PML and its degradation by arsenic trioxide in interferon-mediated neuro-inflammation

Doctoral thesis

to obtain a doctorate (PhD)

from the Faculty of Medicine

of the University of Bonn

Manon Chevallot-Beroux

from Troyes, France

2023

Written with authorization of

the Faculty of Medicine of the University of Bonn

First reviewer: Prof. Dr. Paolo Salomoni

Second reviewer: Prof. Dr. Hiroki Kato

Day of oral examination: 16.12.2022

From the Deutsches Zentrum für Neurodegenerative Erkrankungen of Bonn

Director: Prof. Dr. Paolo Salomoni

Table of Contents

List of abbreviations

Promyelocytic leukemia	PML
Deoxyribonucleic acid	DNA
Ribonucleic acid	RNA
Ribosomal RNA	rRNA
Acute Promyelocytic Leukemia	APL
Retinoic acid receptor α	RARα
Retinoic acid response elements	RARE
Retinoic acid	RA
PML nuclear body	PML-NB
Tripartite motif	TRIM
Really interesting gene	RING
Nuclear localization signal	NLS
Nuclear exclusion signal	NES
PML oncogenic domain	POD
Nuclear domain 10	ND10
Small Ubiquitin Like-Modifiers	SUMO
SUMO-interacting motif	SIM
RING domain, two B-boxes and a coiled-coil domain	RBCC
Reactive oxygen species	ROS
Intrinsically disorder proteins	IDP
Intrinsically disorder protein region	IDPR
Liquid-liquid phase separation	LLPS
Mitotic accumulation of PML protein	MAPP
Protein inhibitor of activated STAT	PIAS1
Casein Kinase	CK2
Cyclin-dependent kinase	CDK
CREB-binding protein	CBP
DNA Topoisomerase II Binding Protein 1	TopBP1
Alternative lengthening of telomeres	ALT
Serine/threonine-protein kinase	CHK2
Death-associated protein 6	DAXX
Histone 3.3	H3.3
PML associated domain	PAD
APEX-mediated chromatin labelling and purification	ALap-seq
Subventricular zone	SVZ
Central nervous system	CNS
Spinocerebellar ataxia	SCA
Interferon	IFN
TAR DNA-binding protein 43	TDP43
Amyotrophic lateral sclerosis	ALS

Frontotemporal lobar degeneration with ubiquitinated Inclusions	FTLD-U
Human immunodeficiency virus 1	HIV-1
Interferon stimulated response element	ISRE
Interferon stimulated gene	ISG
Transforming growth factor β	TGF-β
Toll-like receptor	TLR
Signal transducer and activator of transcription 1	STAT1
Lipopolysaccharide	LPS
Pattern recognition receptors	PRRs
Melanoma differentiation-associated gene 5	MDA5
Retinoic acid inducible gene-I	RIG-I
Cyclic GMP-AMP synthase	cGAS
Interferon regulatory factor	IRF
Interferon stimulated gene factor 3	ISGF3
Cerebrospinal fluid	CSF
Aicardi Goutières Syndrome	AGS
Deoxynucleotide triphosphate	dNTP
Adenosine deaminase acting on RNA	ADAR1
Double strand RNA	dsRNA
Adenosine to inosine RNA editing	A-to-I RNA editing
Mitochondrial antiviral-signaling	MAVS
Systemic lupus erythematosus	SLE
Janus kinase	JAK
Alzheimer’s disease	AD
Positron emission tomography	PET
Magnetic resonance imaging	MRI
Neurofibrillary tangles	NFTs
Mild cognitive impairment	MCI
Early onset AD	EOAD
Late onset AD	LOAD
Amyloid precursor protein	APP
Presenilin	PSEN
Accelerated Food and Drug Administration	FDA
Arsenic trioxide	ATO
All-trans retinoic acid	ATRA
Blood brain barrier	BBB
Wildtype	wt
Knock-out	KO
Bone marrow derived macrophage	BMDM
Dulbecco's Modified Eagle Medium	DMEM
Fetal bovine serum	FBS
Eagle's minimum essential medium	EMEM

Polyinosinic-polycytidylic acid	pI:C
IFN-α/β receptor	IFNAR
Cluster of Differentiation 68	CD68
Differentially expressed genes	DEGs
Gene ontology	GO
Peripheral blood mononuclear cells	PBMCs
Transcription factor enrichment analysis	TFEA
Middle cerebral artery occlusion	MCAO

1. Introduction

1.1. The nucleus and its substructures

The nucleus is a double-membraned organelle found in most eukaryotic cells and was initially defined as an organelle containing the genetic material. Over the last century, the major breakthroughs in technology and advancements in imaging have allowed the discovery of many dynamic sub-nuclear structures (figure 1) unravelling many functions of the nucleus.

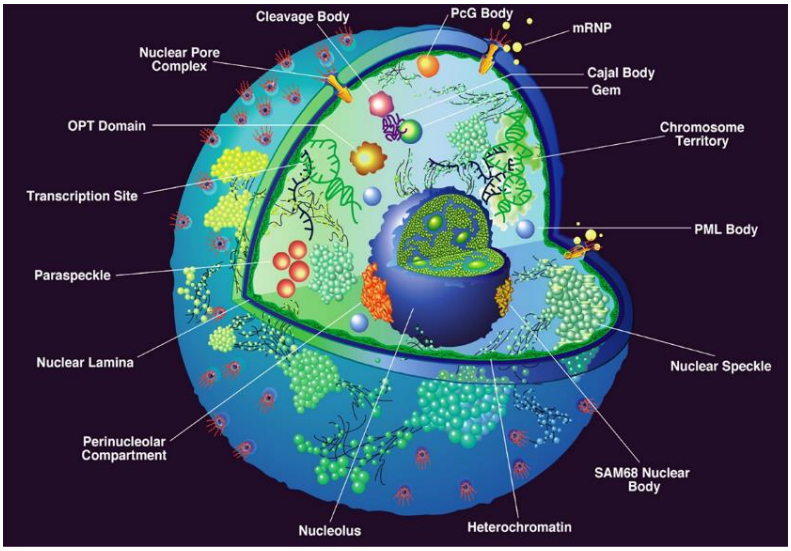

Fig. 1: Nucleus organization.
(Spector & Gasser, 2003)

The nucleus stores the genetic material in a highly organized fashion. It is firstly divided into chromosomes having, each, a defined occupancy called the chromosome territories (Gilbert et al., 2004). Transcriptionally repressed DNA regions are tightly packed into heterochromatin, a nuclear domain composed of nucleosomes carrying H3K9me3 modification (Penagos-Puig & Furlan-Magaril, 2020). Shorter DNA regions containing repressed genes are found in Polycomb Group bodies (Pirrotta & Li, 2012).

Among the transcriptionally active regions, the nucleoli are one of the most condensed and active domains of the nucleus. They are organized into a condensed-liquid phase defined as liquid-like droplets containing high concentration of proteins, RNA and other molecules. The nucleoli contain indeed RNA and high concentrations of proteins required to rapidly and efficiently transcribe and process nascent ribosomal RNA (L. Zhu

et al., 2019). While the nucleoli are the transcription site for ribosomal RNA (rRNA), hundreds other transcription sites are found in the nucleus, where non rRNAs are transcribed (Jackson et al., 1993). These transcription factories are dynamic and highly concentrated in RNA polymerases, transcription factors, RNA processing factors, RNA transcripts and chromatin loops (Szentirmay & Sawadogo, 2000). In the vicinity of high-transcription sites, Cajal bodies can be found in several cells types, such as neuronal and cancer cells. The Cajal bodies are the site of modification for small nuclear and nucleolar RNAs as well as site of assembly and trafficking of small nuclear and nucleolar ribonucleoproteins. They have recently been shown to play a role into telomerase assembly and length regulation (Mao et al., 2011).

One of the nuclear organelles, the promyelocytic leukemia (PML) nuclear bodies (PML-NBs) will be the focus of this thesis and will be described more in details in the following chapter.

1.2. The Promyelocytic Leukemia protein

1.2.1. PML in Acute Promyelocytic Leukemia

PML protein was first discovered in Acute Promyelocytic Leukemia (APL) patients. This rare disease accounts for 10 % to 15 % of the Acute Myeloid Leukemia cases and it is, in 95 % of APL cases, triggered by the mono-allelic chromosome translocation t(15:17)(q21;q22), forming a fusion gene between the *pml* gene and the *retinoic acid receptor α* gene (RARα) (Alcalay et al., 1991; Bennett et al., 1976; Borrow et al., 1990; Castoldi et al., 1994; de Thé et al., 1990; Golomb et al., 1980; Lemons et al., 1990; Pandolfi et al., 1991; Rowley et al., 1977). The resulting PML-RARα chimeric protein represses the transcription of genes involved in granulocytic differentiation by two mechanisms (figure 2). The first mechanism is the binding of the PML-RARα chimeric protein to Pu.1 promoter as well as the retinoic acid response elements (RARE) domains and Pu.1-binding sites. Which in turn recruits corepressor proteins and subsequently prevents transcription (K. Wang et al., 2010).

The second mechanism is that the PML-RARα complex induces the hypermethylation of the target-gene promoters by recruiting DNA methyltransferase (Thomas, 2019; Z.-Y. Wang & Chen, 2008). In addition to the transcriptional repression, the PML-RARα complex formation causes the loss of function of the pro-senescence PML protein, consequently inhibiting the p53-dependent senescence activation (Insinga et al., 2004). To summarize, this fusion protein prevents the differentiation of promyelocytes in which the PML-dependent senescence pathway is inactive (Korf et al., 2014).

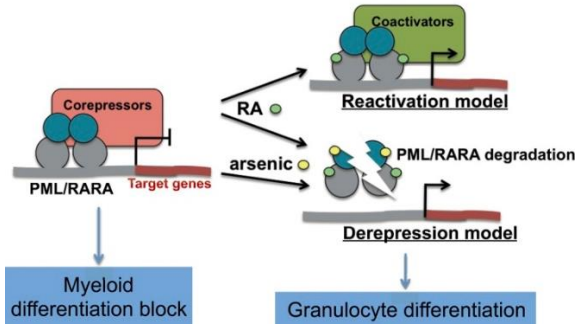

Fig. 2: Model of action of Retinoic acid (RA) and arsenic trioxide in APL cells. (de Thé et al., 2012)

The loss of p53-dependent senescence activation is observed in multiple forms of human cancer. It is suggested to occur due to PML loss of function either by disorganization of PML and therefore of the PML-NBs such as in APL, or by complete loss of PML protein such as in lung and prostate cancer.

1.2.2. PML isoforms

The human *pml* gene is located on chromosome 15q22. It is composed of nine exons dispersed over 35 kb which are translated into 7 groups of isoforms by alternative splicing (PML-I to PML-VII), increasing the diversity of functions of PML (Jensen et al., 2001). Structurally, PML belongs to the tripartite motif (TRIM) family as TRIM19. The TRIM, located on the first 3 exons, is highly conserved and common to all isoforms. It is constituted of a really interesting gene (RING) domain, two zinc-fingers B-boxes and a coiled-coil domain (RBCC) (Jensen et al., 2001; Reymond et al., 2001). Furthermore, all isoforms, except PML-VII, contain a nuclear localization signal (NLS) encoded in the exon 6 and are therefore localized in the nucleus whereas the isoform PML-VII is cytoplasmic. The largest isoform, PML-I, harbors a nuclear exclusion signal (NES) in exon 9 in addition of the previously mentioned NLS and can therefore be found in both cytoplasm and nucleus (Condemine et al., 2006; Hsu & Kao, 2018; Jensen et al., 2001; Nisole et al., 2013) (figure 3). PML-I is also the most abundant isoform *in vivo* and shares the highest homology with the 3 murine isoforms (Condemine et al., 2006; Lin et al., 2004; Salomoni et al., 2008).

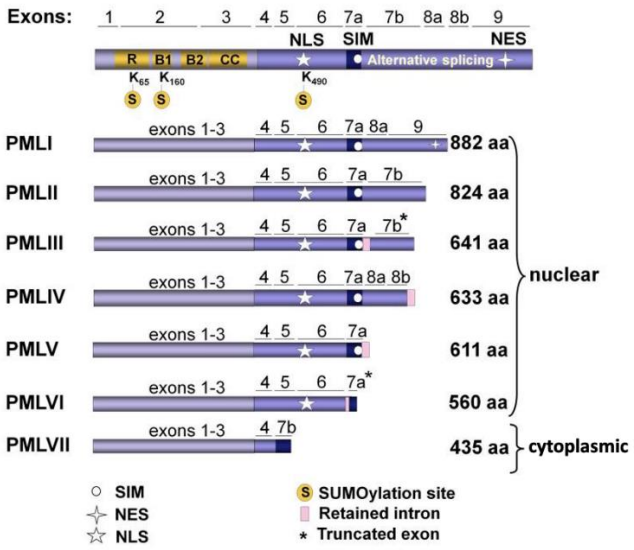

Fig. 3: Human PML protein isoforms.
SIM: SUMO-interacting motif, NES: nuclear exclusion signal, NLS: nuclear localization signal, aa; amino acids (Maroui et al., 2012a).

1.2.3. PML-NBs biogenesis

The PML protein has the ability to form dynamic nuclear foci associated with the nuclear matrix and referred to as PML nuclear bodies (PML-NB), Kremer bodies, PML oncogenic domains (PODs) or nuclear domain 10 (ND10) (Lallemand-Breitenbach & de Thé, 2010; Salomoni et al., 2008). PML is an essential component of the PML-NBs by forming the scaffolding polymeric spherical shell. Nonetheless, one important fact to keep in mind while working in PML field is that most of PML protein pool is in the diffuse nuclear fraction (Lallemand-Breitenbach & de Thé, 2010).

The PML-NBs are highly dynamic and their presence and number vary greatly from 0 to 30 PML-NBs per nucleus depending on cell type, tissue, cell cycle progression and stimuli/stress. The PML-NBs display heterogeneity not only in morphology, with a spherical “donut”-like shape of 0.1 to 1 µm (figure 4A) but also in composition with about 166 transient interacting partners found in the inner core of the PML-NBs (Bernardi & Pandolfi, 2007a; Lallemand-Breitenbach & de Thé, 2010; Salomoni et al., 2008; van Damme et al., 2010).

PML is post-translationally modified by the binding of Small Ubiquitin Like-Modifiers (SUMO), via a process named SUMOylation which is induced by oxidative stress and regulates the protein complex stability. PML carries three SUMOylation sites, K65, K160

and K490, and a SUMO-interacting motif (SIM) (figure 3). For several decades, the biogenesis of PML-NBs was believed to be achieved through a SUMO-SIM interaction between PML proteins. In 2014, Sahin et al. eventually tackled this theory by showing that PML-NB nucleation does happen in a model lacking the three SUMO-binding sites as well as the SIM (figure 4B). Partner recruitment of these PML-NBs was nonetheless affected as the SUMOylation sites and the SIM are necessary for the NB stability and interacting partner recruitment (Lallemand-Breitenbach et al., 2001; Sahin Umut et al., 2014).

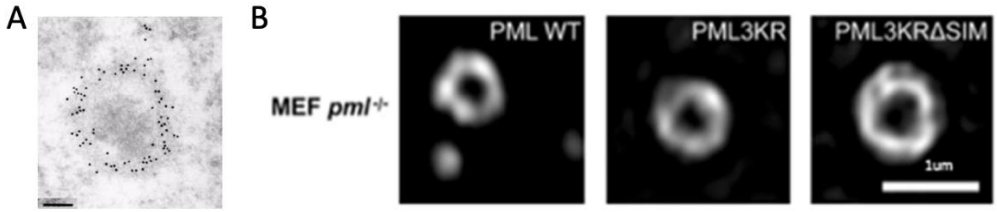

Fig. 4: SUMO-SIM interaction is not required for PML-NB formation.
(A) displays the “donut”-like shape of the NBs by immuno-gold electron microscopy, scale bar of 0.1 µm (Lallemand-Breitenbach & de Thé, 2010). The lack of the 3 SUMOylation sites (3KR) and the deletion of the SIM (ΔSIM) do not impair the NB formation (B) (Sahin Umut et al., 2014).

The PML-NB biogenesis is explained as a two-step mechanism: a PML nucleation via the RBCC domain and disulfide bonds formation upon oxidation; followed by a stabilization and partner recruitment in the PML-NBs (figure 5).

For the initial multimerization, PML as part of the TRIM protein family, has a RBCC motif which is known to play an important role in oligomerization (Jensen et al., 2001; Salomoni et al., 2008). In addition, recent studies have showed that the multimerization of the zinc-finger PML proteins is triggered by oxidation. PML is a cysteine-rich and a reactive oxygen species (ROS) sensor protein, becoming highly oxidized when associated with the nuclear matrix, triggering the formation of disulfide bonds between PML proteins, which then assemble into the outer shell of the PML-NBs (Jeanne et al., 2010; Sahin Umut et al., 2014; Stuurman et al., 1992; X.-W. Zhang et al., 2010).

Following the first step of PML nucleation, UCB9, a SUMO E2 ligase, is recruited into the soluble inner fraction of the PML-NBs to SUMOylate PML. The PML-bound SUMO and the SIM of PML will then be used as docking sites for interacting partner proteins

through SIM-SUMO interactions. UCB9 and PML, the latter of which has also been shown to have a E3 ligase activity as a TRIM protein (Chu & Yang, 2011; Gärtner & Muller, 2014; Reuter et al., 2017), will then SUMOylate the interacting proteins in situ, reinforcing both the interaction, the post-translational modifications and the sequestration of partner proteins (Maroui et al., 2012a; Sahin Umut et al., 2014; Salomoni et al., 2008).

The biogenesis of PML-NBs is thought to be a redistribution of PML from the diffuse nuclear fraction into matrix-associated bodies in response to cellular stresses such as oxidative stress and also upon treatment with arsenic. An increase of PML transcription accounting for the formation of PML-NBs was, so far, only observed upon interferon (IFN) α/β and γ stimuli (Chelbi-Alix et al., 1995; Lallemand-Breitenbach & de Thé, 2010; Sahin Umut et al., 2014). However, it is worth noting that most of the studies on the biogenesis of PML-NBs use overexpressing wild-type or mutant PML transfected cell lines, therefore the transcription and protein level upon stimuli cannot be assessed.

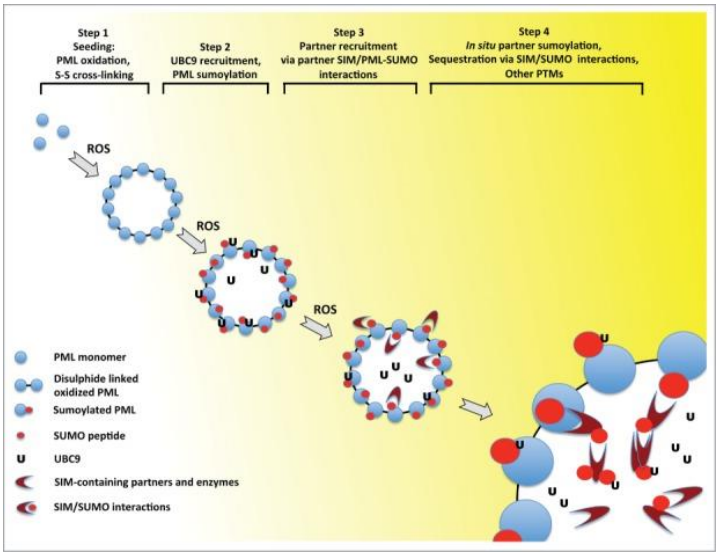

Fig. 5: PML-NBs biogenesis.
(Sahin Umut et al., 2014)

1.2.4. PML, a disordered protein, forming a liquid-liquid phase separation system

Intrinsically disorder proteins (IDPs) or intrinsically disorder protein regions (IDPRs) are proteins or regions lacking secondary/tertiary unique structure which was formerly considered essential for the protein to be functional (DeForte & Uversky, 2016; Dunker

et al., 1998, 2005). However, during the last decades, it has extensively been shown that IDPs and IDPRs are functional and mostly involved in signaling and control pathways (Iakoucheva et al., 2002) as well as molecular recognition (Uversky et al., 2005). They are also commonly involved in protein-protein and protein-DNA or -RNA interactions due to the structural flexibility which gives them faster kinetics for interactions (Dunker et al., 2005). Higher organisms show higher percentage of IDPRs, about 40 % of the whole proteome, which could be explained by the higher complexity in signaling and regulation pathways in such organisms compared to bacteria or archeabacteria (DeForte & Uversky, 2016; Dunker et al., 2001, 2005; van der Lee et al., 2014).

As one of the characteristics of the IDPs and IDPRs is its interaction with RNA and DNA, Frege & Uversky investigated the disorder level in human nucleus (Frege & Uversky, 2015). For this, only the human curated proteins from the Nuclear Protein Database (Dellaire et al., 2003) were analyzed by the PONDR-FIT® metapredictor (Xue et al., 2010). The resulting 185 nuclear proteins show that the nucleus is strongly disordered with most of its proteins having an intrinsically disorder score higher than 30 % (figure 6) (Frege & Uversky, 2015). The disorder score is calculated using neural network predictor which identifies disordered regions and is applied on protein FASTA sequence (Xue et al., 2010). This score represents the disorder level of the protein, i.e the higher the percentage, the higher the disorder.

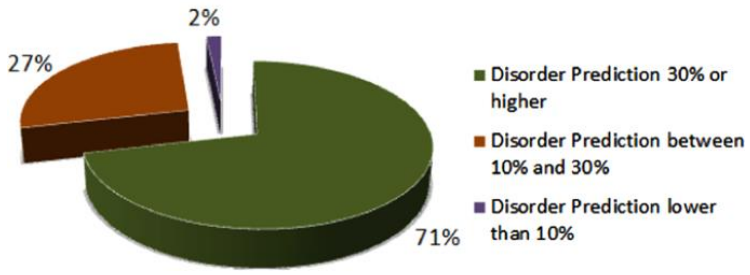

Fig. 6: Distribution of the human curated nuclear proteins depending on their disorder prediction score calculated by PONDR-FIT predictor.
PONDR stands for Predictor of Naturally Disordered Region (Frege & Uversky, 2015).

IDPs and IDPRs are found in many membraneless organelles such as cleavage bodies, SAM68 nuclear bodies, nuclear speckles, Cajal bodies, nucleolus and stress granules

(Banani et al., 2016; Ditlev et al., 2018; Frege & Uversky, 2015; Molliex et al., 2015). These organelles are formed by the phenomenon of liquid-liquid phase separation (LLPS) and are characterized as condensed liquid-like droplets containing proteins, RNA and other molecules. They have a very rapid response upon stress first by their fast formation and client recruitment as a membraneless structure, but also thanks to the high concentration of proteins which facilitate spatiotemporal reactions (Frege & Uversky, 2015; Jo & Jung, 2019; Murthy & Fawzi, 2020; Shin & Brangwynne, 2017).

In the membraneless organelles, protein recruitment is dependent on the client and scaffold valency, as well as on the scaffold stoichiometry. This recruitment can be reversed very quickly, supporting in this way the fast response of cellular bodies to stress (Banani et al., 2016; Ditlev et al., 2018) (figure 7).

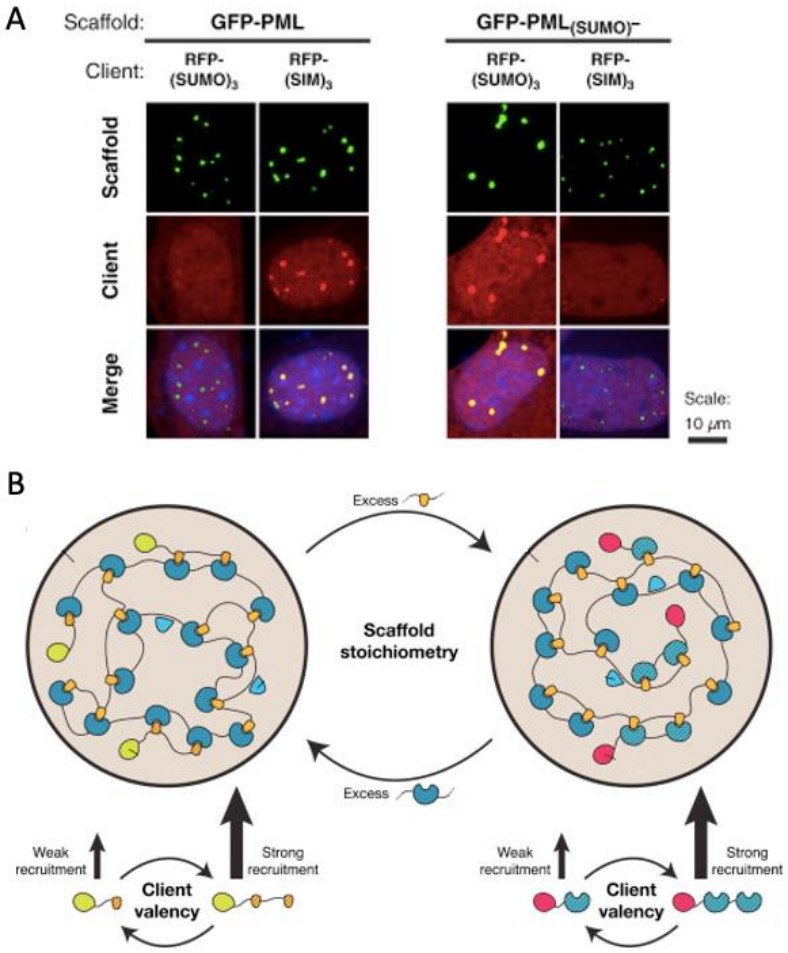

Fig. 7: Client recruitment in cellular bodies depends on the client and scaffold valency and scaffold stoichiometry.

(A) SUMO-depleted NBs recruit SUMOylated clients while PML-NBs recruit SIM-containing clients. (B) Model of cellular bodies composition and dynamic (adapted from Banani et al., 2016).

Interestingly, PML harbors some IDPRs which are slightly different between PML isoforms (figure 8). The difference in disorder at the C-terminal region might explain their specific interaction partners and functions (Frege & Uversky, 2015; Salomoni et al., 2008). Also, PML functions such as the protein-protein interaction and the involvement in signaling pathways, are most likely facilitated by the IDPRs, as their protein flexibility increases the interaction kinetics (Dunker et al., 2005; Salomoni et al., 2008).

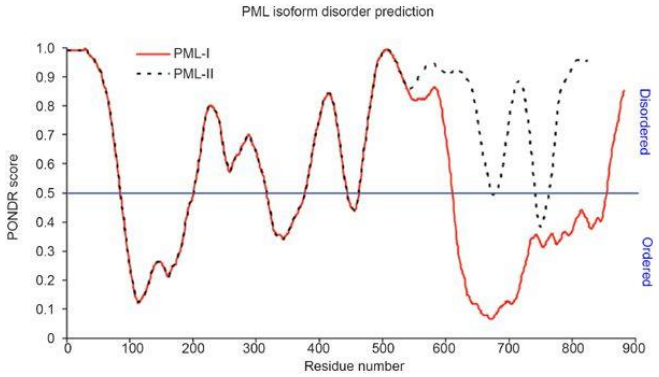

Fig. 8: PML isoforms I and II display different disordered regions by PONDR analysis. (Salomoni et al., 2008)

Banani et al. have shown that highly SUMOylated PML-NBs recruit SIM-containing clients, however, a reduced PML SUMOylation shifts the recruitment towards SUMO-containing clients (figure 7). In addition, the higher the number of SIM or SUMO in the clients, the more their recruitment is favored in the PML-NBs (Banani et al., 2016; Ditlev et al., 2018). This suggests that the composition of cellular bodies affects the partner recruitment and is therefore tightly associated to the PML-NBs functions.

It is important to note that the previously mentioned studies were made *in silico*, but yet, no proof of PML-NBs forming by LLPS *in cellulo* has been achieved. Furthermore, the PML-NBs would be the first LLPS-forming organelle which would have a shell structure. At last, a lot is still to be discovered about how PML carries off its functions in relation to the biogenesis of PML-NBs.

1.2.5. PML-NBs degradation

PML-NBs are highly dynamic sub-nuclear structures: several factors can trigger not only their assembly as described previously, but also their degradation.

At physiological state, the PML-NBs were shown to be degraded during the cell cycle. At the G2/M-phase transition, they first accumulate in the cytoplasm as the nuclear envelope breaks down, forming larger structures called mitotic accumulation of PML protein (MAPP). During the M/G1-phase transition, the bodies are broken down in order to pass through the newly formed nuclear pore and eventually form the progeny PML-NBs (Lång et al., 2019).

As previously mentioned, in various cancers the loss of PML is due to PML protein degradation rather than PML transcription downregulation. At the same time, Protein inhibitor of activated STAT (PIAS1) and Casein Kinase 2 (CK2) are found overexpressed and activated. PIAS induces the SUMOylation of PML and promotes the interaction of PML with CK2 which, in turn, induces the phosphorylation of PML ser517. The phosphorylation of PML is suggested to enhance its ubiquitination and degradation (Scaglioni et al., 2006).

In *in vitro* cancer cells, hypoxia induces PML degradation by, supposedly, CDK1 and CDK2-dependent PML phosphorylation on ser518. However, a lot is still to be understood about PML degradation under hypoxia (Rabellino et al., 2012). Other studies have revealed that PML degradation is dependent on ERK2/Pin1 in breast cancer cell lines (Lim et al., 2011) and is mediated by E6AP, an ubiquitin E3-ligase (Louria-Hayon et al., 2009).

More recently, transforming growth factor β (TGF-β) was shown to induce PML degradation. Upon TGF-β, the nuclear isoforms are SUMOylated, triggering the formation of PML-NBs. Interestingly, upon TGF-β, only the PML-NBs composed of the PML IV isoform recruits and interacts with Caspase-8, which thereafter induces its degradation (El-Asmi et al., 2019).

Lastly, PML-NBs were shown to be degraded upon Arsenic trioxide, a drug approved to treat APL patients (detailed in part 1.4.1.1). At first, arsenic trioxide binds the RING domain of PML and triggers the phosphorylation of PML, inducing the transfer of the nucleoplasmic PML to the nuclear matrix associated PML-NBs (Nisole et al., 2013).

Then, Arsenic trioxide triggers the conjugation of several SUMO peptides to the SUMO binding sites of PML: the lysines K65, K160 and K490 (figure 3), forming a SUMO chain on these amino acids. The resulting enhanced SUMOylation leads to the recruitment of the RING Finger protein 4 (RNF4), a poly-SUMO-specific ubiquitin ligase, which deposits ubiquitin on poly-SUMOylated proteins. The 11S complex and 20S core of the proteasome are then recruited to the PML-NBs and consequently trigger the degradation of PML (figure 9). Interestingly, the SIM of PML is not required for the RNF4 recruitment, however, it is necessary for both PML ubiquitination and proteasome recruitment to the PML-NBs upon Arsenic trioxide. This also explains the resistance to arsenic trioxide of the nuclear isoform PML VI, which does not contain a SIM. Intriguingly, the cytoplasmic isoform, PML VII, does not get SUMOylated and thus not degraded upon Arsenic trioxide (Lallemand-Breitenbach et al., 2008; Maroui et al., 2012b; Nisole et al., 2013).

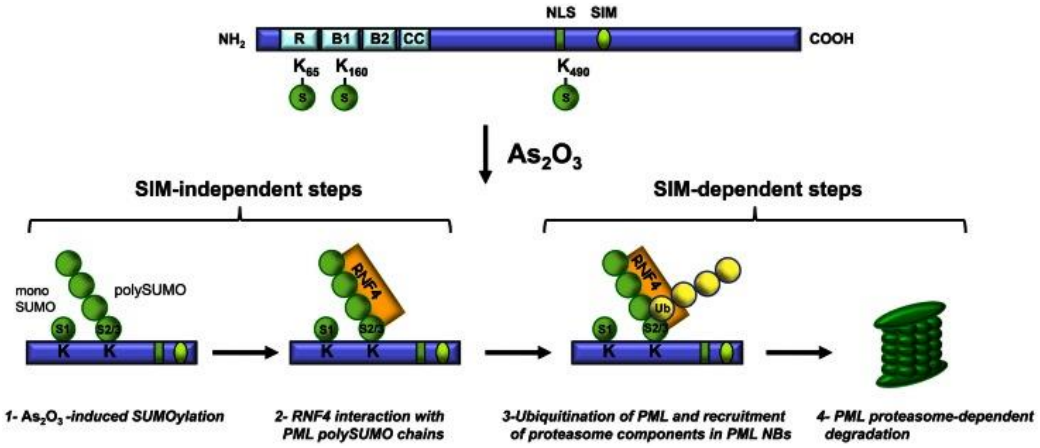

Fig. 9: PML degradation upon arsenic trioxide.
As_2O_3: arsenic trioxide, SIM: SUMO-interacting motif, NLS: nuclear localization signal, NES: nuclear exclusion signal (Nisole et al., 2013).

1.2.6. Biological function of PML-NBs

The PML-NBs are involved in many cellular processes such as tumor suppression, apoptosis, senescence, antiviral response, inflammation, immunity, metabolism and many more. This variety of functions is due to their high number of interacting partners with more than 120 proteins proven to physically interact with PML (figure 10). The high number of PML isoforms and their properties to interact with different proteins via their

different C-terminal region contribute to the plethora of functions of the PML-NBs (Nisole et al., 2013). Despite its numerous functions, it is noteworthy that PML -/- mice are perfectly viable and healthy. They present an increased risk of spontaneous tumorigenesis, but no significant metabolic defects were observed under physiological conditions (Trotman et al., 2006).

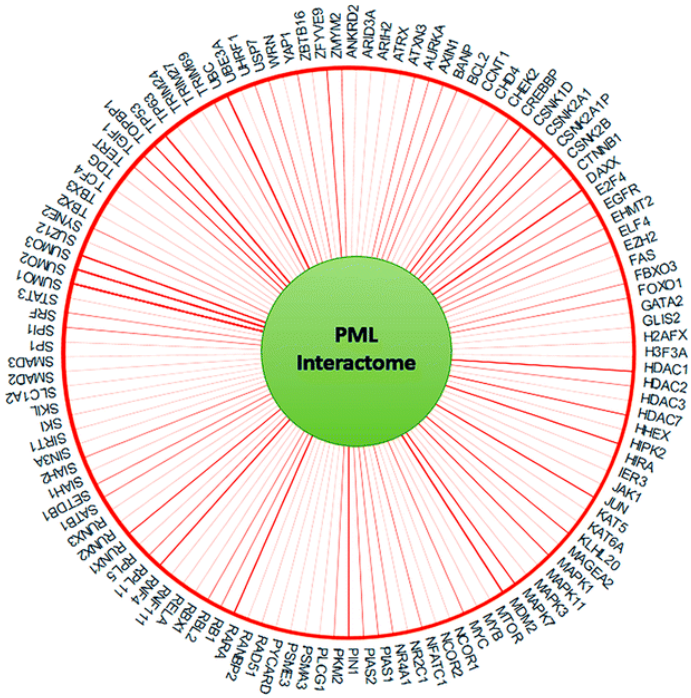

Fig. 10: PML interactome.
(Guan & Kao, 2015)

The PML-NBs achieve their function through several mechanisms: protein sequestration to inhibit their function, protein recruitment to activate their function, facilitation of protein interaction, post-translational modifications of PML-NBs-interacting protein, transcriptional and translational regulation, protein stability, etc. The cellular processes and their mechanism of regulation are detailed in the following parts (Bernardi & Pandolfi, 2007b; Guan & Kao, 2015; Lallemand-Breitenbach & de Thé, 2010).

1.2.6.1. PML as tumor suppressor

Since its discovery in APL, PML was found downregulated at its protein level but not transcriptionally in several cancers. This suggests that, first, PML is regulated at a translational/post translational level, but it also indicates a function of PML as tumor

suppressor (Guan & Kao, 2015). This function of PML is achieved through several independent mechanisms.

First, PML-NBs regulate p53-dependent apoptosis by stabilizing p53. Upon Ras expression, p53 and CREB-binding protein (CBP) are recruited into the PML-NBs, where p53 gets acetylated. This allows p53 to induce the p53 target gene expression triggering the apoptosis or cellular senescence (Ferbeyre et al., 2000; Pearson et al., 2000). In addition, PML-NBs have been shown to stabilize p53 by sequestering the p53-ubiquitin ligase, Mdm2, to the nucleolus (Bernardi et al., 2004). On the same note, PML isoform IV overexpression leads to p53-dependaent apoptosis and cell senescence (Quignon et al., 1998). The PML-NBs also regulates p53-independent apoptosis. The recruitment of DAXX into the PML-NBs upon mitogenic activation is necessary for the induction of DAXX-mediated apoptosis (Zhong et al., 2000).

Taken all together, these finding show that the downregulation of PML in cancer cells impairs, via several independent mechanisms, the activation of the p53-dependent and p53-independent apoptosis and senescence induction.

Oppositely, PML was suggested to be oncogenic in primary glioblastoma cells with a reduced growth and invasion index in PLM knock down cells (Amodeo et al., 2017).

1.2.6.2. PML function in genome stability and DNA damage response

PML contributes to DNA damage response and DNA repair (Chang et al., 2018). Upon ionizing-radiation-induced DNA damage, PML recruits and stabilizes DNA Topoisomerase II Binding Protein 1 (TopBP1) and other DNA repair proteins at the single-stranded DNA foci. TopBP1 is a DNA topoisomerase repairing the DNA damage (Xu et al., 2003). In addition, PML-NBs were found at persisting IR-induced DNA damage foci contributing to DNA repair via the homologous recombination machinery (Vancurova et al., 2019).

To maintain the genome stability, PML can also induce cell apoptosis upon DNA damage. PML mediates the auto-phosphorylation of Serine/threonine-protein kinase (CHK2), which triggers its activation and subsequently the induction of apoptosis (S. Yang et al., 2006).

In addition, PML has been found to colocalize with telomeres in cells presenting an active alternative lengthening of telomeres (ALT) mechanism (I. Chung et al., 2012). The PML-NBs are the site of synthesis of telomeres by ALT which is therefore abrogated upon the loss of PML. It is worth mentioning that only a few human cancers use the ALT mechanism, while the majority of them rely on the telomerase to extend the shortening telomeres (J. M. Zhang et al., 2021).

1.2.6.3. PML as a regulator of transcription

The PML-NBs present several mechanisms to regulate transcription. First, PML-NBs can regulate the chromatin opening or closing by recruiting numerous chromatin-modifier proteins into the PML-NBs. The heterochromatin protein HP1, the histone chaperones ATRX, DAXX and DEK, but also some histone acetyltransferase (CBP, MOZ, TIP60), histone deacetylase (HDAC7, SIRT1) and histone methyltransferase (SETDB1) have been found to localize in the PML-NBs (Corpet et al., 2020). The newly synthesized histone variants histone 3.3 (H3.3) are recruited to the PML-NBs in a DAXX dependent manner, preventing the accumulation of the non-incorporated H3.3 (Delbarre et al., 2013). In addition, PML is required for ATRX- and DAXX-mediated deposition of H3.3 in PML associated domains (PADs), a heterochromatin domain associated with PML-NBs (Delbarre et al., 2017). It is important to mention that the PML-NBs do not contain neither chromatin nor RNA in normal conditions (Boisvert et al., 2000). However, as previously mentioned, telemetric DNA is found in PML-NBs in ALT and tumour cells, and viral DNA is recruited in the PML-NBs upon viral infection (detailed in 1.2.6.7). Despite not containing chromatin, the PML-NBs are closely associated with transcriptionally active regions, as suggests the presence of nascent RNA and highly acetylated chromatin domain at the vicinity of the PML-NBs (Boisvert et al., 2000; J. Wang et al., 2004). This was later confirmed by immuno-TRAP, a biotin-labelling DNA method allowing to find chromatin loci associated to the PML-NBs (Ching et al., 2013), as well as by APEX-mediated chromatin labelling and purification (ALap-seq) (Kurihara et al., 2020). The PML-NBs can also indirectly regulate transcription by recruitment, post-translational modification, sequestration or activation of many transcription factors, such as p53, as detailed previously.

1.2.6.4. PML role in metabolism

PML has been shown to regulate many metabolic genes, however, the role of PML in metabolism is still controversial. Under high fat diet, a study has shown that the PML -/- mice present an accelerated fat accumulation due to the loss of transcriptional repression of adipogenic transcription factors by PML (M. K. Kim et al., 2011). In contradiction, another study showed that the PML -/- mice are protected from obesity induced upon high fat diet, thanks to an accelerated rate of fatty acid metabolism (Cheng et al., 2013).

1.2.6.5. PML in central nervous system pathophysiology

At postnatal stages, PML is present in the subventricular zone (SVZ) of the neocortex and in few neuronal cells in the hippocampus and cerebellum, where it regulates neurogenesis. PML -/- mice exhibit an impaired differentiation and an increased proliferation of the neural progenitor cells leading to a thinner cortical wall and swollen SVZ (Regad et al., 2009; Salomoni & Betts-Henderson, 2011).

At adult stage, PML expression is no more restricted to the SVZ but it is present in almost all central nervous system (CNS) areas such as the hippocampus, the brain stem and the cerebellum, where it achieves different functions (figure 11). In the adult SVZ, PML is required for adult neurogenesis by regulating neuroblast migration (Amodeo et al., 2017). Following the defect in postnatal neurogenesis, Butler et al. showed that that the PML -/- mice present a low anxiety level and an impairment in conditioned and spatial learning. They suggested that the hippocampal plasticity was impaired due to a reduced synaptic transmission in the CA1 (Butler et al., 2013). In addition, Arc, a protein involved in synaptic plasticity by regulating the transcription of genes associated with synaptic strength, was found to colocalize and associate with PML-NBs in hippocampal neurons (Bloomer et al., 2007).

In the suprachiasmaticus nucleus, PML is essential for the transcription and nuclear localization of Per2, a clock regulator gene and for the transcription of other key clock regulator genes. Upon PML loss, mice exhibit a lack of precision and stability in circadian rhythm (Miki et al., 2012).

PML role was also investigated in polyQ diseases such as Huntington’s disease and spinocerebellar ataxia (SCA). These neurodegenerative diseases are caused by

expanded repeats of CAG in the causative gene, forming a chain of glutamine residues called polyQ tract. The accumulation of polyQ proteins leads to damage in mitochondria and in the ubiquitin proteasome system which, eventually, triggers the degeneration of specific neuronal populations (Fan et al., 2014). In Purkinje cells, the most affected cell type of SCAs, PML is highly expressed under physiological conditions and was found to colocalize with Ataxin mutants in patient samples of SCA1, SCA7, SCA3, SCA17 (Takahashi et al., 2003; Yamada et al., 2001). The recruitment of Ataxin7 in PML-NBs, specifically formed by PMLIV, was shown *in vitro* to promote their ubiquitin-dependent proteasomal degradation which eventually prevents their aggregation. Furthermore, the disruption of PML-NBs by Cadmium increases the mutant Ataxin7 aggregation. Inversely, up-regulating PML expression and enhancing the PML-NBs formation by an *in vitro* interferon-β (IFNβ) treatment increase the proteasomal degradation of mutant Ataxin7 and its aggregates. (Janer et al., 2006). Similarly, IFNβ treatment of the SCA7 preclinical model, $SCA7^{266Q/5Q}$ knock-in mice, induces the clearance of mutant Ataxin7 and an improvement of the SCA7-associated cerebellar dysfunctions, such as locomotor function, balance and motor coordination (Chort et al., 2013). More generally, Guo et al. demonstrated that PML-NBs promote the degradation of several nuclear misfolded proteins, such as the polyQ proteins mutant ataxin1 and mutant huntingtin causing respectively SCA1 and Huntington's disease, but also the degradation of TAR DNA-binding protein 43 (TDP43) associated with Amyotrophic lateral sclerosis (ALS) and frontotemporal lobar degeneration with ubiquitinated inclusions (FTLD-U). After their recruitment into the PML-NBs, PML performs the SUMOylation of the misfolded proteins, followed by RNF4-mediated ubiquitination which signals their proteasomal degradation (L. Guo et al., 2014; Janer et al., 2006). This newly revealed function of PML could be of interest for several neurodegenerative diseases caused by misfolded proteins and protein aggregation.

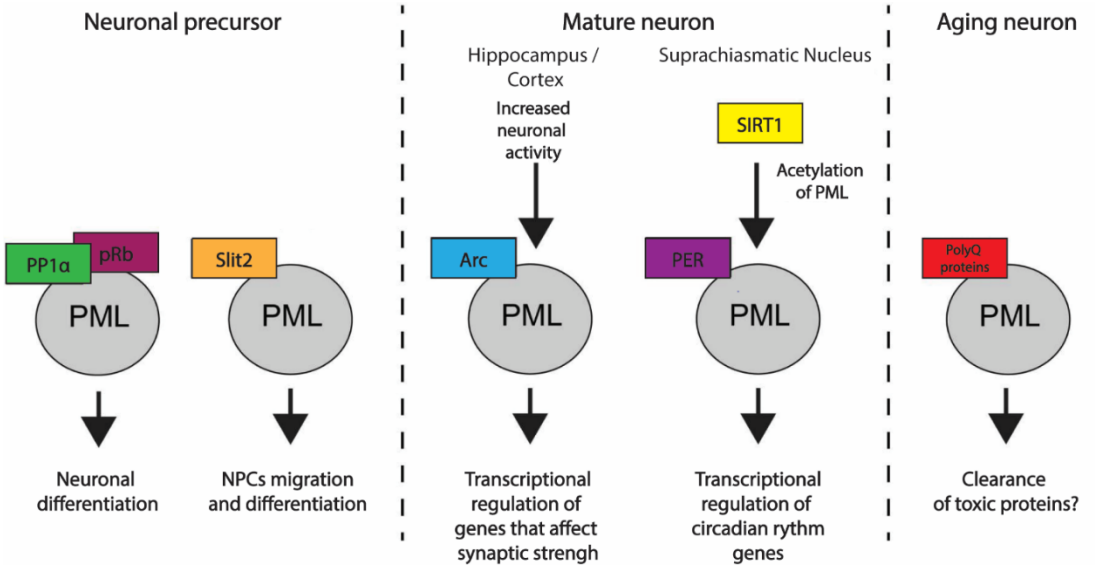

Fig. 11: PML functions in the brain.
(adapted from Korb & Finkbeiner, 2013)

As described above, in the CNS, PML has mostly been studied in neuronal cells and their precursors. It was also believed that PML was not, or very lowly expressed in glial cells, which explain the almost non-existent literature about PML in glial cells.

Palibrk et al. studied the response of PML -/- mice in a neonatal hypoxia-ischemia model caused by a permanent occlusion of the carotid artery at day 9. Interestingly, they discovered that PML-NB numbers were increased in microglia in this model and that PML is required for the microglia response upon hypoxia-ischemia. Indeed, the PML -/- mice showed a reduced/abrogated activation of the microglia. Furthermore, PML was shown to have a protective role from the hypoxia-ischemia-induced tissue loss and apoptosis, as well as a better tissue regeneration. The latter was due to a defect in de novo production of neuronal progenitor and PML role in neuron differentiation (Palibrk et al., 2016).

1.2.6.6. PML as a stress sensor

PML is required to sense and mediate the stress response upon several stimuli. Upon basal oxidative stress, PML-NBs mediate the p53-dependent anti-oxidant response in order to protect the cells against ROS. While upon acute ROS exposure, PML-NBs assembly is enhanced which in turn mediates p53-dependent cell death. Furthermore, silencing PML led to higher ROS level and DNA damages. It is worth mentioning that

the PML-/- mice have a prolonged live span under chronic oxidative stress due to their lack of oxidative stress response, which was suggested to delay aging (Niwa-Kawakita et al., 2017).

1.2.6.7. PML in the viral response

PML has been shown to have an antiviral function against DNA viruses and RNA viruses.

PML-NBs have the ability to repress viral replication during the early infection stage and also at later stage (figure 12). Upon nuclear entry of nuclear replicating viruses, the PML-NBs recruit and silence the viral genome by epigenetic regulation conducted by PML-NBs interacting partners such as hDAXX and ATRX. At a later stage, the PML-NBs repress the viral replication by entrapping the newly assembled nucleocapsids of varicella-zoster virus (Scherer & Stamminger, 2016). Upon human immunodeficiency virus 1 (HIV-1), the PML-NBs translocate to the cytoplasm and inhibit the viral retrotranscription in a cell type dependent manner (Dutrieux et al., 2015; Kahle et al., 2015).

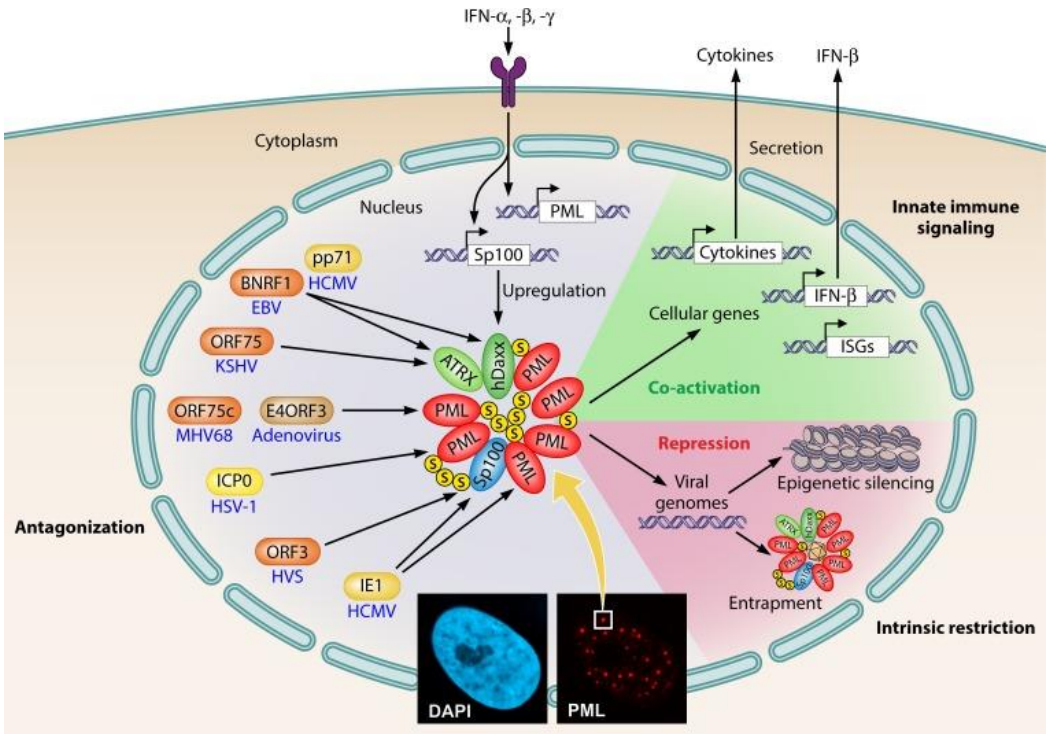

Fig. 12: Mechansims of action of PML against viruses.
(Scherer & Stamminger, 2016)

The antiviral activity of PLM-NBs has been bypassed by virus evolution. The viruses have deployed different mechanisms to inactivate the antiviral functions of the PML-NBs such as p53-dependent apoptosis, IFN response activation as well as replication repression. For instance, herpes virus type 1 is able to ubiquitinate and induce the proteasomal degradation of the SUMOylated PML-NBs-interacting partners as well as triggering the dispersion of the PML-NBs by inhibiting the SUMOylation of PML and therefore its PML-NBs formation (Scherer et al., 2014). Similarly, cytomegaloviruses and gammaherpesviruses trigger the dispersion or degradation of the PML-NBs, while adenoviruses induce their rearrangement into a nuclear track-like structure, eventually inhibiting their functions (Scherer & Stamminger, 2016). Cytomegaloviruses are also able to inhibit the IFN-mediated response by sequestering IFN-stimulated gene factor 3 once bound to PML-NBs (Y. E. Kim & Ahn, 2015). Other viruses employ mechanisms to disrupt the association of PML-NBs components such as hDAXX-ATRX complex which acts as a silencer of the viral genome (Scherer & Stamminger, 2016).

Recently, PML presence was shown to be required for human papillomavirus infection, which uncovers a new role of the PML-NBs in addition to their antiviral functions (Guion & Sapp, 2020).

1.2.6.8. PML in inflammation and innate immunity

Pml promoter contains IFN stimulated response elements (ISRE) making PML an IFN stimulated gene (ISG) (Stadler et al., 1995). In addition to *pml* transcription, IFN stimuli enhance PML-NBs formation which is required to induce p53-dependent apoptosis (Chelbi-Alix et al., 1995; Fu et al., 2015; Regad et al., 2001). IFNα was also indicated to induce TGFβ-mediated apoptosis, where cytoplasmic PML, PML VII isoform, was required for TGFβ signaling activation (El-Asmi et al., 2019). In addition to the role of PML inducing p53 activation, PML is required to mediate apoptosis upon p53 activation. p53 binding sites were discovered in *pml* gene, making PML a p53 target (de Stanchina et al., 2004).

Upon IFNγ stimulation, the role of PML is controversial. Initially, PML was considered as a repressor of IFNγ-induced STAT1α transcriptional and DNA binding activity in mouse embryonic fibroblasts (Choi et al., 2006). However, in 2011, Bougrini et al. showed that the silencing of nuclear PML isoforms led to a reduced IFNγ-induced STAT1 activation, while the overexpression of nuclear PML isoforms increases IFNγ-induced STAT1 phosphorylation, DNA binding activity and eventually the ISG expression (el Bougrini et al., 2011).

Interestingly, PML SUMOylation is required to induce STAT1 activation upon IFNγ treatment (el Bougrini et al., 2011), but also to enhance global SUMOylation upon IFNγ stimulation (El-Asmi, McManus, Thibault, et al., 2020; Maroui et al., 2018). The analysis of the SUMO proteome upon IFNα reveals that STAT1 is first deSUMOylated 45 minutes after induction and then increased after 16 hours of induction (Maroui et al., 2018). The later SUMOylation of STAT1 was shown to inhibit its phosphorylation and subsequently its activation which provides a negative feedback loop in the IFN-mediated signaling (Maarifi et al., 2015).

Lastly, PML was suggested to be involved in the Toll-like receptor (TLR)/NF-κB signaling pathway. Upon LPS-induced sceptic shock, the PML -/- mice were found to be more resistant than the wt mice. This is due to an impairment in TLR4 signaling activation and therefore in chemokines and cytokine release by the PML -/- macrophage upon lipopolysaccharide (LPS), suggesting an impairment in the NF-κB pathway (Lunardi et al., 2011).

1.3. Interferon signaling in disease

1.3.1. Interferon signaling upon viral infection

The nucleic acid sensing pathways were initially found to be induced upon viral infections to activate the immune response through the IFN signaling pathway and fight viral infections. Following a viral infection, the pattern recognition receptors (PRRs), such as TLRs, NOD-like receptors or retinoic acid inducible gene-I-like (RIG-I-like) receptors, and also cytoplasmic DNA receptors, such as the cyclic GMP-AMP synthase (cGAS), sense the accumulated cytoplasmic viral double stranded DNA or RNA.

One of the endosomal receptors, TLR3, senses double stranded RNA and leads to the phosphorylation of TBK1 and IKKε by TRAF6 and TRIF. Once phosphorylated, TBK1 phosphorylates IFN regulatory factor 3 (IRF3), which then translocates to the nucleus and induces the transcription of IFNβ and IFN regulatory factors 7 (IRF7). The primary signal is further amplified by a positive feedback loop where the IFN-α/β receptor (IFNAR) undergoes a dimerization upon IFN binding, recruiting JAK1 and TyK2 which phosphorylate the STAT proteins. The IFN stimulated gene factor 3 (ISGF3) complex, comprising phosphorylated STAT1-STAT2 dimer with IRF9, is formed and binds to ISRE inducing the transcription of the ISGs (figure 13). It is worth noting that *pml* is an ISG (Stadler et al., 1995), as well as *ifnb* (Schafer et al., 1998), which therefore induces an amplification by the IFNβ feedback loop (figure 13).

The nucleic acid sensing pathways are also induced by cytosolic RNA helicase such as RIG-I and the melanoma differentiation-associated gene 5 (MDA5), which activate mitochondrial antiviral-signaling (MAVS) and IRF3 upon RNA sensing (d'Angelo et al., 2021).

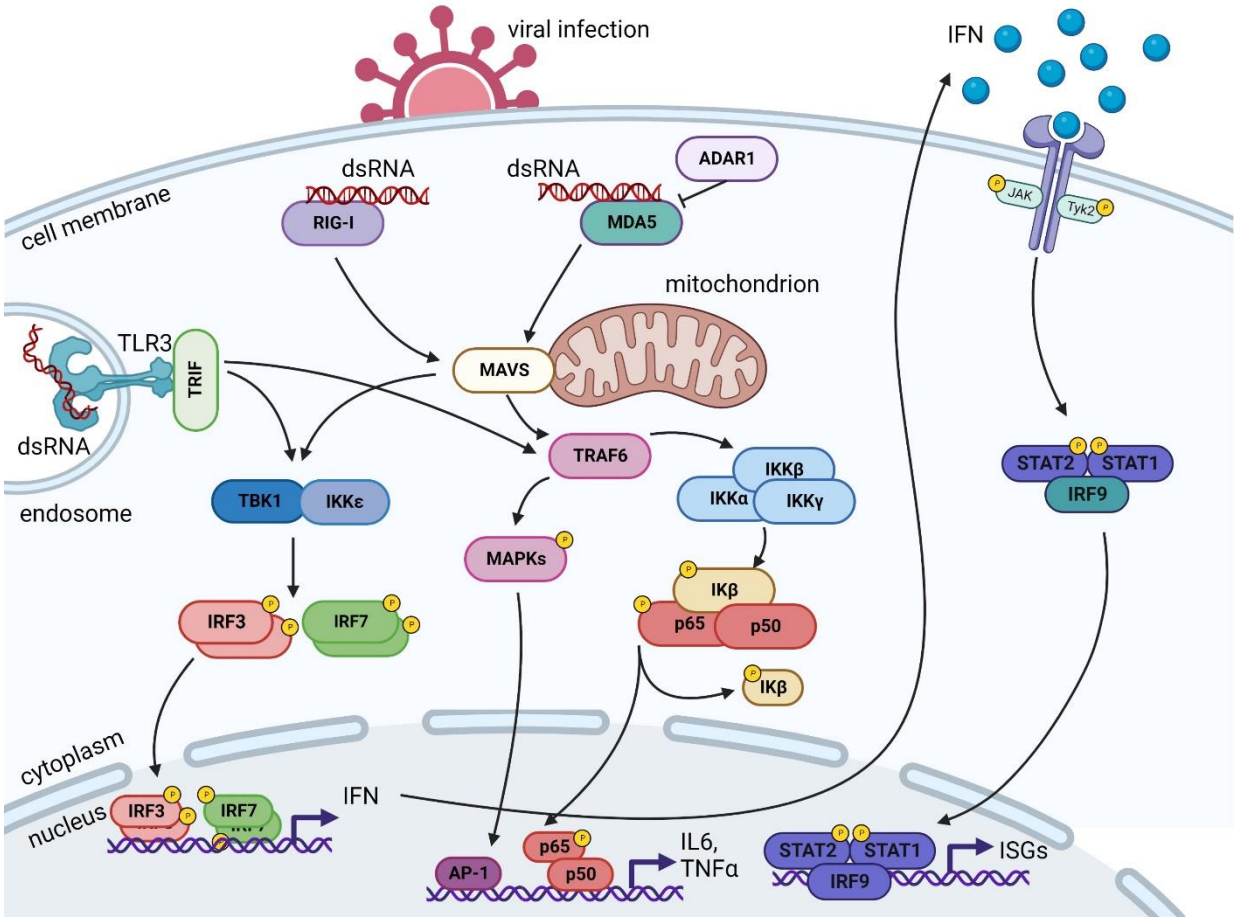

Fig. 13: Simplified inflammatory pathways upon viral infection.
Created with BioRender.com.

1.3.2. Type I interferonopathies

The type I interferonopathies group 13 several autoimmune diseases having in common one or several mutations in the IFN signaling pathway (2017 classification of the International Union of Immunological Societies). Due to these mutations, the organism fails to discriminate between self and non-self nucleic acid, triggering the activation of the nucleic acid sensing pathway by the host RNA/DNA and subsequently the IFN signaling pathway. The patients show high level of type-I IFN in the cerebrospinal fluid (CSF) and serum (d'Angelo et al., 2021).

Aicardi Goutières Syndrome (AGS) was one of the first interferonopathies to be identified. It is a rare disease described as an autoimmune neurological disease where the nervous system is greatly affected. Babies with early-onset AGS, around 20 % of the cases and usually the most severe form, are born with small blood vessels inflammation called chilblains, liver dysfunctions as well as neurological abnormalities.

Babies with a late-onset start showing microcephaly, cognitive and developmental delay after few weeks or months. The AGS infants will develop calcification of the basal-ganglia and cerebellar dentate nuclei, white matter abnormalities, seizures, skin lesion and more symptoms (Abe et al., 2014; Behrendt & Roers, 2013; d'Angelo et al., 2021; G. Rice et al., 2007). The babies suffering the most severe form of AGS, around 40 % of the cases, die in early childhood, while few patients will reach adulthood with severe neurological and physical disabilities (Crow & Rehwinkel, 2009).

AGS is hereditary in an autosomal recessive manner with mutations in genes encoding intracellular nucleic acid degradation enzymes: TREX1, RNASEH2B, RNASEH2C, RNASEH2A, SAMHD1, ADAR1; or in an autosomal dominant manner with a mutation in *IFIH1* coding for MDA5. All the reported mutations lead to a constitutive activation of the IFN response leading to a chronic overproduction of type I IFN (Crow, 2016; G. I. Rice et al., 2014).

Loss-of-function mutations of the 3' → 5' exonuclease TREX1 or of one of the 3 RNAse H2 enzyme subunits (RNASEH2A, RNASEH2B, RNASEH2C) result in an accumulation of the reverse transcription products. This accumulation of endogenous nucleic acid is most likely due to the loss of nuclease activity of these proteins and will then be sensed by the cGAS-STING DNA sensing pathway, inducing a pro-inflammatory response. It is worth noting that the main function of RNAse H2 enzymes is to degrade RNA/DNA hybrid and to keep the genomic stability by removing the ribonucleotides of genomic DNA (Gall et al., 2012; Gray et al., 2015; Hemphill et al., 2021; Stetson et al., 2008b).

Similarly, mutations in the deoxynucleoside triphosphohydrolase SAMHD1 lead to an activation of the cGAS-STING pathway. However, the mechanism of activation of the cGAS-STING pathway is still not fully understood from the currently known SAMHD1 functions. SAMHD1 is also important for the genome integrity by balancing the deoxynucleotide triphosphate (dNTP) pools. In AGS, its loss of function might contribute to an increase of dNTP availability, promoting DNA synthesis (Crow, 2016; Park et al., 2021).

The adenosine deaminase acting on RNA (ADAR1) marks the endogenous double strand RNA (dsRNA) by catalyzing the deamination of adenosine to inosine RNA editing (A-to-I RNA editing). This mechanism prevents the endogenous dsRNA to activate the

inflammatory response (Liddicoat et al., 2015). Although the mechanism inducing IFN response is still unclear, supporting evidences show that loss of ADAR1 induces an accumulation of cytoplasmic dsRNA coming from genomic repetitive elements, specifically the Alu elements which are then recognized by MDA5 and lead to IFNβ production (H. Chung et al., 2018; Nakahama et al., 2021; G. I. Rice et al., 2012). The immunopathology induced by ADAR1 alteration was recently shown to be dependent on ZBP1, with ADAR1 being a negative regulator of ZBP1 (Hubbard et al., 2022; Jiao et al., 2022). Moreover, ADAR1 might play a role in inhibiting the retrotransposition of the retrotransposable element LINE1 by A-to-I RNA editing (Orecchini et al., 2017).

MDA5 senses exogenous viral dsRNA and induces the inflammatory response via MAVS. In AGS, although the mechanism is not clearly known, it has been suggested that gain-of-function mutations of MDA5, such as G821S, A946T, M845K, R822Q and R779H, lead to a lower activation threshold of MDA5 which could induce the RNA sensing pathway by endogenous dsRNA binding (Crow & Manel, 2015; G. I. Rice et al., 2014; Yu et al., 2021).

1.3.2.1. Aicardi Goutières Syndrome therapies

Unfortunately, no cures exist for AGS patients, only symptomatic treatments are used to increase the patient's quality of life. The current approaches for potential therapies target 1) the production of endogenous nucleic acids and specifically the retrotransposable elements, 2) the upstream nuclei acid sensing pathway and 3) the downstream IFN signaling response pathway.

The first approach is based on the hypothesis that the retroelements are accumulating by lack of control from mutated TREX1, SAMHD1 or RNAse H2 enzymes, therefore inhibiting the reverse transcription would prevent their accumulation. Inspired by the HIV reverse transcriptase therapy, a pilot study showed a reduction of IFN signaling in patients treated with reverse transcriptase inhibitors used in HIV patients, such as abacavir, lamivudine and zidovudine. However, no significant neurological improvement was found, which was most likely due to the too advanced disease stage of the patients in the trial (G. I. Rice et al., 2018).

The second approach is to inhibit the nucleic acid sensing pathway. Even though it is not understood mechanistically, antimalarial drugs, such as X6 (J. An et al., 2018),

hydroxychloroquine or quinacrine (J. An et al., 2015), have been shown to inhibit c-GAS. These drugs have actually been used for decades in patients with systemic lupus erythematosus (SLE), one of the 13 interferonopathies (Tonduti et al., 2020).

Another approach is based on immunotherapies targeting the IFN-α/β receptor. This appears to be a more promising approach for inhibition of the inflammatory response. However, these therapies, such anifromulab and sifalimumab, are not yet tested for AGS, but are accepted or in the advanced phase of clinical trials for SLE patients (Greth et al., 2017; Morand et al., 2022; Takeuchi et al., 2020).

The last approach is targeting the IFN signaling pathway, which can be done through immunotherapies or by inhibiting janus kinase (JAK). The latest seems to be the most promising so far: several clinical trials are currently ongoing to assess the efficacy of JAK inhibitors in AGS patients. To cite only few drugs in current trials: Baricitinib which is currently in phase II (Vanderver et al., 2020), Ruxolitinib (Mura et al., 2021) and Tofacitinib (S. Zhang et al., 2021). Among these drugs in trial for AGS patients, two of them, Baricitinib and Tofacitinib, are FDA-approved medications for chronic inflammatory disorder such as rheumatoid arthritis and psoriatic arthritis (Campanaro et al., 2021). Tofacitinib-treated patients show a significant decrease in symptoms compared to placebo-treated patients, however, they did not reach a significantly higher remission rate (Fleischmann et al., 2012). Furthermore, it is worth noting that therapies based of JAK inhibitors have also shown increased risks of major adverse cardiovascular events, malignancies, herpes zoster, bacterial infections and thromboembolism when used against rheumatoid arthritis (Song et al., 2022; Ytterberg et al., 2022).

In summary, currently no therapies are FDA-approved for frontline treatment of AGS patients. Even though the JAK inhibitors seem promising to ameliorates the disease, their efficiency is relative. Even in the context of rheumatoid arthritis disease, which presents milder symptoms than AGS, JAK inhibitors do not induce remission but only ameliorate symptoms. Secondly, the safety of JAK inhibitors is highly discussed as previously detailed. Therefore, there is still a strong urge to find a new treatment, in combination with others or by itself.

1.3.2.2. Aicardi Goutières Syndrome mouse models

Like many disease mouse models, the AGS mouse models are based on mutations found in AGS patients. One of the most common models to study AGS is the TREX1 -/- murine model. The mice have a reduced lifespan of 6 months and die of inflammatory myocarditis. Like AGS patients, they present peripheral immune response and IFN signaling, however, this model does not reproduce the brain inflammation and encephalopathy seen in AGS patients. This autoimmune phenotype triggered by TREX1 -/- is cured by IRF3 knock out, IFNAR KO and Rag2 KO (Behrendt & Roers, 2014; Stetson et al., 2008a).

Another widely studied model is the ADAR1 -/- murine model. This model, which is embryonic lethal (E11.5-E12.5), shows high IFN and ISG expression, but no neuro-inflammation nor CNS phenotypes. ADAR1 p.K999N mouse mutant is the first model showing an asymmetric and sparse inflammation in neurons and microglia, however, no basal ganglia calcification or gliosis were observed in this model. A second hit, such as a viral infection might be required to trigger the other AGS phenotypes (X. Guo et al., 2021).

Loss of RNAse H2 triggers the death of E11.5 embryos. Unlike the ADAR1 -/- mice, the death is due to cell cycle arrest induced by p53-inducible genes activated by genome instability. Importantly, in patients, the activity of the RNAse H2 complex is only reduced but not abrogated: no bi-allelic mutations are reported in any subunits of this complex (Behrendt & Roers, 2014).

In AGS, several gain-of-function mutations in MDA5 lead to a constitutively active IFN signaling due to the lack of exogenous/endogenous RNA binding discrimination. The MDA5 G821S mutation is one of the mutations found in human which has been reproduced into a mouse model (Funabiki et al., 2014; Onizawa et al., 2021). A chronic inflammation was reported in kidneys and liver, as well as a high level of inflammatory cytokines in multiple organs, including the brain. Interestingly, crossing the MDA5 GS mutant with IFNAR -/- mice ameliorated the pathology, suggesting that IFNβ is contributing to the disease, but other cytokines might as well. Also, it is worth noting that MDA5 is constitutively active in this model and cannot be further induced by RNA ligands (Funabiki et al., 2014). The MDA5 G821S also reported spontaneous encephalitis, one of the AGS patient phenotypes (Onizawa et al., 2021).

The existing models are very useful to understand the pathway by which a mutation in RNA sensing genes leads to an activation of inflammation, however, they do not recapitulate all the phenotypes observed in patients such as the neurological disorders. Only the MDA5 GS model indicated a high level of IFNβ transcript in the brain, but no further studies have been reported. It would be crucial to find a model with CNS inflammation leading to neurological disorders to better understand the neurological pathology found in the AGS patients.

1.3.3. Interferon in Alzheimer's Disease

1.3.3.1. Epidemiology and pathology

Alzheimer's disease (AD) is part of the neurodegenerative diseases and is the most common form of dementia, representing about 60-80 % of dementia cases. Worldwide, recent statistics counted about 50 million people having dementia, with 60 % of them living in low- or middle-income country (Ferri & Jacob, 2017; Tiwari et al., 2019). As the population is progressively aging and advanced age is the greatest risk factor for AD and dementia, the disease prevalence is predicted to rapidly increase, reaching more than 131 million of people affected by dementia in 2050 and therefore, making AD a major socio-economical problem (Edwards et al., 2019; Tiwari et al., 2019). The percentage of AD cases increases from 3 % of people aged of 65-74 years-old, to 17 % of people being 75-84, to finally reach 32 % of the population older than 85 years-old ("Alzheimer's Disease Facts and Figures," 2019). Gender seems also to be a preeminent AD risk factor; women represent almost two-third of the AD-diagnosed patients (Podcasy & Epperson, 2016).

Dementia is a clinical syndrome which has been characterized by progressive cognitive decline in memory, language, behavior and personality, which results in an impairment in performing daily-life tasks or activities. AD diagnosis is assessed on living people showing dementia by CSF and positron emission tomography (PET) biomarker analysis, magnetic resonance imaging (MRI) assessing the hippocampal volume, or by post-mortem evaluation of brain tissue (Rabinovici et al., 2019; Weller & Budson, 2018). The hallmark pathological characteristics of AD brains are extracellular amyloid-β plaques

(figure 14), intracellular neurofibrillary tangles (NFTs) in neocortical regions (figure 14), brain inflammation, synaptic impairment and neuronal loss.

Surprisingly, the presence of senile plaques and NFTs can also be found in healthy patients presenting no cognitive impairment (Rabinovici et al., 2019)(figure 14).

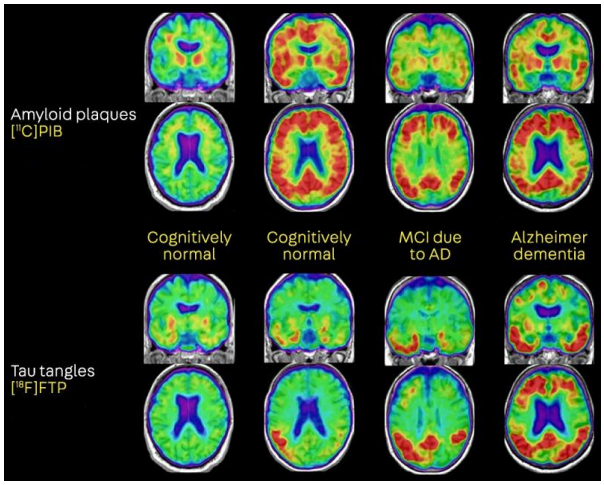

Fig. 14: The presence of amyloid-β and tau revealed by PET is not always associated with Mild Cognitive Impairment or AD.
(Rabinovici et al., 2019)

AD neuropathology appears decades before the clinical onset is assessed. During the preclinical phase, amyloid-β aggregation occurs exponentially and reaches almost the maximal level before any cognitive impairment appears. NFTs formation starts later than amyloid-β deposition and is gradually increasing with the cognitive impairments and neuronal loss. During this mild cognitive impairment (MCI) phase, the patients manifest a memory impairment greater than their age-peers, which will rapidly declines within a few years, until reaching the clinical onset of dementia and being diagnosed as AD patients (Bateman et al., 2012; Caselli & Reiman, 2013; Long & Holtzman, 2019) (figure 15).

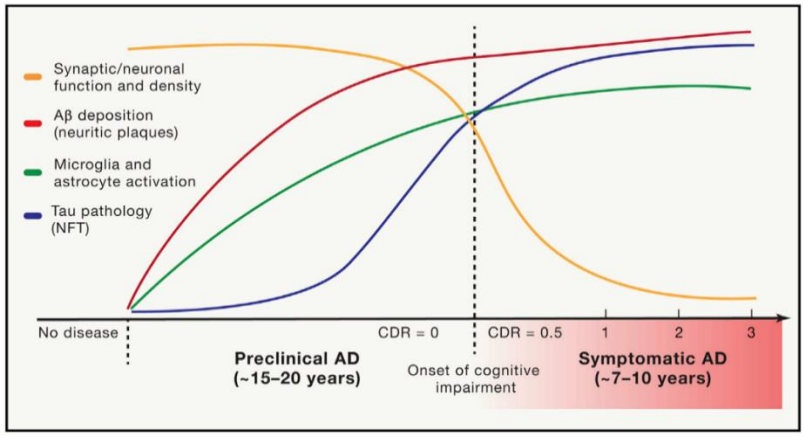

Fig. 15: The evolution of AD disease.
(Long & Holtzman, 2019)

AD patients are divided into two groups, the early onset AD (EOAD) with an onset inferior to 65 years-old and the late onset AD (LOAD) with an onset superior to 65 years-old (Kunkle et al., 2019; Mendez, 2019). EOAD, which represents less than 5 % of the AD cases, is mostly characterized by a genetic predisposition, called Familial Alzheimer's Disease. It follows a more aggressive course than the LOAD (Mendez, 2019). Among AD patients, 1 % present an autosomal dominant mutation on the Amyloid precursor protein (APP), Presenilin-1 (PSEN1) and/or Presenilin-2 (PSEN2) genes, triggering the eventual AD outcome (Guerreiro et al., 2012; Kunkle et al., 2019; Rogaeva, 2002).

The most prevalent AD form, LOAD, mainly affects the aged population in a sporadic manner. The life expectancy is of average from 4 to 8 years after LOAD onset ("Alzheimer's Disease Facts and Figures," 2019). Beyond the environmental and acquired risk factors, such as cerebrovascular diseases, hypertension and obesity, the genetic risk factors in AD were discovered by Genome Wide Association Studies (GWAS) (Grupe et al., 2007; Guerreiro et al., 2012; Kunkle et al., 2019; M. V. F. Silva et al., 2019). Allelic and genotypic variants of genes involved in amyloid-β process (*app, psen1, psen2*), cholesterol metabolism (*apoe, clu, abca7*), endocytosis (*bin1, picalm, cd2ap, epha1 and sorl1*) and in unknown pathways (such as *pld3*) have already been identified as prevalent in AD (figure 16), but many others are yet to be discovered (Guerreiro et al., 2012; Karch & Goate, 2015; Kunkle et al., 2019). Interestingly, several risk variants are mainly expressed in microglia, such as *trem2*, *cd33, cr1, ms4a, spi1, inpp5d, plcg2*¸ as well as a*poe* which is more expressed in glial cells than in neurons (K.-L. Huang et al., 2017; Sierksma et al., 2020). This has changed the idea that the

neurons are responsible for AD, and suggests the microglia as also a potential cause of AD. These risks variants are involved in immune response, such as but also a microglia transcription factor, Pu

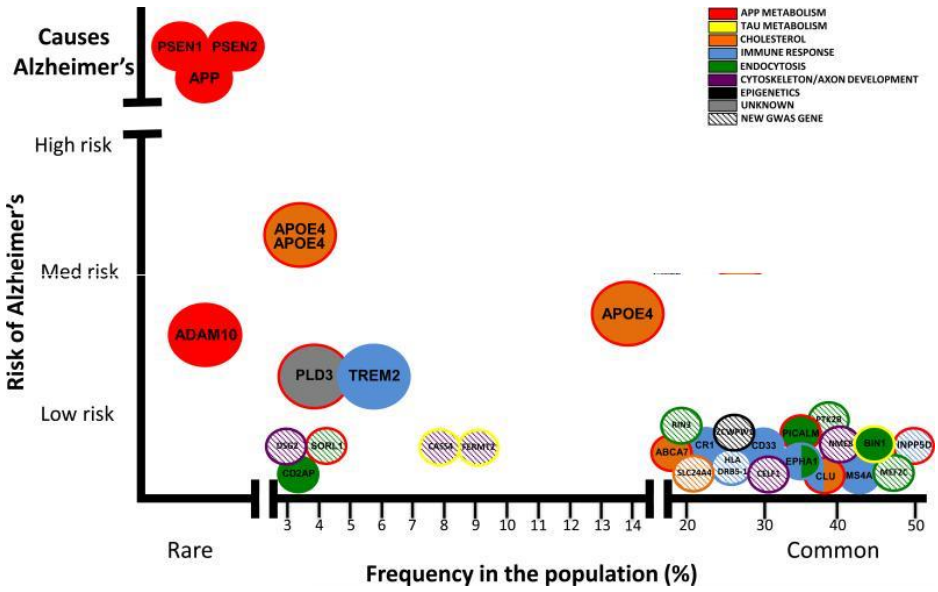

Fig. 16: Genetic risk factors in AD.
(Karch & Goate, 2015)

1.3.3.2. Current therapies and new prospective

One of the main challenges in discovering a cure to AD is that the pathological-brain changes happen decades before the clinical onset. The amyloid-β deposition and Tau pathology are far too extended at the onset of cognitive impairment making it already too late to be cured after diagnosis.

Symptomatic therapies for all AD patients are currently used for improving the MCI either by inhibiting the acetyl cholinesterase or by blocking NMDA receptors to avoid an excess of neuronal stimulation leading to excito-toxicity (“Alzheimer’s Disease Facts and Figures,” 2019; Se Thoe et al., 2021). However, these symptomatic treatments do not stop nor slow the disease progression down.

During the last few years, the research focused on tackling AD at early stage during the preclinical phase. To do so, an early detection of the pathology and the prevention of amyloid-β and Tau deposition are both required. Therefore, reliable AD biomarkers are widely investigated to find a less expensive and less invasive test than the amyloid-β

and Tau PETs, MRI or the detection of amyloid-β level in CSF. Amyloid-β, Tau and neurofilament light in plasma have been shown to be associated with early AD pathology, though the detection method must be very sensitive. Other blood biomarkers have been published; however, the results were often not reproducible (Khoury & Ghossoub, 2019; Rabinovici et al., 2019).

Preventing amyloid-β and Tau deposition is believed to prevent neuronal loss and cognitive impairment. As a results, several strategies (Chen et al., 2017; Tiwari et al., 2019) are being investigated: 1) inhibiting the oligomerization by using small molecules inhibitors, by blocking amyloid channels, or by overexpressing amyloid-β-degrading enzymes, 2) degrading the aggregates by immunotherapies or using β-sheets breakers, 3) Tau-directed therapies.

Unfortunately, most of the clinical trials failed because of unfavorable pharmacodynamics and pharmacokinetics (L. K. Huang et al., 2020; Tiwari et al., 2019), however, a recent hope for MCI AD patients has emerged with the accelerated Food and Drug Administration (FDA) approval of ADUHELM in June 2021.

Aducanumab is a recombinant human monoclonal antibody targeting soluble and insoluble amyloid-β oligomers present in ADUHELM. The clinical trials have shown that AD patients presenting MCI have a reduction of amyloid-β load by PET scan upon treatment with ADUHELM (figure 17), which led to the fast FDA approval. However, it is important to keep in mind that the cognitive impairment has still to be assessed (Cummings et al., 2021; fda & cder, 2021; Sevigny et al., 2016).

In parallel, recent advances in nanoparticle research give a new promising approach for an AD therapy, as nanoparticles would allow the drugs to penetrate the blood brain barrier and prevent their degradation.

Lastly, anti-neuroinflammation therapy has been extensively investigated in the last years, since the neuronal death is correlated to neuroinflammation (X. Huang, 2020).

A

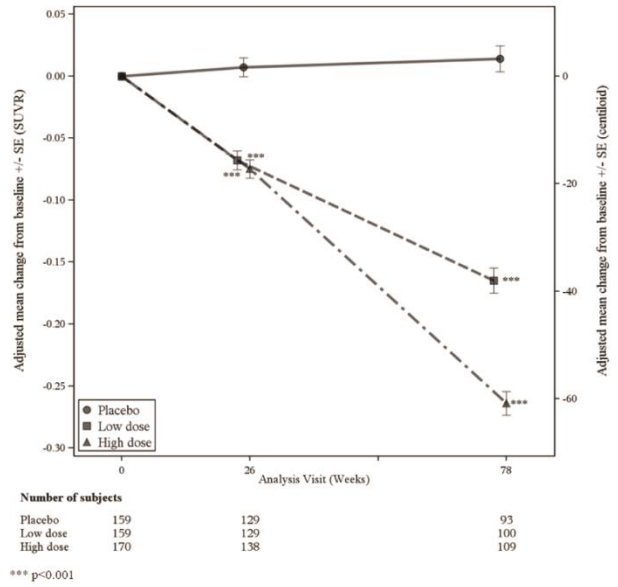

Number of subjects			
Placebo	159	129	93
Low dose	159	129	100
High dose	170	138	109

*** p<0.001

B

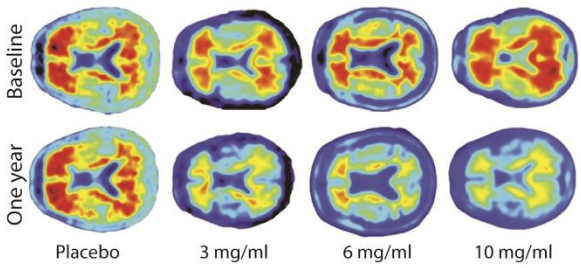

C

Biomarker Endpoint at Week 78[1]	ADUHELM High dose	Placebo
Amyloid Beta PET Composite SUVR	N=170	N=159
Mean baseline	1.383	1.375
Change from baseline	-0.264	0.014
Difference from placebo	-0.278, p<0.0001	
Amyloid Beta PET Centiloid	N=170	N=159
Mean baseline	85.3	83.5
Change from baseline (%)	-60.8 (-71%)	3.4
Difference from placebo	-64.2, p<0.0001	
CSF p-Tau (pg/mL)	N=17	N=28
Mean baseline	100.11	72.55
Change from baseline	-22.93	-0.49
Difference from placebo	-22.44, p=0.0005	
CSF t-Tau (pg/mL)	N=17	N=28
Mean baseline	686.65	484.00
Change from baseline	-112.44	-0.39
Difference from placebo	-112.05, p=0.0088	

[1]P-values were not statistically controlled for multiple comparisons.

Fig. 17: Amyloid beta load by PET in AD patients treated with placebo, low dose or high dose of ADUHELM (study 1 of the clinical trials of ADUHELM) (A).
PET scan of AD patients treated with placebo or Aducanumab (B). Biomarker results of AD patients treated with placebo and high dose of ADUHELM (study 1 of the clinical trials of ADUHELM), (adapted from fda & cder, 2021 and Sevigny et al., 2016).

1.4. Arsenic trioxide against diseases

Arsenic is a non-toxic natural element mostly present in the Earth's crust. Small quantities exist in water and rocks at the surface of Earth and once in presence of oxygen, the arsenic is oxidized and turns into highly toxic arsenic trioxide (ATO). A high exposure to ATO, most commonly coming from water and food, can trigger skin lesions, organ damage, respiratory disorders and cancer. It was even used as poison in the 17th – 19th century (Medda et al., 2021; Sanyal et al., 2020). Nonetheless, arsenic derivatives have been used for hundreds of years already in Chinese medicine with the principle of "attacking the poison with poison" and it is only a few decades ago that the western medicine started to use ATO as a treatment (Au, 2011).

1.4.1. Arsenic trioxide against cancer

1.4.1.1. Arsenic trioxide in Acute Promyelocytic Leukemia

In 2001, Trisenox®, the injectable form of ATO was approved by the FDA for treating APL patients relapsing and failing to respond to standard therapy. ATO triggers, on one hand, the degradation of the PML/RARα complex via PML oxidation and the 11S proteasome recruitment, therefore de-repressing the differentiation. On the other hand, ATO enhances the formation of new PML-NBs from the non-rearranged *pml* allele. These newly synthetized and functional PML-NBs are able to recruit and post-translationally modify PML-NBs partners. Among others, the activation of p53 will lead to the apoptosis of APL cells.

In 2018, the FDA extended the use of ATO in combination with all-trans retinoic acid (ATRA), a vitamin A derivative, for treating newly diagnosed APL patients. ATRA in itself allows for a 70 % remission rate in patients through its two mechanisms of action. The first being that ATRA binds the RARα moiety of the PML/RARα chimeric protein, which reactivates of the transcription of the RA-induced genes and hence allows the myelocytic differentiation (Figure 18). The second is that ATRA treatment results in the degradation of the PML/RARα complex, lifting the PML-RARα transcriptional repression and therefore induces differentiation, leading to a transient remission in patients (de Thé et al., 2012; de Thé & Chen, 2010; Jeanne et al., 2010; Thomas, 2019).

When combined, ATRA and ATO re-activate and de-repress the genes involved in differentiation, while ATO leads to the apoptosis of the APL cells. The combined ATRA

and ATO therapy gets rid of the undifferentiated cancerous cells by senescence or differentiation initiation, turning APL from a severe and fatal disease into the most curable subtype of adult acute leukemia with a complete remission rate of 90 % in APL patients (de Thé et al., 2012; Hu et al., 2009; Stahl & Tallman, 2019; Thomas, 2019; Z.-Y. Wang & Chen, 2008).

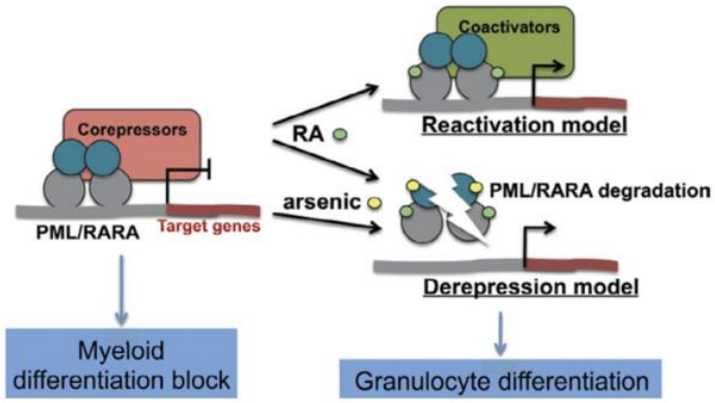

Fig. 18: ATO and ATRA, two drugs efficiently targeting the PML-RARA complex. (de Thé et al., 2012)

1.4.1.2. Arsenic trioxide against peripheral solid tumors

After seeing the beneficial effects in APL, ATO has been investigated in other peripheral cancers from which several mechanisms of action have been discovered. In models of cervical cancer, prostate cancer, lung cancer, pancreatic cancer and breast cancer, ATO induces caspase3/9-dependent cell apoptosis via high oxidative stress (AM et al., 2016; Chow et al., 2004; Hoonjan et al., 2018). In liver cancer, breast cancer, nasopharyngeal cancer and ovarian cancer, ATO induces a cell cycle arrest in G2/M or in S-phase also resulting in apoptosis (Hoonjan et al., 2018; Y. Yang et al., 2012; N. Zhang et al., 2009). Unlike in the previously mentioned cancers, ATO leads to a reduction of the tumor size in gastric cancer by impeding the tumor vascularization via an inhibition of the vascoendothelial growth factor protein expression (Xiao et al., 2006).

The promising results obtained *in vitro* or in cancer models were unfortunately not reproduced in clinical trials. Several clinical trials using ATO in patients having peripheral solid tumors, such as liver cancer, breast cancer, colon cancer and few others, did not reveal significant improvement of the disease (Fang & Zhang, 2020; Kindler et al., 2008). Eventually, the key of using ATO in cancer might be the combined treatment with

chemotherapy and/or radiotherapy, as done in APL patients combining ATO and ATRA treatments.

1.4.1.3. Arsenic trioxide against CNS cancer

In CNS, ATO effects have been widely investigated in glioma models. In addition to the previously described apoptosis and cell cycle arrest, ATO was shown to induce autophagy, oxidative damages and inhibition of tumor stem cells. Most importantly, ATO was recommended to be used in addition of chemotherapy and radiotherapy leading to synergy (Fang & Zhang, 2020). In glioblastoma cell lines, ATO-induced cell death was reduced in PML KO cells, suggesting a crucial role of PML in the apoptosis induced by ATO (Amodeo et al., 2017).

However, an additional obstacle to keep in mind when dealing with the CNS, is the ability, or lack thereof, of the drug to cross the blood brain barrier (BBB). In a study on APL patients having cancer relapses in the CNS, the ATO concentration in the CSF was 17,7 % of the one measured in blood plasma. It is worth noting that ATO was administered orally to patients. This result indicates that only a small proportion of ATO is able to cross the BBB (Au et al., 2008). However, by coupling ATO to mannitol, which has been shown to transiently open the BBB, the level of ATO in the CSF reached a similar concentration as in the blood plasma. In this study, no control patients with only ATO were reported. Mannitol and ATO were both injected intravenously (Rapoport, 2000; H. Wang et al., 2014). In addition to mannitol, the permeability of ATO through the BBB could also be improved with the use of nano-carriers (Fang & Zhang, 2020).

1.4.2. Arsenic trioxide against autoimmune diseases

In autoimmune or immune-related diseases, ATO's main function is to induce the death of the cells responsible for the inflammation.

In multiple sclerosis, ATO has been shown to induce mitochondria-dependent apoptosis of the CD4+ T cells, which have a major role in the disease. The CD4+ T cells infiltrate in the brain and initiate the inflammatory response which in turn induces demyelination. Therefore, by inducing the apoptosis of the CD4+ T cells, ATO reduces the microglia

activation, the inflammatory cytokine expression levels and overall, delays the disease onset and decreases the severity of the disease (K. An et al., 2020).

Similarly, ATO reduces the inflammation in graft-versus host disease by inducing T cell apoptosis and therefore lowering both cytokine synthesis and secretion (Gao et al., 2015; C. Li et al., 2015).

ATO was suggested as treatment in autoimmune diseases with type-I IFN signature in systemic sclerosis patients. As such, in plasmacytoid dendritic cells, low concentrations of ATO (1 μmol/L) inhibit the phosphorylation of IRF7 and the IFN-α release, but not of the other cytokines. However, a high concentration of ATO (5 μmol/L), induces apoptosis of CpG-A induced plasmacytoid dendritic cells via the mitochondrial pathway, but independently of ROS formation (Ye et al., 2020).

In APL cells, ATO inhibits NF-κB activation and leads to apoptosis by down-regulating the NF-κB-induced anti-apoptotic proteins (Kerbauy et al., 2005; Mathieu & Besançon, 2006).

1.5. Hypothesis and impact of the thesis

Neuroinflammation plays a key role in interferonopathies and neurodegenerative diseases, such as AD (Guzman-Martinez et al., 2019; Kwon & Koh, 2020; Leng & Edison, 2021). Tackling neuroinflammation is thus a recent, interesting and promising angle of research to cure or slow down neurological diseases.

PML plays an important role in inflammation: it was shown to be induced by IFNs (Chelbi-Alix et al., 1995; Regad & Chelbi-Alix, 2001; Stadler et al., 1995) and more importantly to be required for inducing peripheral immune response upon viral and bacteria-like infection (el Bougrini et al., 2011; Lunardi et al., 2011; Regad et al., 2001; Regad & Chelbi-Alix, 2001; Scherer & Stamminger, 2016). However, the role of PML in immune cells of the brain is mostly unknown. This thesis therefore focuses on the role of PML in microglia at steady state and in IFN-related neuro-inflammation, as well as the effect of ATO, a FDA-approved drug degrading PML, against IFN-mediated neuro-inflammation.

In the first part, the effects of PML deletion in microglia on microglia and brain function are described using a newly created murine line. Phenotypes and brain function were assessed at steady states. Furthermore, preliminary results on PML role in bacteria-like induced inflammation are presented.

In the second part, we hypothesized that PML, being an ISG, is induced in microglia in IFN-related inflammatory models. We thus studied PML upon pI:C stimulation and in interferonopathy models. Furthermore, ATO was shown to degrade PML (Lallemand-Breitenbach et al., 2008; Maroui et al., 2012a; Nisole et al., 2013) and to lower peripheral inflammation in several models (K. An et al., 2020; Gao et al., 2015; Kerbauy et al., 2005; C. Li et al., 2015; Mathieu & Besançon, 2006; Ye et al., 2020), we therefore investigated the effects of PML KO as well as ATO in IFN-mediated neuro-inflammation. To do so, pI:C stimulated mice and interferonopathy murine model were pretreated with ATO and analyzed.

The third part presents preliminary data about PML in AD. IFN response was shown to be induced in microglia surrounding amyloid-β plaques as the latest contain nucleic acids in AD murine model (Roy et al., 2020). Our aim was to determine whether PML is induced in plaque-associated microglia and, if so, to investigate the functions of PML in AD microglia. In this regard, we first described PML levels in human brains from AD patients and in the APP/PS1 model, a murine AD model presenting amyloid-β deposit, glial inflammation but no NFTs. Furthermore, in order to analyze PML function in microglia in AD, we created a new murine model in which PML is deleted from microglia in the APP/PS1 background.

This thesis represents the first study addressing the function of PML in microglia at steady state but also upon interferon-related inflammation and in neurodegenerative diseases, such as AD. It also demonstrates a new role of ATO against neuroinflammation. Altogether, this thesis, through the study of PML in microglia, presents the potential of ATO as an anti-neuroinflammatory drug.

2. Materials & Methods

2.1. Reagents

Tab. 1: Reagents list

Product	Catalogue number Provider	Applications
Methoxy-X04	4920 Tocris	Immunofluorescence
TrueBlack® Lipofuscin Autofluorescence Quencher	23007 Biotium	Immunofluorescence
Hoescht	H1399 ThermoFisher Scientific	Immunofluorescence
REDExtract-N-AmpTM Tissue PCR Kit	R4775 Sigma Aldrich	DNA extraction Genotype
DreamTaq Green PCR Master Mix	K1082 ThermoFisher Scientific	Genotype
LPS (Lipopolysaccharides)	L6143-1MG Sigma Aldrich	*In vivo* / *in vitro* treatment
Poly I:C	P1530 Sigma Aldrich	*In vivo* / *in vitro* treatment
Arsenic Standard for AAS	39436-250ml Sigma Aldrich	*In vivo* / *in vitro* treatment
Adult Brain Dissociation Kit, mouse and rat	130-107-677 Myltenyi Biotech	Microglia isolation
Myelin Removal beads	130-096-733 Myltenyi Biotech	Microglia isolation
Cd11b microbeads	130-093-634 Myltenyi Biotech	Microglia isolation
Mouse TNFα ELISA set II	558534 BD OptEIA™	ELISA
Mouse IFNγ ELISA set	555138 BD OptEIA™	ELISA
Mouse IL-10 DuoSet®	DY417 R&D system	ELISA
Mouse IFNβ DuoSet®	DY8234 R&D system	ELISA
Mouse CXCL10/IP-10/CGR-2 DuoSet®	DY466 R&D system	ELISA
Mouse IL-6 DuoSet®	DY406 R&D system	ELISA
VeriKine™ Mouse IFNβ ELISA	42400-1 PBL Assay science	ELISA on serum
Human Aβ42 Ultrasensitive ELISA Kit	KHB3544 Invitrogen	ELISA on brain extract
TMB Substrate Reagent set	555214 BD OptEIA™	ELISA
STOP solution	DY994 R&D system	ELISA

cOmplete™ EDTA-free Protease Inhibitor Cocktail	11873580001 Roche	Protein extraction
PhosSTOP™	4906837001 Roche	Protein extraction
Pierce BCA assay	23225 Pierce	Protein extraction
4x Laemmli Sample Buffer	1610747 Biorad	Protein extraction
4-15 % Mini-PROTEAN® TGX™ Precast protein Gel	4561083 Biorad	Western Blot
Trans-Blot Turbo Mini 0.2 µm Nitrocellulose Membrane	1704158 Biorad	Western Blot
Pierce BCA assay	23225 Pierce	Protein extraction
Amersham ECL Prime Western Blotting Detection Reagent	RPN2232 Cytiva	Western Blot
RNeasy® Plus Mini Kit	74134 Quiagen	RNA isolation
High-Capacity cDNA Reverse Transcription Kit	4368814 Applied Biosystem	cDNA synthesis
Fast SYBR™ Green Master Mix	4385610 Applied Biosystem	qPCR
SMARTer Stranded Total RNA-seq kit v2 & v3 - Pico Input Mammalian	634413 & 634487 Takara Bio	RNA seq library preparation
FD Rapid GolgiStain™ Kit	PK401A FD Neurotechnologies	Golgi staining

Tab. 2: Antibodies list.

Antibody (anti-)	Catalogue number Provider	Applications
Ms-PML	05-718 SCBT	IF 1:200 WB 1:500
Hu-PML H238	sc-5621 SCBT	IF 1:100
Iba-1	234 008 Synaptic system	IF 1:500
NeuN	ab177487 Abcam	IF 1:1000
GFAP	ab4674 Abcam	IF 1:500
CD68	MCA1957 Biorad	IF 1:300
Pu.1	MA5-15064 Invitrogen	IF 1:300
Ms-DAXX	sc-7152 SCBT	IF 1:200 WB 1:500
Amyloid-β, 6E10	SIG-39300 Covance	IF 1:1000
p-STAT1	9167S CST	WB 1:500
STAT1	9172S CST	WB 1:500
p-MAPK P38	9211S CST	WB 1:500
MAPK P38	9212S CST	WB 1:500

p-S6	9234BC CST	WB 1:1000
S6	2317S CST	WB 1:1000
β-actin	A5541 Sigma-Aldrich	WB 1:2000
α-tubulin	62204 Thermo Fisher	WB 1:2000
p-TBK1	5483S CST	WB 1:500
TBK1	sc-73115 SCBT	WB 1:500
SUMO2/3	ab3742 Abcam	WB 1:200
SUMO2/3	4971S CST	IF 1:500
Cleaved caspase-3	9661S CST	IF 1:200
NF-κB p65	8242S CST	IF 1:500
Ki67	ab16667 Abcam	IF 1:300

2.2. Human tissue samples

Human samples were provided by the Netherlands Brain Bank under the project 1292, “The role of histone chaperones and associated proteins in neurodegenerative diseases”. The samples were provided fixed and embedded in paraffin.

2.3. Animal models & genotyping

All the mice were housed in individually ventilated cages under standard conditions (22 °C, a 12-hour light/dark cycle and free access to water and food). The animal research institute DZNE was responsible of the animal care and the experiments were approved by the LANUV, the governmental ethical committee (AZ 81-02.04.2018.A259, AZ 84-02.04.2015.A218, AZ 81-02.04.2019.A462).

- Animal models

The deletion of PML in microglia was achieved by using the LoxP/cre system. PML fl/fl mice were derived from Taconic Artemis in a C57BL/6NTac background. Briefly, *pml* exon3 is floxed by two LoxP sequences and can be cut off by a Cre, which leads to a deletion of PML in cre-expressing cells (figure 19).

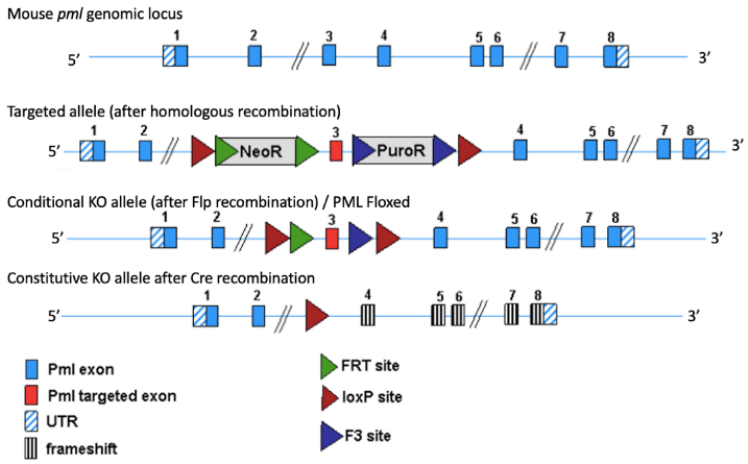

Fig. 19: Cartoon of PML conditional locus before and after recombination.

In this study, we used the Csf1r-cre, standing for Colony Stimulating Factor 1 Receptor, which is specifically expressed in pre-dendritic cells, conventional dendritic cells, plasmacytoid dendritic cells, monocytes, macrophages and microglia. The deletion of PML therefore occurs in the previously mentioned cell types as early as the Cre expression starts. In microglia, PML is deleted at embryonic day E8.5 (Wieghofer and Prinz, 2016).

The APP/PS1 line (B6.Cg-Tg(APPswe,PSEN1dE9)85Dbo/Mmjax, JAX034832) was purchased from the Jackson Laboratory. This model is one of the most commonly used mouse models for studying the mechanisms and neuropathology of AD and for investigating treatment options. This model mimics one of the major phenotypes in Alzheimer patients: the presence of beta amyloid plaques. This mouse line carries the Swedish mutation in the app gene and expresses a chimeric mouse/human amyloid precursor protein as well as the mutant human protein prenisilin 1 (PS1-dE9). Both mutations lead to an overproduction of the amyloid-β peptide and, as a result, to the formation of amyloid-β plaques.

- Genotyping

To genotype the mice, the DNA was extracted from the mouse ear snips using the REDExtract-N-Amp^{TM} Tissue PCR Kit. Briefly, the ear snips were incubated in 40 µl of extraction solution +10 µl of Tissue Preparation solution for 20 minutes at 50 °C, followed

by 5 minutes at 95 °C. Then, 50 µl of Neutralization buffer B was added to stop the reaction. The genotype was carried out as described in the table 3. The primers used for PCR are listed in table 4.

Tab. 3: List of genes genotyped with their PCR mix and program details.

Gene of interest	**PCR mix**	**PCR program**	**PCR product (base pairs)**
PML floxed	- 10 µl DreamTaq Green PCR Master Mix - 1 µl Primer PML F Fw - 1 µl Primer PML F Rev - 7 µl dH_2O - 1 µl of extracted DNA	- 95 °C, 5 min - 94 °C, 30 sec - 60 °C, 30 sec - 72 °C, 1 min - GOTO 2, 35x - 72 °C, 10 min - 4 °C, ∞	Wt: 170 Floxed allele: 289
PML recombination	- 10 µl DreamTaq Green PCR Master Mix - 1 µl Primer PML recombination Fw - 1 µl Primer PML recombination Rev - 7 µl dH_2O - 1 µl of extracted DNA	- 95 °C, 5 min - 95 °C, 30 sec - 60 °C, 30 sec - 72 °C, 90 sec - GOTO 2, 40x - 72 °C, 10 min - 4 °C, ∞	wt/wt ≈ 1,400 Fl/Fl ≈ 1,500 Recombined ≈ 300
Csf1r cre	- 10 µl REDExtract-N-Amp PCR Reaction Mix - 1 µl Primer Cre- Int control Fw - 1 -µl Primer Cre-Int control Rev - 1 µl Primer Csf1r Fw - 1 µl Primer Csf1r Rev - 5 µl dH_2O - 1 µl of extracted DNA	- 94 °C, 3 min - 94 °C, 30 sec - 57.1 °C, 45 sec - 72 °C, 1 min - GOTO 2, 35x - 72 °C, 10 min - 4 °C, ∞	Int ctrl: 324 Cre: 236
APP/PS1 tg	- 10 µl DreamTaq Green PCR Master Mix - 1 µl Primer APP/PS1 Fw - 1 µl Primer APP/PS1 Rev - 7 µl dH_2O - 1 µl of extracted DNA	- 95 °C, 10 min - 94 °C, 30 sec - 54 °C, 1 min - 72 °C, 1 min - GOTO 2, 34x - 72 °C, 5 min - 4 °C, ∞	Int ctrl: 324 Tg: 608
Synapsin cre, Cx3cr1 cre-ERT2, L(7)-Pcp2 cre	- 10 µl DreamTaq Green PCR Master Mix - 1 µl Primer Cre- Int control Fw - 1 µl Primer Cre-Int control Rev - 1 µl Primer Cre Fw - 1 µl Primer Cre Rev - 5 µl dH_2O - 1 µl of extracted DNA	- 94 °C, 3 min - 94 °C, 30 sec - 54.2 °C, 1 min - 72 °C, 1 min - GOTO 2, 34x - 72 °C, 2 min - 4 °C, ∞	Int ctrl: 324 Cre: 100

Tab. 4: List of primers for genotype PCR

Primers	Sequence
PML F Fw	TTG GCA TCA GCC TTC TAT GC
PML F Rev	AAG GAG GCT CTA GGA CCT AGA GG
PML recombination Fw	CAA AGC CAC ACC ATA CTC ATC C
PML recombination Rev	AAG GAG GCT CTA GGA CCT AGA GG
Csf1r Fw	AGA TGC CAG GAC ATC AGG AAC CTG
Csf1r Rev	ATC AGC CAC ACC AGA CAC AGA GAT C
Cre-Internal control Fw	CTA GGC CAC AGA ATT GAA AGA TCT
Cre-Internal control Rev	GTA GGT GGA AAT TCT AGC ATC ATCC
APP/PS1 Fw	AAT AGA GAA CGG CAG GAG CA
APP/PS1 Rev	GCC ATG AGG GCA CTA ATC AT
Cre Fw	GCG GTC TGG CAG TAA AAA CTA TC
Cre Rv	GTG AAA CAG CAT TGC TGT CAC TT

2.4. *In vivo* ATO+pI:C treatment

The effect of ATO on the response to IFN-induced inflammation was studied upon Polyinosinic-polycytidylic acid (pI:C), a synthetic analogue of double stranded RNA. Wt mice or the Knock-out (KO) group (PML F/F, Csf1r cre/+) and its control group (PML wt/wt, Csf1r cre/+) were injected by i.p. with either PBS or 2.5 µg/g of ATO and sacrificed 24 hours later; or with 300 µg of pI:C dissolved in PBS at a concentration of 5 mg/ml, or with 2.5 µg/g of ATO and 24 hours later with 300 µg of pI:C. Mice were sacrificed by CO_2 asphyxia for organ and blood collection 5 or 12 hours after pI:C treatment.

2.5. *In vivo* ATO treatment of the MDA5 RQ mice

The effect of ATO in the interferonopathy model MDA5 R822Q was investigated by daily i.p. injection of 2.5 µg/g of ATO, for 6 days in MDA5 R822Q mice and their control wt mice in the Haus fur Experimentelle Therapie, UKB, by Burcu Sivri. Body temperature and weight were monitored daily by Burcu Sivri. Mice were sacrificed one day after the last injection for organ collection. Genotyping of the MDA5 R822Q mice was performed by Burcu Sivri.

2.6. Behavioral tests

To assess their locomotion, anxiety and memory, 3 month-old wt and PML KO mice were subjected to a panel of behavioral tests, as described below:

Open field: the mice were placed in a 25-cm-wide box which is divided into a central and a peripheral zone. The distance and movement of the animal within the zones were automatically recorded to assess the fear vs. exploratory behavior (Walsh & Cummins, 1976).

Elevated plus maze: the mice were placed for 5 minutes on a 1-meter-high platform composed of 4 arms of which 2 have walls, called the closed arms, and 2 arms have no walls, the open arms. The time spent on the closed arms was calculated and was related to anxiety (Lister, 1987).

Rotarod: the mice were place on a rotating rod for 5 minutes four times per day for 4 days with one hour of rest between each trial. The speed of the rod increased with time from 4 to 40 rpm. The time spent on the rod until fall was recorded (Jones & Roberts, 1968).

Object location memory: the mice were placed in a 25-cm-wide box for 20 minutes for 3 consecutive days. On the fourth day, two different objects were placed in the box in opposite corners, the mice had 20 minutes to familiarize with the objects before returning back in their cage. 90 minutes later, the mice were reintroduced in the box in which one of the object was changed of location. The mice were recorded for 6 minutes and the discrimination index, expressing the exploration time of the newly located object, was calculated as follow : $DI= ((t_{novel} - t_{familiar}) / (t_{novel} - t_{familiar}))*100$ (Vogel-Ciernia et al., 2013).

Water maze: the mice were placed in a 1.5-meter-diameter pool filled with opaque water at 24 °C. For 7 consecutive days, the mice attempted to reach an escape platform placed one cm below the surface of the water. The starting point was changed daily, while the platform stayed unmoved. The time needed to reach the platform was recorded for each trial, and the trial was terminated after 60 seconds when the platform was not found (Hodges, 1996).

2.7. Primary microglia cell culture

Primary microglia were cultured for *in vitro* assays. Briefly, P0-P3 day-old pups were decapitated and the brain was harvested in ice-cold PBS. The meninges were carefully removed to prevent the culture contamination with fibroblasts. Each brain was then manually disrupted by a P1000 pipette in Dulbecco's Modified Eagle Medium (DMEM) complemented with 20 % FBS and 1 % penicillin/streptomycin (mgMedia). The brain

lysate was passed through a 70 µm cell strainer. Then, the obtained cell suspensions were spun down at 700 x g for 5 minutes, resuspended in 10 ml and placed in a poly-L-lysine coated T25 cm^2 flask. The following day and every second day, half of the media was replaced with fresh mgMedia supplemented with 10 % L929 supernatant. After 7-10 days, the co-culture was ready to be used: the microglia are sitting on top of an astrocyte layers and can be easy detached by “shaking” the flask and re-plated for further experiments.

2.8. Primary bone marrow derived macrophages (BMDM) culture

Hind legs were collected from 3 month-old mice. The bone marrow was flushed from the tibiae and femurs and passed through a 70 µm cell strainer. 14.10^6 were plated per 150 mm non-treated dishes into DMEM (11960, Gibco) supplemented with 10 % FBS, 1 % penicillin/streptomycin, 1 x Glutamax (35050061, Gibco) and 20 % of freshly added L929 supernatant. At day 4, half of the media was renewed. At day 6, the cells were detached with the Cell dissociation buffer (13151-014, Gibco) and re-plated for further experiments.

2.9. Cell lines

The immortalized murine microglia cell line, BV2, was purchased from ATCC (CRL-2469™). The BV2 cells were cultured at 37 °C, 5 % CO_2, 90 % of humidity in DMEM (30-2002, ATCC) supplemented with 10 % FSB, 1 % penicillin/streptomycin and 20 % of freshly added LADMAC Conditioned Media. Once reaching 80 % of confluency, i.e. every 5-7 days, the BV2 were subcultivated at a ratio 1:2 or 1:4. In the meantime, the media was renewed every 2-3 days.

The LADMAC cell line was purchased from ATCC (CRL-2024™) and was used to produce the conditioned media necessary to the BV2 culture. The LADMAC cells were cultured at 37 °C, 5 % CO_2, 90 % of humidity in Eagle's minimum essential medium (EMEM) (30-2003, ATCC) supplemented with 10 % FSB and 1 % penicillin/streptomycin. The conditioned media was produced as follow: 0.5 million (Mio) LADMAC cells were plated in T175 cm^2 flasks; after 7 days, the supernatant was filtered at 0.2 µm and stored at -20 °C. This conditioned media contained growth factors secreted by the LADMAC cells which supports the proliferation of the BV2 cells.

The L929 cell line was used for producing the L929 Supernatant necessary for primary microglia and BMDM culture. The L929 cells were cultured at 37 °C, 5 % CO_2, 90 % of humidity in DMEM (D5671, Sigma-Aldrich) supplemented with 10 % FSB, 1 % HEPES, 1x Glutamax (35050061, Gibco) and 1 % penicillin/streptomycin. The L929 supernatant was produced as follow: 0.47 Mio LADMAC cells were plated in 54 ml of complete medium T175 cm^2 flasks; after 7 days, the supernatant was filtered at 0.2 µm and stored at -20 °C.

The human HL60 is a cell line derived from peripheral blood lymphocytes isolated from a woman suffering from APL. The HL60 cells were cultured at 37 °C, 5 % CO_2, 90 % of humidity in RPMI 1640 (31870-025, Gibco) supplemented with 2mM Glutamine, 10 % FBS and 1 % penicillin/streptomycin. As the cells may start to differentiate after 6 weeks of culture, the cells were not kept more than 2 weeks in culture. The cell density was maintained between 0.1 and 1 Mio cells.

2.10. *In vitro* treatment

BMDMs, primary microglia and BV2 were pretreated with 2.5 µM of ATO for 24 hours followed by a stimulation of 150 µg/ml pI:C for 6 h. Supernatant was collected, spun down for 3 minutes at 1200 rpm and stored at -80 °C for cytokines quantification by ELISA. Cells were harvested for RNA isolation or protein extraction as described below.

2.11. Microglia isolation from adult mouse brains

Microglia were isolated from murine brains using the Adult Brain Dissociation Kit from Miltenyi Biotech (Bergisch Galdbach, Germany) in accordance to the manufacturer's guidelines. Briefly, brains were freshly isolated and mechanically and enzymatically digested at 37 °C in the gentleMACS™ Dissociator with Heaters. The brain lysates were passed through a 70 µm cell strainer and cleared out of red blood cells. The cell suspensions obtained by sucrose gradient were then incubated with CD11b MicroBeads (Miltenyi Biotech) for 15 minutes at 4 °C followed by a separation in MS columns (Miltenyi Biotech) using a magnetic field on a MACS MultiStand and QuadroMACS (Miltenyi Biotech). The microglia population isolated was then processed for further analysis, such as RNA isolation or protein extraction.

2.12. Immunofluorescence on cells

Cells plated on poly-L-lysine coated coverslips were washed 2 times with cold PBS and fixed for 8 minutes with 4 % PFA at room temperature. The coverslips were washed and incubated for 1 hour in blocking buffer (5 % goat serum in PBS-Tween 0.1 %) at room temperature, followed by an overnight incubation at 4 °C with the primary antibodies diluted in blocking buffer. The following day, the coverslips were incubated at room temperature for 2 hours with the fluorescent secondary antibodies before being counterstained with Hoechst (1:10,000 in dH_2O) for 8 minutes at room temperature. The coverslips were mounted on microscope slides and the staining was imaged using a confocal fluorescent microscope (LSM880, Zeiss).

2.13. Immunofluorescence on frozen-fixed tissues

Freshly isolated brains were washed in PBS and fixed for 20 hours in 4 % PFA at 4°C. After 2 washes in PBS, the brains were dehydrated in 30 % sucrose solution until the brains sunk. The brains were then snap frozen on dry ice and stored at -80 °C. Sections of 30 µm were cut on a Cryostar™ NX70 cryostat and stored in cryosolution (475 mM glucose, 7 mM of $MgCl_2$,$6H_2O$ dissolved in 100 ml of PBS, and supplemented with 100 ml of glycerol). Before staining, the sections were washed 3 times with PBS and an antigen retrieval was performed by incubating the sections in citrate antigen retrieval solution (10 mM citric acid, 0.05 % of Tween-20 in PBS, pH6) for 8 minutes at 95 °C. Once cooled down, the sections were washed with PBS and incubated for 1 hour in blocking buffer (5 % goat serum, 2.5 % of BSA, 0.05 % triton in PBS) supplemented with 0.2 % of Triton-X100. The primary antibody diluted in blocking buffer was incubated on the sections overnight at 4 °C. The following day, the sections were washed in PBS 3 times for 10 minutes, incubated with the secondary antibodies for 2 hours at room temperature, washed 2 more times with PBS and then counterstained with DAPI for 10 minutes. The sections were then carefully placed on microscope slides, dried and mounted with ROTI®Mount Aqua. The staining was imaged using a confocal fluorescent microscope (LSM880, Zeiss).

2.14. Immunofluorescence on paraffin-embedded human brain samples

Paraffin sections of human brain samples were cut at the microtome with a thickness of 6 µm. Before the staining, the deparaffinization was performed: the slides were incubated for 30 minutes at 60 °C in order to melt the paraffin and incubated 2 times for 10 minutes in Xylene. The sections were then rehydrated by consecutive incubation of 2 x 10 minutes in ethanol 100 %, ethanol 90 %, ethanol 70 % and dH_2O. The slides were incubated in citrate Antigen retrieval solution (10 mM citric acid, 0.05 % of Tween-20 in PBS, pH6) for 8 minutes at 95 °C for the antigen retrieval. 1 x True Black® solution was applied for 10 minutes on the sections to quench the Lipofuscin. The sections were then incubated in blocking buffer (5 % goat serum, 0.15 % Triton in PBS) for 1 hour at room temperature, followed by the primary antibody incubation overnight at 4 °C in blocking buffer. On the second day, the secondary supplemented with Methoxy-X04 (10 µM) was applied for 2 hours at room temperature before mounting the sections. The staining was analyzed and imaged using a confocal fluorescent microscope (LSM880, Zeiss).

2.15. Golgi staining of freshly isolated brains

Golgi staining was performed on brains isolated from mice which have performed the panel of behavioral studies (described in 2.7). The staining was performed using the FD Rapid GolgiStain™ Kit according to the manufacturer's guidelines. Briefly, the freshly isolated brains were incubated in impregnation solution for 2 weeks, then in the solution C for 72 hours. Sections of 100 µm were cut on a Cryostar™ NX70 cryostat and mounted on gelatin-coated slides. After drying overnight, the sections were stained, dehydrated and mounted. Imaging of Golgi staining was performed in brightfield and extended depth focus was applied to z-stack images.

2.16. Protein extraction & Western Blot

2.16.1. Total protein extraction by RIPA

Cells isolated from brain or from cell culture were washed with PBS once and lysed with freshly-prepared RIPA buffer (25 mM Tris·HCl (pH 7.5), 150 mM NaCl, 1 % Nonidet P-40, 0.5 % NaDOC, 0.1 % SDS) supplemented with 1 mM of sodium orthovanadate, 1 mM of NaF and 1x of cOmplete™ Protease Inhibitor Cocktail (Roche) for 20 minutes on

ice. The lysates were sonicated 2 times for 10 seconds on ice and centrifuged for 30 minutes at 4 °C. Supernatants were transferred to a pre-chilled Eppendorf tube and protein concentration was determined by Pierce BCA assay (Pierce). A 4x Laemmli buffer was added to the extracts prior to be used for Western Blot or stored at -20 °C.

2.16.2. Total protein extraction by Laemmli buffer

Cells were lysed directly in 1x Laemmli buffer in order to detect SUMOylated proteins. Samples were stored -20 °C until use.

2.16.3. Total brain protein isolation

A piece of a brain was dissected and lysed in HEPES-sucrose buffer (20 mM HEPES, 320 mM sucrose) by mechanical dissociation using pestles. The samples were diluted and the protein concentration determined by BCA assay (Pierce). 4x Laemmli buffer was added to the extracts prior to be used for Western Blot or stored at -20 °C.

2.16.4. Western Blot

Samples were separated on home-made SDS-PAGE gels or on Mini-PROTEAN® TGX™ Gels (Biorad) and transferred on Trans-Blot Turbo Mini 0.2 µm Nitrocellulose Membrane (Biorad). After 1 hour of incubation in blocking buffer (5 % non-fat milk in PBS-0.1 % Tween-20 (PBS-T)) at room temperature, the membrane was incubated overnight at 4 °C in primary antibody solution . The next day, the membrane was washed 3 times in PBS-T and incubated with the appropriate HRP-secondary antibodies diluted in blocking buffer at room temperature for 2 hours. The protein of interest was detected using the Amersham ECL™ Prime Western Blotting Detection Reagent (Cytiva) and developed in the ChemiDoc™ MP Imaging System (Biorad).

2.17. ELISA on *in vitro* supernatant of cell culture

Pro-inflammatory cytokines were quantified in the supernatant of *in vitro* microglia or BMDMs after treatment by ELISA. The supernatant was stored at -80 °C until analysis. The cytokines, IL-6, IL-10, IFNβ, TNFα, IFNγ, Cxcl10 were determined according to the

manufacturer's guidelines. Briefly, the ELISA plate was coated overnight with a capture antibody. The plate was washed and incubated for 1 hour with blocking buffer (10 % FBS or 1 % BSA in PBS). 50 µl of supernatant or standards were incubated for 2 hours on the plate, followed by an incubation of the detection antibody, then an HRP-conjugated antibody and finally the TMB substrate solution. After the reaction was stopped by adding the Stop solution, the absorbance was read on the spectrophotometer (Biorad) at 450 nm – 560 nm. The concentration of each sample was determined using the obtained standard curve.

2.18. ELISA on *in vivo* serum

After treatment, the mice were sacrificed by cervical dislocation and the blood was collected from the heart with a 21 Gauge needle. The blood was stored at 4 °C overnight in Eppendorf tube for clotting. After centrifugation at 1000 x g for 5 minutes, the serum was collected and stored at -80 °C until analysis. The cytokines IL-6, IL-10, TNFα, IFNγ, Cxcl10 were determined according to the manufacturer's guidelines as described in 2.17. IFNβ levels were quantified using a more sensitive kit, the VeriKine™ Mouse IFNβ ELISA. The quantification was achieved according to their guidelines. Shortly, the samples or standards with the detection antibody solution were incubated for 3 hours at RT on a pre-coated plate. Then the plate was incubated with the stabilized chromogen solution and the reaction stopped with the stop solution. The absorbance was read on the spectrophotometer (Biorad) at 450 nm. The concentration of each sample was determined using the obtained standard curve.

2.19. Amyloid β quantification by ELISA from murine brains

A small piece of freshly isolated brains were snap frozen and stored at -80 °C until sample processing. The samples were homogenized in 150 µl of 5 M Guanidine HCl in 50 mM Tris pH8 with pre-cooled pestles. The homogenized samples were incubated for 3 hours at 400 rpm at RT. 50 µl of the samples was diluted 1:10 in 1x PBS supplemented with protease inhibitor. The supernatants of the samples obtained by centrifugation at 16,000 x g for 20 minutes at 4 °C were stored at -80 °C. The protein concentration was determined by BCA assay. The Amyloid β quantification was performed using the Human Aβ42 Ultrasensitive ELISA Kit (Invitrogen) according to their guidelines. Briefly,

1.5 µg of each sample or standard was loaded in the pre-coated ELISA plate. 50 µl of Hu Aβ42 US detection antibody was added to the samples and standards for 3-hour incubation at room temperature. After 4 washes, incubation of primary antibody solution, followed by the incubation of the stabilized chromogen were sequentially performed for 30 minutes each. After adding the stop solution, the absorbance was read on the spectrophotometer (Biorad) at 450 nm. The concentration of each sample was determined using the obtained standard curve.

2.20. RNA isolation & RT-qPCR

2.20.1. RNA isolation

The RNA isolation was performed using the RNeasy® Plus Micro Kit (Qiagen) according to the manufacturer's guidelines. Briefly, the brain-isolated cells or cultured cells were washed in PBS once and lysed in 350 µl of RLT buffer. gDNA was eliminated by passing the lysates through a gDNA eliminator column. Equal volume of 70 % ethanol was added to the lysates which was then added to an RNeasy spin column in order to bind the RNA to the silicon column. The column-bound RNA was washed two times with RPE buffer, dried and eluted using 10-20 µl of RNAse-free H_2O. RNA concentration was determined by ND-1000 Nanodrop™ Spectrophotometer (ThermoScientific).

2.20.2. Reverse transcription

Reverse transcription (RT-PCR) was performed using High-Capacity cDNA Reverse Transcription Kit (ThermoFisher) according to the manufacturer's guidelines. Briefly, the isolated RNA was added to the reaction mix composed of RT Buffer, RT Random primers, dNTP Mix, MultiScribe™ Reverse Transcriptase and RNAse-free H_2O. The RT-PCR program is the following: 25 °C for 10 minutes, 37 °C for 2 hours and 85 °C for 5 minutes, after which the samples were stored at -20 °C.

2.20.3. Real time PCR

Real Time PCR (qPCR) was performed using the 2x Fast SYBR Green Master mix (Applied Biosystems). cDNA was added to a mix of Fast SYBR Green, dedicated

primers (table 5) at a final concentration of 500 nM and RNAse-free H_2O to a final volume of 10 µl. The qPCR program is the following: 95 °C for 20 seconds, followed by a cycle of 95 °C for 3 seconds and 60 °C for 30 seconds repeated for 40 times. The luminescence is measured at every cycle and the relative gene expression was generated using the $2^{-\Delta\Delta Ct}$ method as described in Livak and Schmittgen (Livak & Schmittgen, 2001).

Tab. 5: qPCR primer sequences

Targeted gene	**Forward sequence**	**Reverse sequence**
m-gapdh	ATGGTGAAGGTCGGTGTGAA	TGGAAGATGGTGATGGGCTT
m-pml	CGACAGTGCCCATGCACAG	AGCTCAGCTGGCCAGCTATTTC
m-isg56	CCCAGAAGGCAGGACAATGT	GCACTTCAGCCATGCAAACA
m-ifnb	CCCTATGGAGATGACGGAGA	CTGTCTGCTGGTGGAGTTCA
m-isg15	GGTGTCCGTGACTAACTCCAT	TGGAAAGGGTAAGACCGTCCT
m-stat1	AGTTCCGACACCTGCAACTGAAGG	GAGATCACCACGACAGGAAGAGAGG
m-daxx Exon7-8	TGTGGCTTCTGTCGCTGATTC	AAGCACGATGATCTCCTCCG
m-sumo3	GGCTCGGTGGTACAGTTCAAG	CCGGAATCGAATCTGCCTCAT
m-hsph1	TGCAGCACTATGCCAAGATTG	TTCTCAACCTTCTTCATTTCTGATTC
m-hspa5	ACCCACCAAGAAGTCTCAGATCTT	CGTTCACCTTCATAGACCTTGATTG
m-hsp90ab1	GCGCACGCTGACTTTGGT	CCTGGAGAGCCTCCATGAAC
m-trem2	AGAAGCGAATGGGAGC	GAGGTGGGTGGGAAGGA
h-gapdh	GCACCGTCAAGGCTGAGAAC	TGGTGAAGACGCCAGTGGA
h-pml	GGTGCAGAGGATGAAGTGCT	AGGAAACCGTGCATGTCC
h-ifnb	AGCTGCAGCAGTTCCAGAAG	AGTCTCATTCCAGCCAGTGC
h-isg15	GCTGGGACCTGACGGT	TTAGCTCCGCCCGCCAG
m-stat1	ATGGCAGTCTGGCGGCTGAATT	CCAAACCAGGCTGGCACAATTG

2.21. Library preparation for RNA-sequencing

For RNA sequencing, isolated RNA using the RNeasy® Plus Mini Kit (Qiagen) was performed as described previously. The column-bound RNA was eluted with 30 µl of RNAse-free H_2O and the quantity and quality of RNA was assessed by the Agilent Bioanalyzer 2100 RNA pico chip. Only samples with a RIN > 6 were subjected to RNA sequencing.

RNA libraries were prepared using SMARTer®Stranded Total RNA-seq kit v2 - Pico Input Mammalian (Takara Bio USA, Inc) according the the manufacturer's guidelines. Briefly, the RNA was first fragmented by incubating at 94 °C for 3-4 minutes with SMART Pico Oligos Mix v2, First-Strand Buffer. cDNA is then synthetized by incubating the

fragmented RNA with SMART TSO Mix v2, RNase inhibitor and SMARTScribe Reverse Transcriptase at 42 °C for 90 minutes and 70 °C for 10 minutes. Indexes and Illumina Adapters were added to the cDNA, in order to distinguish the pooled libraries from each other, by running a PCR (94 °C for 1 minute, [98 °C for 15 seconds, 55 °C for 15 seconds, 68 °C for 30 seconds] x 5 and 68 °C for 2 minutes) on the following mix: cDNA, SeqAmp BC PCR Buffer, SeqAmp DNA polymerase and 3' and 5' unique index couple per sample. The purification of the libraries was conducted using SRI beads and magnetic separation. 40 µl of SRI beads were added to each sample and incubated for 8 minutes to allow the DNA to bind the beads. The DNA-bounded beads were washed two times with 80 % ethanol and dried before eluting the cDNA from the beads with 52 µl of nuclease-free H_2O. The beads were discarded and once again, 40 µl of SRI beads were added to each sample. The beads were washed two times, dried and the cNDA was eluted from the beads in ZapR Master Mix which is used to deplete by cleavage the mitochondrial cDNA fragment (originating from mitochondrial RNA). The ZapR Master Mix contained ZapR Buffer, ZapR v2 and R-Probes v2 and was incubated at 37 °C for 60 minutes, 72 °C for 10 minutes. The final RNA-seq Library amplification was then performed, in which the library fragments not cleaved by the previous reaction were further enriched. SeqAmp CB PCR Buffer, PCR2 Primers v2 and SeqAmp DNA polymerase were added to the samples and the following PCR was performed: 94 °C for 1 minute, [98 °C for 15 seconds, 55 °C for 15 seconds, 68 °C for 30 seconds] x 13. The libraries were purified using the SRI beads as described previously. 100 µl of beads were added to the samples, bound by the cDNA, washed two times with 80 % ethanol, dried and resuspended in 20 µl of Tris Buffer. The beads were discarded and the libraries were stored at -20 °C until sequencing. DNA concentration and quality of the libraries were assessed using respectively the Qubit dsDNA HS kit (ThermoFisher) and the Agilent High sensitivity DNA kit (Agilent).

The sequencing was performed by the DZNE sequencing facility, PRECISE.

3. PML role in homeostatic microglia and upon bacteria-like stimulation

3.1. Results

3.1.1. PML-NBs in the brain

The functions of PML in the brain has mainly been investigated in neurons as PML protein and PML-NBs are mostly present in neuronal cells at steady state in adult mice (Figure 20). Among neurons, the number of PML-NBs varies depending on the neuronal type and its brain region. The highest number of PML-NBs per nuclei are found in the Purkinje cells with more than 20 PML-NBs per cell, oppositely to neurons in the cerebellar granule layer which do not present any PML-NBs. In the cortex, the layers 2-3 harbors around 10 PML-NBs per neuronal nucleus, while the fifth layer has very few of them. Sparse PML-NBs are found in the hippocampus (figure 20A).

In glial cells, such as astrocytes and microglia, hardly any PML-NBs were found in adult mice at steady state (figure 20B). This likely explains the lack of research about PML functions in glial cells.

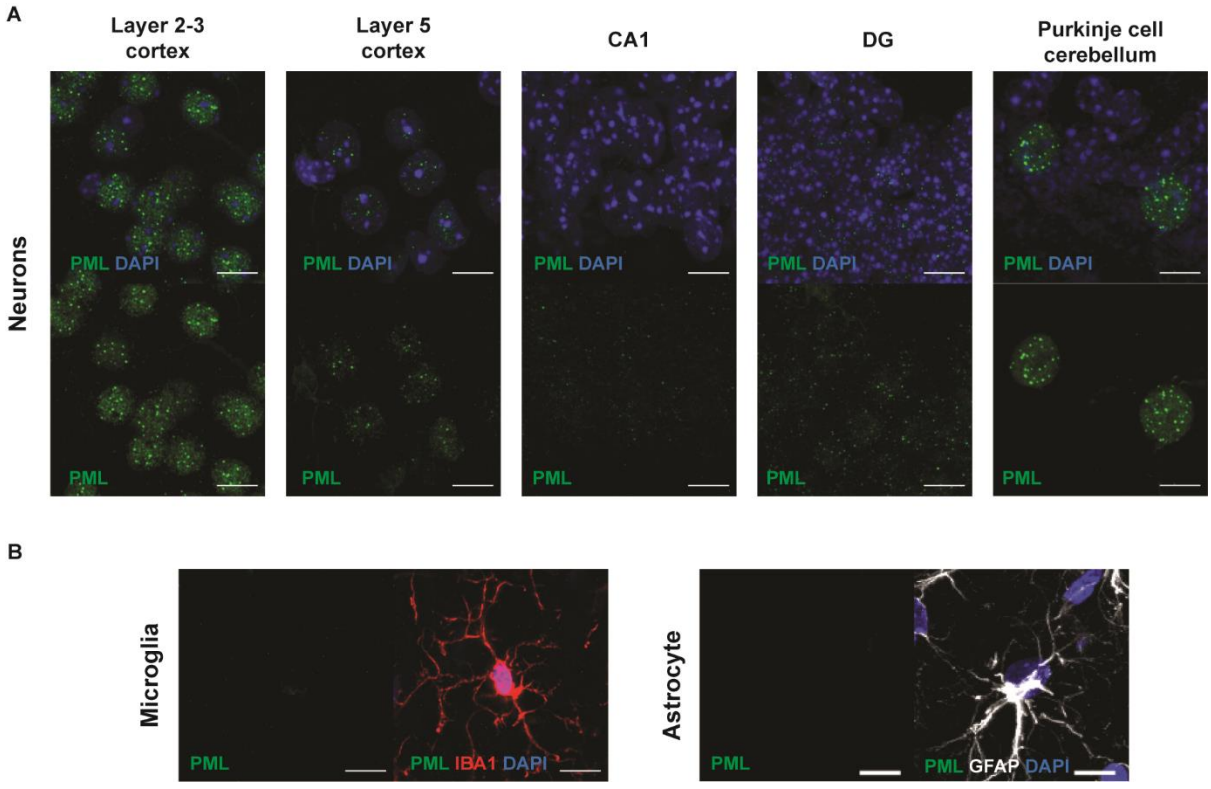

Fig. 20: PML-NBs in different brain cell types in adult mouse.

Representative confocal images of PML-NBs in neuronal nuclei (A) and in glial cells (B). Scale bars, 10 µm.

3.1.2. PML in microglia, from development to aging

As shown previously, at steady state in adult microglia, almost no PML-NBs are found in microglia. However, as PML is a stress sensor protein, we investigated the presence of PML-NBs during development and upon aging, where microglia have an active role such as pruning and debris clearance. As indicated in figure 21, from postnatal day 0 (P0) to P20, every microglia harbored one large PML-NB, which disappeared during adulthood from around 1 month old. Upon aging, hardly any PML-NBs were observed in microglia at 20 months old. Interestingly, at early postnatal stage, P0-P3, an intense nuclear staining and a fainter cytoplasmic staining of PML were observed. Overall, we concluded that PML was more expressed in microglia in young pups and that the formation of one PML-NB was induced during development. We could speculate that, during development, PML-NB formation was triggered in response to stress and/or to achieve specific functions. This will not be further studied in this thesis.

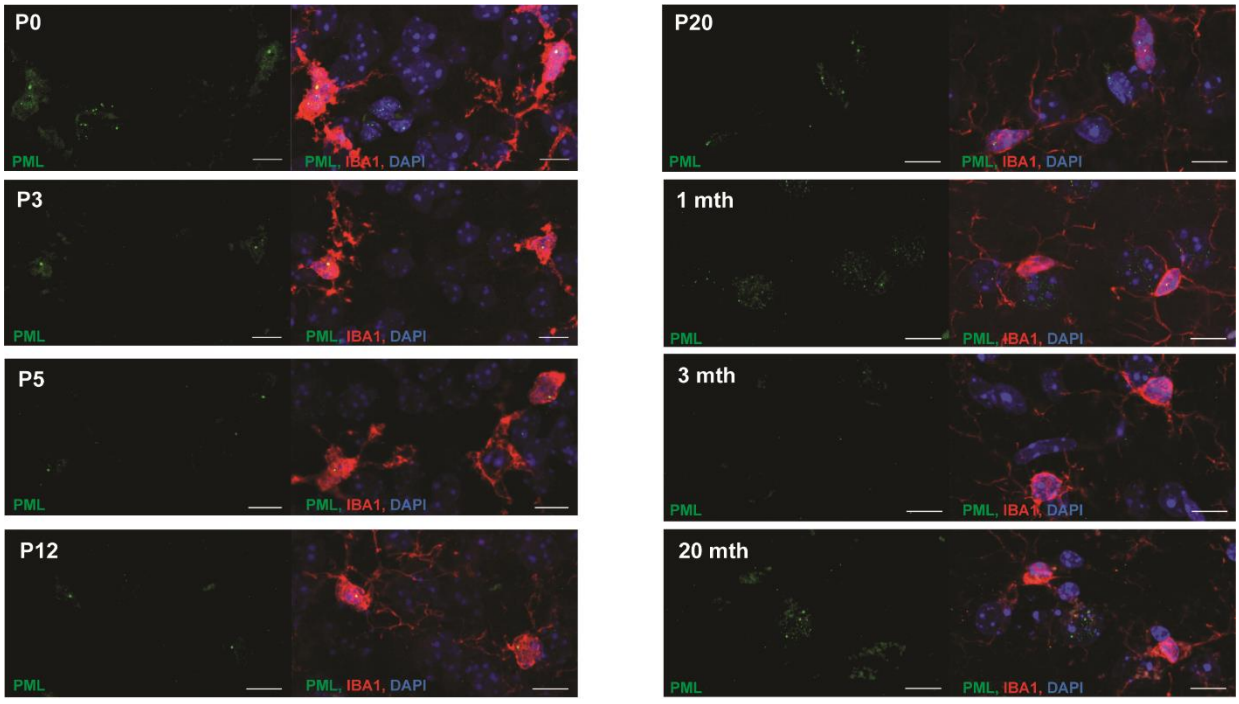

Fig. 21: PML-NBs in microglia from development to aging.
Representative confocal images of PML-NBs in microglia. Scale bars, 10 µm.

3.1.3. Assessment of PML deletion efficiency in microglia

In order to investigate PML functions in microglia, we created a mouse line using the Cre-loxP system (detailed in Material & Methods 2.3, Figure 19). PML fl/fl mice were crossed with a mouse line carrying *Cre* under the Csf1r promoter which is constitutively active from E8.5 in microglia, dendritic cells, monocytes and macrophages. PML fl/fl, Csf1r Cre mice, microglia and BMDMs will be referred, respectively, as PML KO mice, PML KO microglia and PML KO BMDMs in the rest of the thesis.

We first assessed the recombination efficiency in brain-isolated microglia and in *in vitro* cultured BMDMs: in both PML KO cell types, total recombination was observed (figure 22 A&D). Furthermore, in brain-isolated PML KO microglia and *in vitro* PML KO cultured BMDMs, P*ml* transcript was significantly decreased compared to wildtype (wt) microglia (figure 22B) and wt BMDMs (figure 22E). In *in vitro* cultured BMDMs and PML KO microglia, PML protein was not detected by western blotting (figure 22 C&G), nor by immunofluorescence in PML KO BMDMs (figure 22F).

Altogether, the data showed that PML deletion was successfully achieved in brain-isolated microglia and in *in vitro* cultured BMDMs. This will allow us to study the role of PML in those cells.

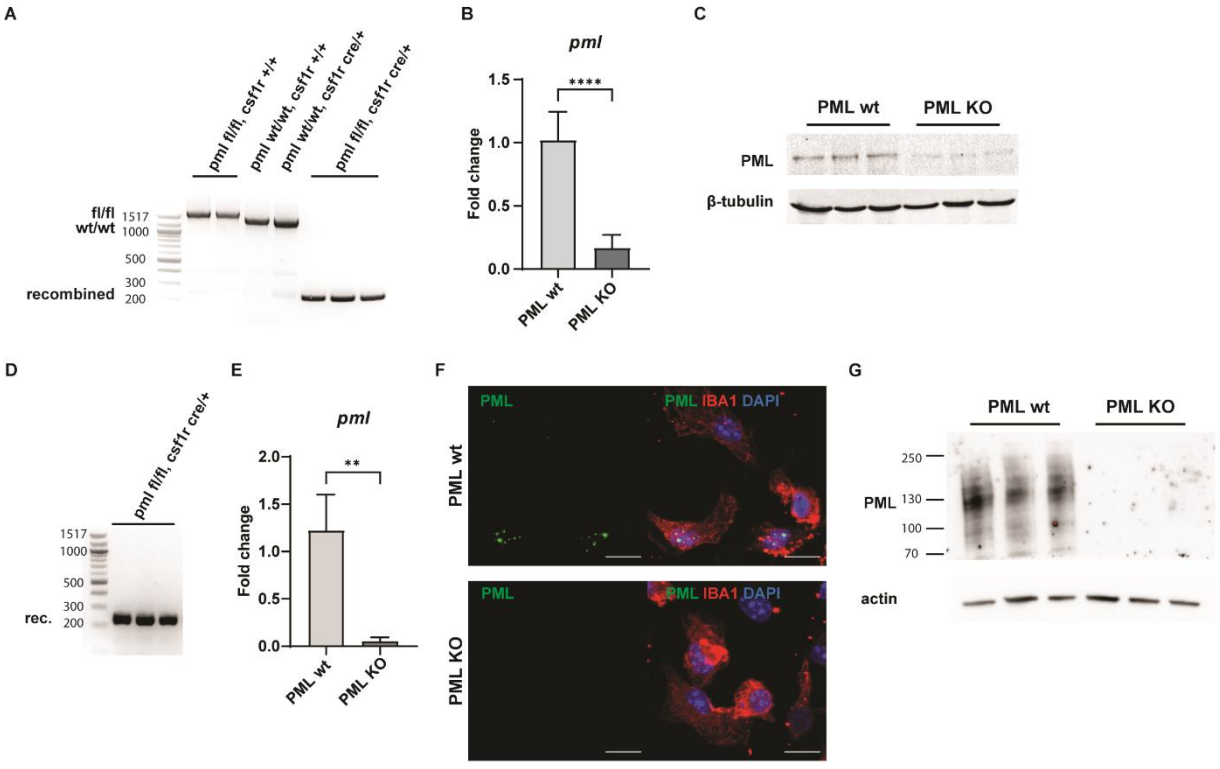

Fig. 22: Assessment of *Pml* deletion in brain-isolated microglia and *in vitro* cultured BMDMs.
(A&D) Recombination of PML fl/fl, csf1r cre/+ is total in microglia (A) and BMDMs (D). The recombined band is around 300 bp, wt band 1400 bp and fl/fl unrecombined 1500 bp.
(B&E) Downregulation of *pml* transcript level in PML KO microglia (B) and BMDMs (E). n=6; t-test.
(C) Western blot assay showing the absence of PML in PML KO brain isolated microglia.
(F) Representative confocal images of PML expression in wt and PML KO BMDMs. Scale bars, 10 µm.
(G) Western blotting analysis of PML in wt and PML KO BMDMs showing the absence of PML in PML KO BMDMs.
All data are represented as mean ± SD. $^{*}p < 0.1$; $^{**}p < 0.01$; $^{***}p < 0.001$; $^{****}p < 0.0001$; ns, not significant.

3.1.4. Cellular phenotype of PML KO microglia

In order to study the effects of *Pml* deletion in microglia, we first quantified the microglia numbers in PML wt and PML KO mice: similar microglia numbers were observed (figure 23B). Interestingly, PML KO microglia harbored a less complex morphology than wt microglia (figure 23A). By quantification, we assessed that PML KO microglia harbored less branches and junctions (figure 23D), despite having, in average, longer branches than wt microglia (figure 23C).

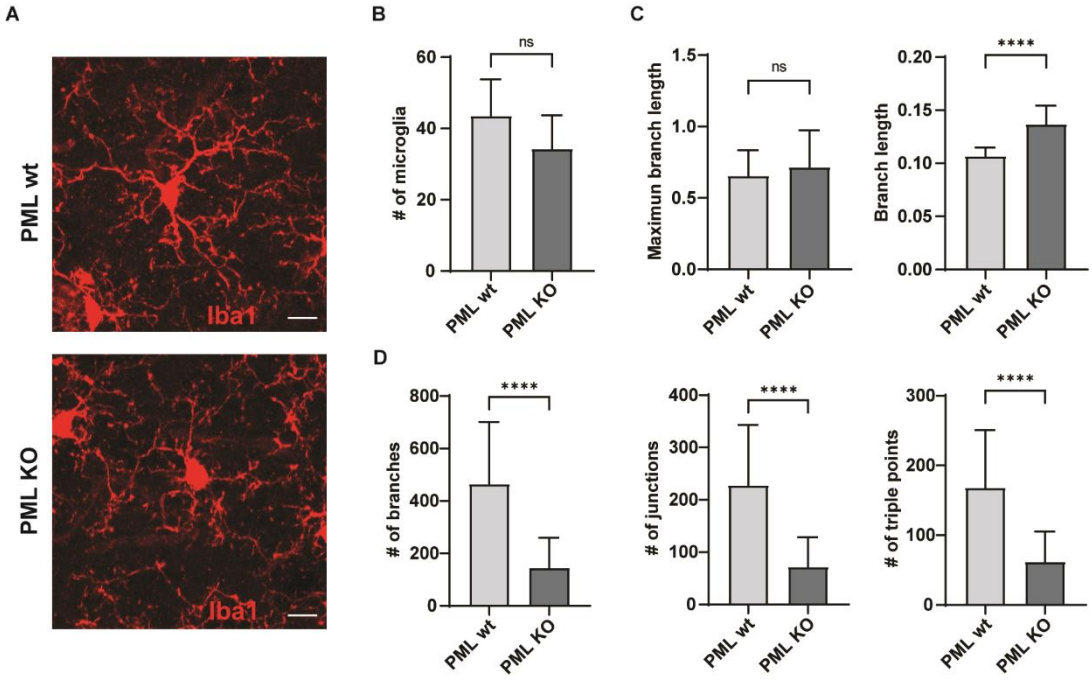

Fig. 23: PML KO microglia present a “less complex” morphology at 3 month-old.

(A) Representative confocal images of microglia in the cortex of PML wt and PML KO mice. Scale bars, 10 µm.
(B) Quantification of microglia number in the cortex of wt and PML KO mice. n=3; t-test.
(C&D) Quantification of the branch length, number of branches and junctions of wt and PML KO microglia showing the increased branch length in PML KO microglia, while the number of branches, junctions and triple points are decreased in PML KO microglia. n=3, 6-19 microglia analyzed per biological replicate; t-test.
All data are represented as mean ± SD. ****p < 0.0001; ns, not significant.

3.1.5. Memory impairment in the PML KO mice

Microglia were shown to be involved in cognitive behavior, memory and learning (Morris et al., 2013). We therefore sought whether the morphological changes induced by PML deletion in microglia would affect the behavior of PML KO mice. For this purpose, 3-month-old wt and KO mice underwent multiple behavioral tests in order to assess the locomotion, anxiety, long- and short-term memory.

According to our data, PML KO mice did not show any sign of impairment in locomotion: KO mice traveled similar distance to wt mice in the Open field test (figure 24A) as well in the Water Maze test (figure 24E). We can then conclude that PML KO mice do not have any motor disability.

Previously, Butler et al. (2013) showed that PML -/- mice presented a reduced anxiety-related behavior, however, in our study, the deletion of PML in microglia did not induce a similar phenotype. Indeed, PML KO mice did not spend more time in the center during the open field test (figure 24A), neither longer time on open arms in the elevated plus maze (figure 24D). The results from these two tests proves that PML KO mice do not show higher level of anxiety than wt mice. This difference to the previous study is likely due to the difference of model, they used a germline KO while we investigated a microglia specific PML KO.

In order to determine any impairment in memory, males and females were analyzed separately as wt males did not show any learning in the water maze nor in the novel object location test. In the water maze, males, both wt and KO, did not show any learning curve expected along time (figure 24E). In both genders, PML KO and wt reached the platform in similar times, indicating no impairment of long term memory in KO mice (figure 24E). Interestingly, the second memory test investigating the short term spatial memory, showed a significantly lower discrimination index for female KO mice (figure

24B): female KO mice did not discriminate between the newly located object and the unchanged one and were interested in both objects similarly.

In conclusion to the behavior tests, we found that PML deletion in microglia did not induce any locomotor deficit, anxiety-like behavior nor short term memory loss, however, a spatial memory impairment was observed in female KO mice.

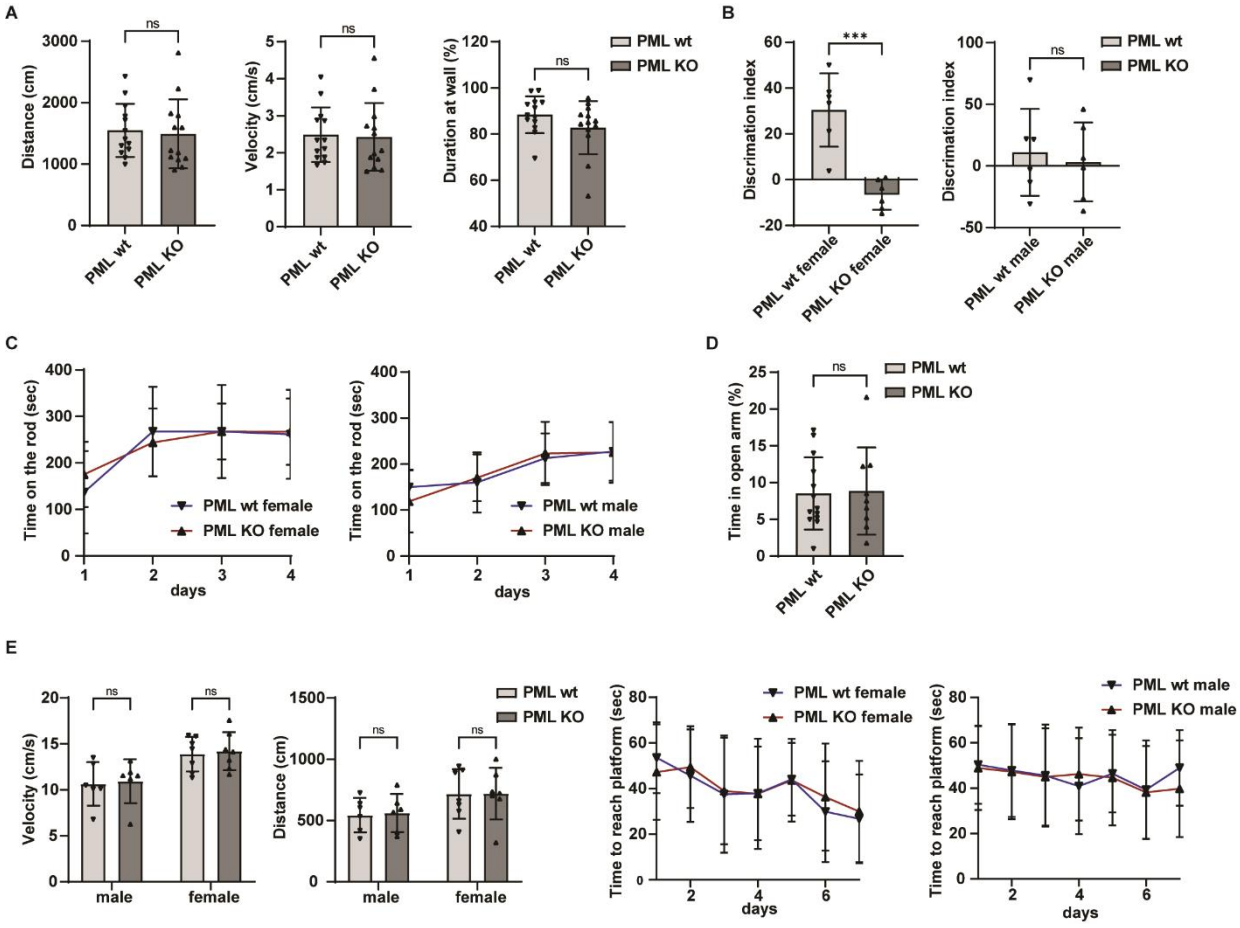

Fig. 24: Deletion of PML in microglia induces an impairment in spatial memory, but not in short term memory, locomotion nor an anxiety-like behavior.
(A) Open field assay: wt and PML KO mice travelled a similar distance with a similar velocity, and spent the same duration at wall. t-test.
(B) Novel object location test: PML KO females display lower discrimination index compared to wt females. Wt and PML KO males have both a very low discrimination index, indicating the lack of recognition of the newly-located object. t-test.
(C) Rotarod test: representation of the time spent on the rod for each day. All mice improve their time spent on the rod, and no difference are observed between wt and PML KO mice.
(D) In the elevated plus maze, wt and PML KO spend similar amount of time in the open arms. t-test.

(E) Water maze test, wt and PML KO mice have similar velocity and swum distance. The time to find the platform is similarly decreasing over the days for wt and PML KO mice. 2-way ANOVA.
All data are represented as mean ± SD. ***p < 0.001; ns, not significant. n=7 females and n=6 males per genotype.

It was shown that spatial learning and spatial memory involve mainly the hippocampus (Haettig et al., 2011; Mumby et al., 2002), and specifically the apical dendrites of CA1 pyramidal neurons (Y. Zhu et al., 2017). We therefore performed a Golgi staining in order to study the CA1 pyramidal neurons. No drastic differences were observed between wt and PML KO neurons as shown with the basal dendrites of CA1 pyramidal neurons (figure 25A). The spines of basal dendrites (figure 25B) and apical dendrites (figure 25C) did not demonstrate any striking difference in density nor in shape.

Altogether, PML deletion in microglia induced a less “complex” morphology of microglia which might be the cause of a spatial memory impairment in female mice. However, the Golgi staining did not show any differences in CA1 pyramidal neurons morphology of spine density or shape. This was not pursued any further.

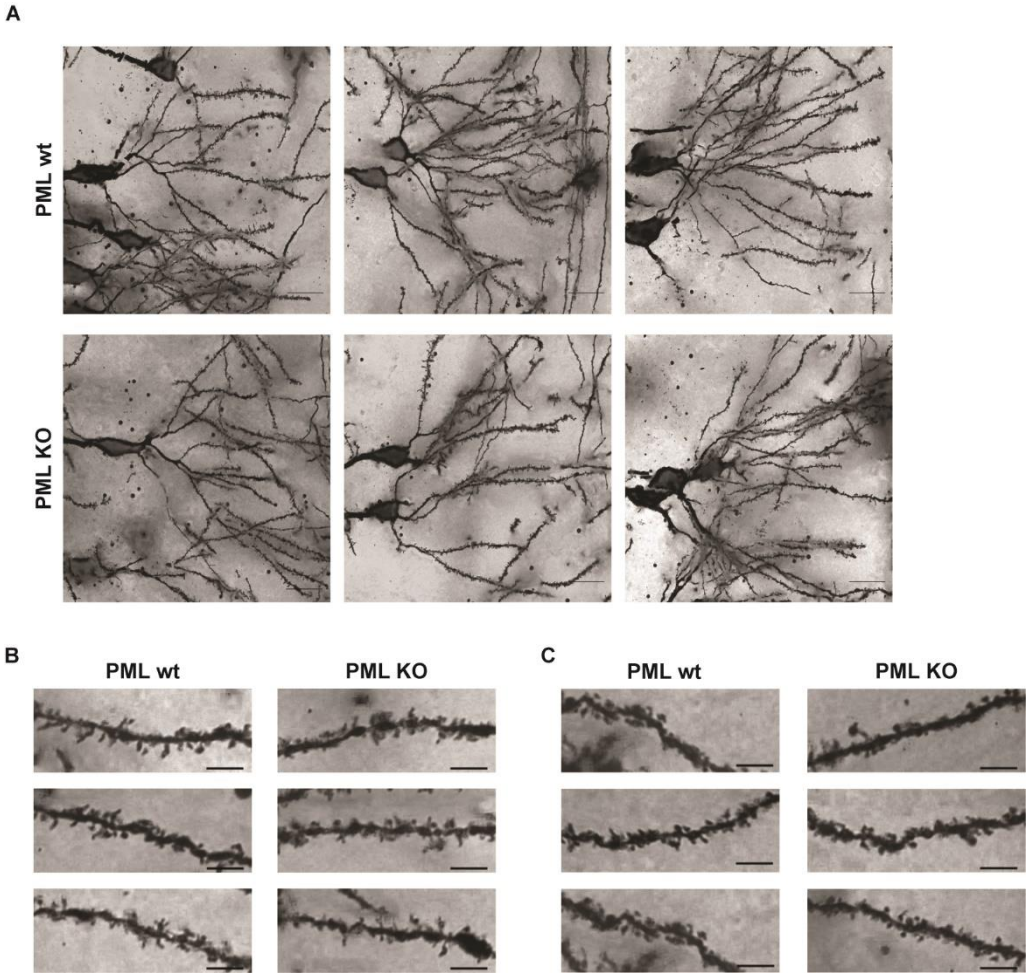

Fig. 25: Golgi staining of CA1 pyramidal neurons.
(A) Representative images from Golgi staining of basal dendrites of pyramidal neurons in the CA1 of PML wt and PML KO mice. Scale bars, 20 µm.
(B&C) Close up images of spines of secondary basal dendrites (B) and apical dendrites (C). Scale bars, 5 µm.

3.1.6. NF-κB translocation, TNFα release and phagocytosis activity are impaired upon LPS in PML KO primary microglia and BMDMs.

From literature, it is known that constitutive PML -/- mice are less sensitive upon LPS-induced septic shock due to the lack of macrophage activation and cytokine production by PML KO cells (Lunardi et al., 2011). Furthermore, in PML -/- mouse embryonic fibroblasts, reduced level of phosphorylation of NF-κB and transcription of NF-κB-target genes were observed without any NF-κB translocation impairment (Ahmed et al., 2017).

As previous studies were conducted in mouse embryonic fibroblasts, we investigated the response to LPS via the NF-κB pathway in PML KO immune cells such as primary microglia and BMDMs. To do so, we stimulated *in vitro* primary microglia and BMDMs

cultures with LPS for 30 minutes or 6 hours and we analyzed the NF-κB p65 translocation, TNFα release and ability to phagocytose.

First, we found that only around 20 % of wt BMDMs showed NF-κB translocation to the nucleus upon 30 minutes of LPS stimulation (figure 26 A&C). Surprisingly, all and only the cells having NF-κB translocated to the nucleus upon LPS harbored PML-NBs (figure 26 A&B). Furthermore, we found that, unlike in a previous study (Ahmed et al., 2017), NF-κB translocation had a tendency to decrease in PML KO BMDMs (figure 26C). These results correlate with the reduced TNFα release observed in PML KO primary microglia upon 6-hour LPS stimulation (figure 26D). Finally, we observed an impaired phagocytosis activity in PML KO primary microglia at steady state and upon 6-hour LPS stimulation (figure 26E).

Taken together, our data showed that in wt BMDMs, only cells containing PML-NBs translocated NF-κB to the nucleus upon LPS stimulation, nonetheless, PML was not fully required for NF-κB translocation as few PML KO cells also showed NF-κB translocation. We also found that PML deletion led to an impairment in TNFα release and phagocytosis activity.

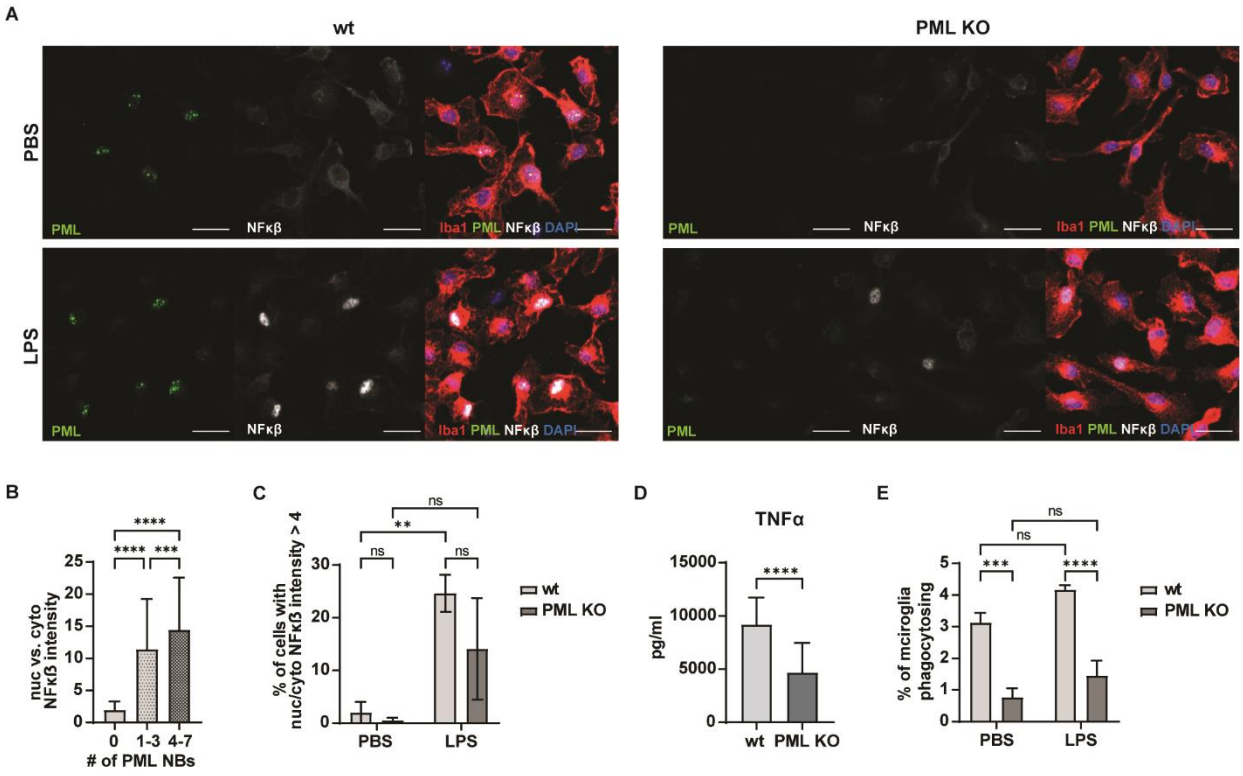

Fig. 26: Impaired NF-κB translocation, TNFα release and phagocytosis activity upon LPS in PML KO cells.
(A) Representative confocal images of NF-κB and PML upon LPS stimulation in BMDMs show that NF-κB translocation is observed in PML-NBs containing cells upon LPS, and is reduced in PML KO cells. Scale bars, 20 µm.
(B) Bar plot presenting the nuclear vs. cytoplasmic NF-κB intensity increasing with the PML-NB number per nucleus upon LPS in wt BMDMs. n=3, 2-way ANOVA.
(C) Bar plot showing the percentage of cells having nuclear vs. cytoplasmic NF-κB intensity superior to 4. n=3, 2-way ANOVA.
(C) Bar plots displaying the reduced release of TNFα cytokines by PML KO primary microglia upon LPS. n>10, 2-way ANOVA.
(D) Bar plots showing the decrease in percentage of phagocytosis cells upon LPS in wt and PML KO primary microglia. n>6, 2-way ANOVA.
All data are represented as mean ± SD. $^{*}p < 0.1$; $^{**}p < 0.01$; $^{***}p < 0.001$; $^{****}p < 0.0001$; ns, not significant.

3.2. Discussion

Several studies have attributed a role to PML in innate immune response, such as viral response and bacteria-like-related inflammation (Lunardi et al., 2011; Regad et al., 2001; Regad & Chelbi-Alix, 2001). However, studies on PML function in brain-immune cells was lacking most likely due to the fact that PML-NBs are not present at steady state in adult glial cells.

In order to study PML function in the immune resident brain cells, the microglia, we created a genetically modified mouse line with PML deletion under the Csf1r promoter, deleting PML in microglia, dendritic cells, monocytes and macrophages. It is important to keep in mind that PML is deleted from embryonic stage as the Csf1r promoter is active from E8.5. This model shows a complete recombination in microglia, which allowed us to understand the role of PML in microglia by studying the effects in the brain following its microglia-specific deletion.

We first found that PML KO microglia harbor a less complex morphology than wt microglia with longer and less numerous branches. It was hypothesized that changed of morphology of PML KO microglia would affect some of the microglial functions in the brain at steady state, such as cognition and learning (Augusto-Oliveira et al., 2019). We thus investigated the effects of PML deletion in microglia on those brain functions by subjecting PML KO mice to behavioral tests to assess the motor capacity, anxiety and memory. PML KO female mice showed a short spatial memory impairment which, from literature, involves the pyramidal neurons of the CA1 hippocampal region (Haettig et al., 2011; Mumby et al., 2002; Y. Zhu et al., 2017). We did not identify any striking difference in pyramidal neuron morphology or spine density and shape by Golgi staining. However, this staining method presents important limitations, such as high background, low resolution and a lack of 3-dimension analysis, making the analysis of spines difficult and not accurate enough to detect slight differences which might be present between our models. These limitations could be overcome by using a reporter line and 2-photon imaging for instance, but, this was not pursued any further.

For this study, it is important to keep in mind that PML is deleted from embryonic stage in our model, the PML fl/fl, Csf1r-Cre. Therefore, the spatial memory impairment could result from a developmental issue, instead of reflecting a role of PML in adult microglia. This hypothesis is supported by the presence of PML NBs during postnatal stage, P0-P20, where its deletion in microglia could, for instance, impair pruning or brain development from postnatal period. In order to differentiate between the role of PML in microglia during development from the role of PML in adult microglia, we will create another murine line, where PML is deleted using an inducible Cre system, the Cre-ERT2, under the microglia specific Cx3cr1 promoter. This will allow us to delete PML in

microglia from any chosen age by Tamoxifen injections, and therefore to specifically assess the role of PML in adult microglia and in brain functions.

Finally, we studied PML role upon bacteria-like infection in BMDMs. It was previously shown that PML -/- mice demonstrate a reduced sensitivity to LPS-induced septic shock, and that PML deletion in mouse embryonic fibroblasts inhibits NF-κB phosphorylation and therefore NF-κB-target gene transcription upon LPS without affecting NF-κB translocation to the nucleus.

Our data showed that only 20 % of wt BMDMs present a translocation of NF-κB p65 to the nucleus upon 30-min LPS stimulation, despite being described as a homogenous population (Mendoza et al., 2022). Surprisingly, these are also the cells harboring PML-NBs. We also observed a reduced NF-κB translocation, TNFα release and phagocytosis activity in PML KO BMDMs. However, it is important to mention that PML-NBs are not required for NF-κB translocation.

Our data demonstrated that not all the BMDMs, wt or KO, are responding to LPS stimulation and that in a pool of wt cells, only the ones harboring PML-NBs have the ability to sense cellular stimuli and to respond to them. In a pool of PML KO cells, we hypothesize that the reduced response to stimuli could be triggered by a compensatory or secondary mechanism which will be further investigated. Furthermore, we speculate that the partial activation of the cell population might also be a self-regulation system from immune cells to avoid generating a too strong response upon bacterial infections. It will be interesting to better understand the role of PML-NBs containing cells compared to the PML-NB lacking cells. Currently, efforts are being made to separate these populations in order to be able to characterize their transcription profile, cytokine release, phagocytosis activity and other biological processes.

4. ATO, an ancient anti-cancer drug, suppresses the IFN response in microglia: implications for interferonopathies.

4.1. Results

4.1.1. PML is upregulated in interferon-driven inflammation models

PML protein is known to act as a stress sensor. In particular, PML transcription and PML-NB formation were shown to be induced upon IFN stimulation in several peripheral cell types (Chelbi-Alix et al., 1995; Regad et al., 2001; Stadler et al., 1995). In this project, in collaboration with Burcu Sivri and Pr. Kato, we sought to investigate PML response in microglia upon IFN-mediated inflammation by using two models.

The first one is an AGS mouse model with a gain-of-function R822Q mutation in MDA5, referred as MDA5 RQ mice in this thesis. This mutation has been reported in patients, but was not yet reproduced in a mouse model. Unlike the MDA5 G821S mice, MDA5 RQ mice have a shorter lifespan compared to wild type mice with a mortality starting from 40 weeks and reaching hundred percent mortality at 105 weeks (data not shown from AG Kato). We observed that MDA5 RQ mice presented a higher number of microglia (figure 27A) which harbored an activated morphology with more numerous and thicker processes (figure 27B). They also showed an increased transcription of IFN stimulated genes (ISGs) (figure 28D). Similarly, MDA5 RQ astrocytes presented a tendency to be more numerous with an activated morphology shown by higher GFAP staining intensity (figure 27 C&D). Despite the increased number of microglia and astrocytes observed, no Ki67 positive cells were detected in the cortex (data not shown).

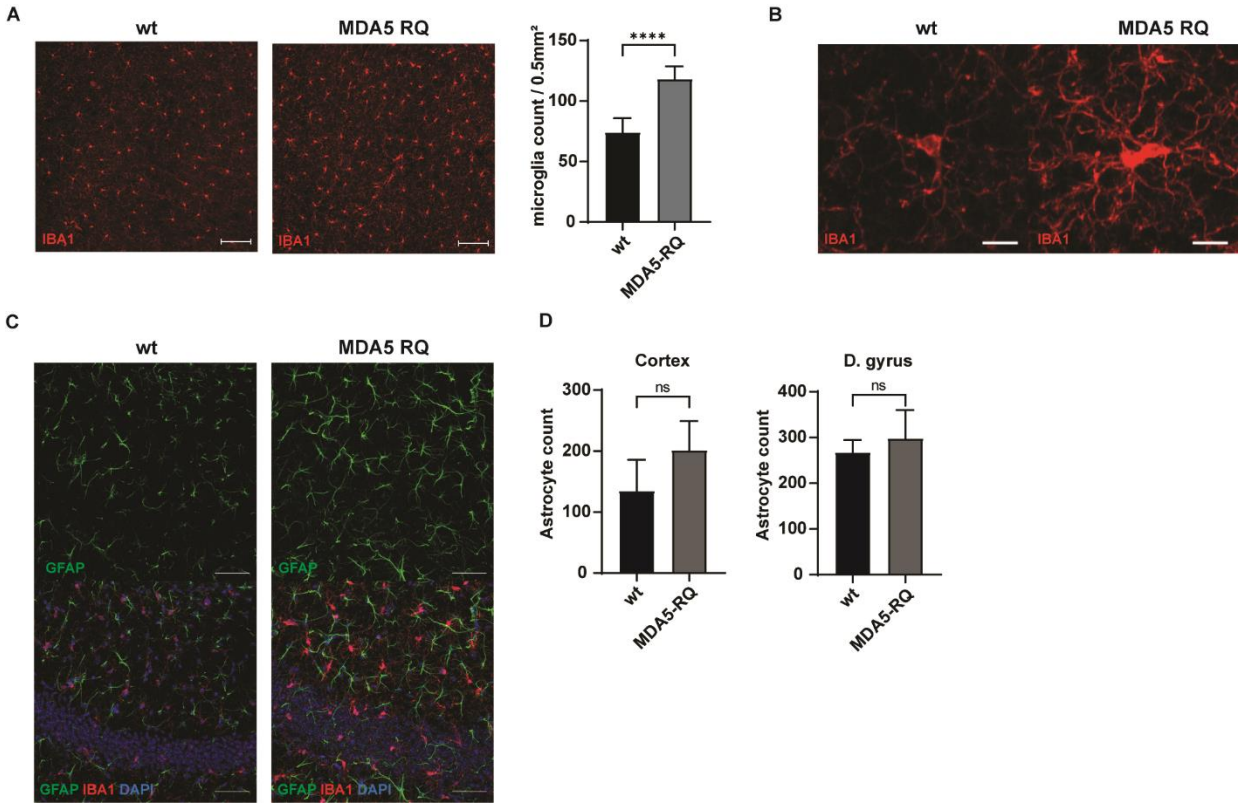

Fig. 27: Description of MDA5 RQ mice.
(A) Representative confocal images of the MDA5 RQ cortex showing an increase in microglia in MDA5 RQ mice. Bar plot shows quantification of microglia in the cortex of wt and MDA5 RQ mice. Scale bar 100 µm. n=3, t-test.
(B) Representative confocal images of the activated morphology of MDA5 RQ microglia. Scale bar 10 µm.
(C) Representative confocal images of the activated morphology of MDA5 RQ astrocytes in the hippocampus. Scale bar 50 µm.
(D) Bar plots showing that MDA5 RQ astrocytes tend to be more numerous in the cortex and dentate gyrus. n=3, t-test.
All data are represented as mean ± SD. $^{****}p < 0.0001$; ns, not significant.
Burcu Sivri took part in the sample collection of all the RQ mice presented in the thesis; Burcu Sivri made the bar plots in (D).

In the second IFN-mediated inflammation model, the IFN response is induced by polyinosinic-polycytidylic acid (pI:C). pI:C is a synthetic analogue of double stranded RNA, which binds to TLR3 or MDA5 and activates the IFN signaling. Wt mice were injected by i.p. with 300 µg of pI:C and sacrificed 5 and 12 hours after injection.

In figure 28 A&B, we observed that PML-NBs numbers in microglia were increased upon pI:C injection in a time-dependent manner and were further more increased in MDA5 RQ microglia. S*tat1* transcription was similarly upregulated in each model, however, *pml* and *ifnb* transcript levels reached the same fold change upon 5-hour and 12-hour pI:C

stimulation as well as in MDA5 isolated microglia. This suggests that the correlation between PML transcription level and NBs formation is not linear. Surprisingly, *isg56* was not induced in isolated microglia upon 5-hour pI:C treatment, but reached the same level upon 12-hour pI:C treatment and in MDA5 RQ microglia (figure 28D).

After observing PML increase in transcription and in PML-NB formation, we wanted to assess the functionality of these PML-NBs by checking DAXX, one of the interacting partners of PML. In pI:C-treated microglia and MDA5 RQ microglia, DAXX co-localized with some PML-NBs, we therefore can assume that the formed PML-NBs are functional (figure 28C).

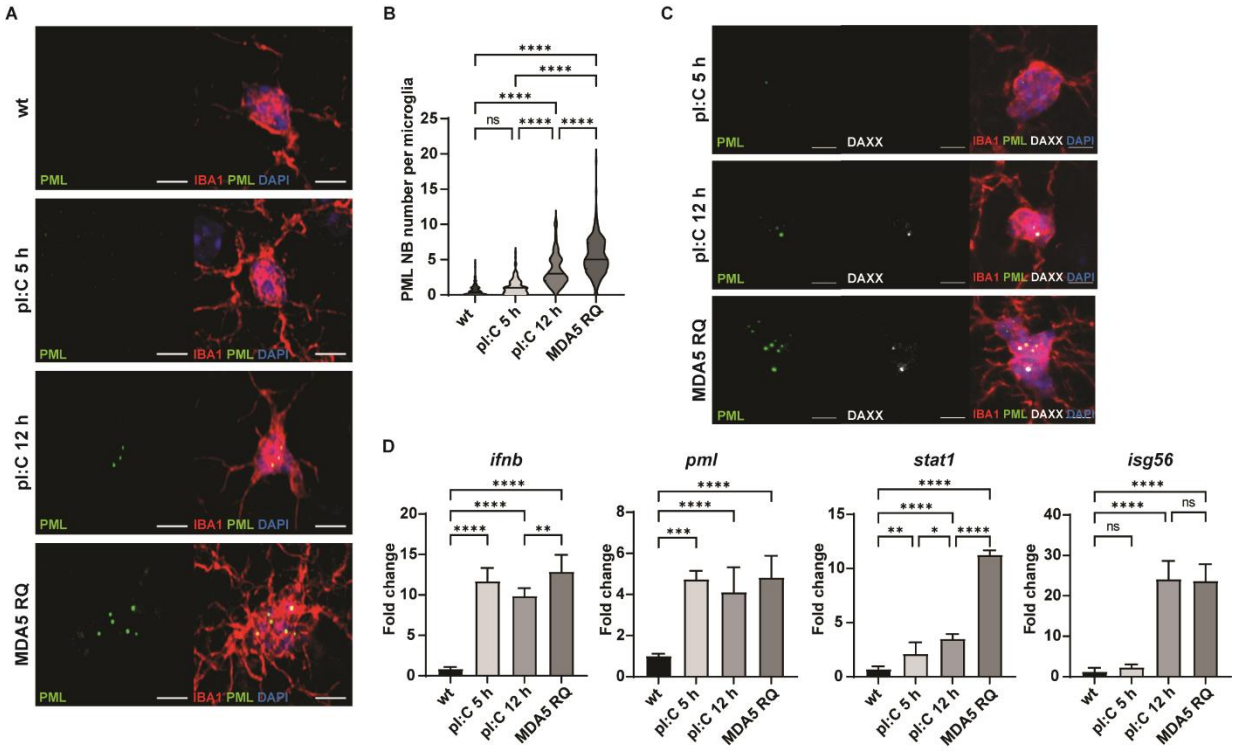

Fig. **28:** PML expression and NB formation are enhanced in IFN-mediated inflammation models.
(A) Representative confocal images of PML-NBs in microglia upon 5 and 12 hours of pI:C stimulation and in the RQ model. Scale bar 5 µm.
(B) Quantification of PML-NB number in microglia represented as violin plots. n=3-4; ordinary one-way ANOVA.
(C) Representative confocal images of DAXX colocalization with PML-NBs. Scale bar 5 µm.
(D) ISG transcription is upregulated in microglia upon 5 and 12 hours of pI:C stimulation and in the RQ model. n=3-4; ordinary one-way ANOVA.
Data are represented as mean ± SD. $^{*}p < 0.1$; $^{**}p < 0.01$; $^{***}p < 0.001$; $^{****}p < 0.0001$; ns, not significant.

4.1.2. PML is an Interferon Stimulated Gene (ISG)

PML has been shown to be an ISG and therefore to be induced upon IFN signaling, however, it is still unknown whether PML transcription or PML- NB formation could also be induced via the primary signaling pathway, such as the IRF transcription factors. To assess it, we looked at PML response upon pI:C in IFNAR -/- mice, kindly provided by AG Kato, UKB. This transgenic mouse model carries a constitutive KO of IFN-α/β receptor (IFNAR), the receptor triggering IFN signaling amplification. In IFNAR -/- BMDMs, the inflammation via IRF3 is abrogated, therefore, IFNβ, IL-6 and IL-10 were not induced upon pI:C stimulation (figure 29C). In addition, the transcription of *ifnb* and other ISGs including *pml* was not induced in *in vitro* pI:C-treated IFNAR -/- BMDMs nor *ex vivo* isolated IFNAR -/- microglia upon pI:C i.p. stimulation (figure 29 B&D). PML protein levels were also not induced upon pI:C in IFNAR -/- BMDMs (figure 29E) and PML-NBs formation was abrogated in IFNAR -/- microglia from pI:C-treated mice (figure 29A).

It is worth mentioning that, at steady state, PML transcript levels were lower in IFNAR -/- microglia (figure 29B) and PML protein levels were lower in IFNAR -/- BMDMs (figure 29E).

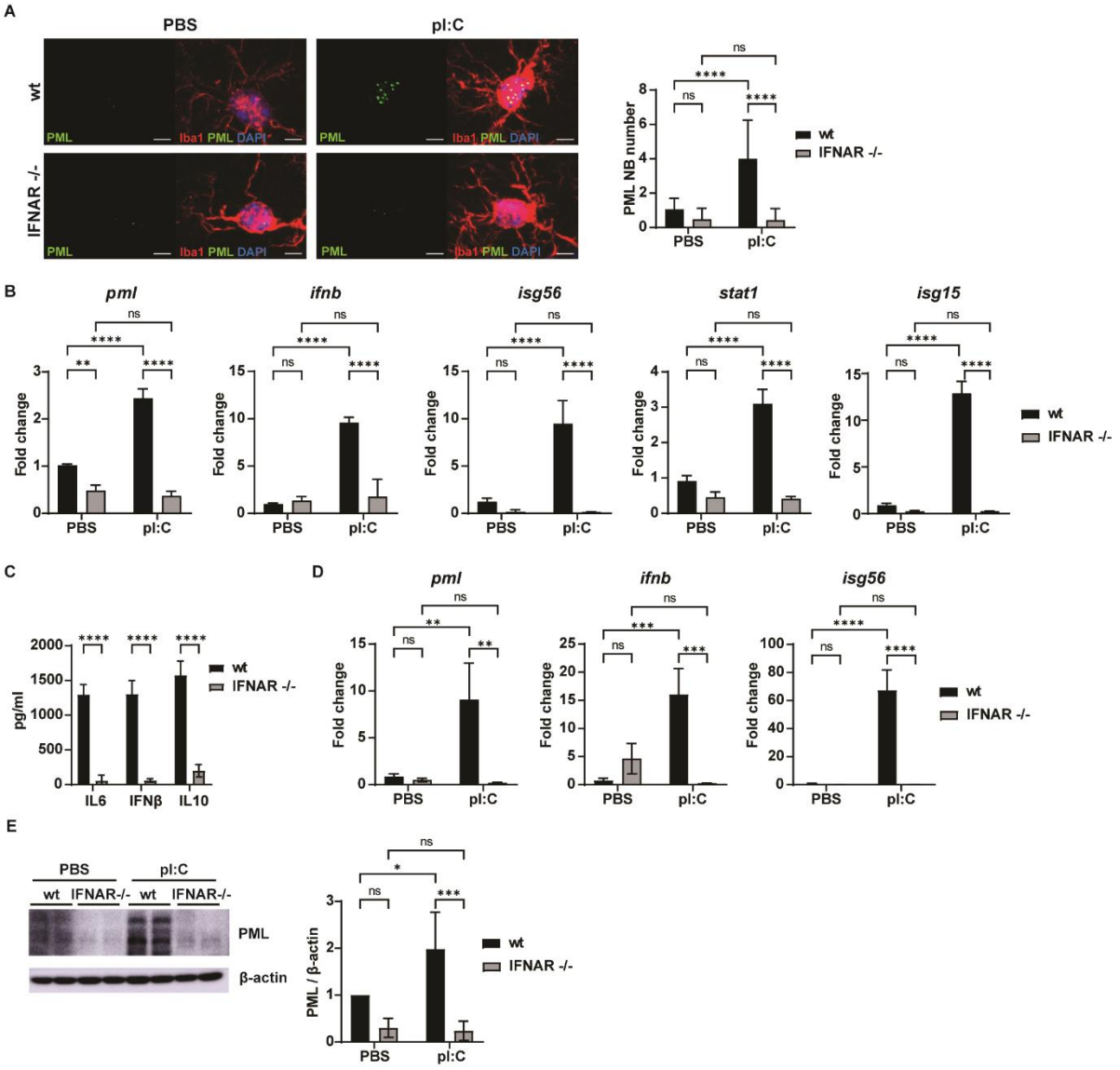

Fig. 29: PML is an ISG.
(A) Representative confocal images of PML-NBs in IFNAR -/- microglia upon pI:C stimulation show that PML-NB formation is not induced by pI:C stimulation in IFNAR -/- microglia. Scale bar 5µm. Bar plots represent the PML-NB number in wt and IFNAR -/- microglia upon PBS and pI:C stimulation. n=3, 2-way ANOVA.
(B) ISG transcription is not induced upon pI:C in IFNAR -/- microglia. n=3, 2-way ANOVA.
(C) Cytokine release is abrogated in IFNAR -/- BMDMs upon pI:C stimulation. n=3, 2-way ANOVA.
(D) ISG transcription is not induced upon pI:C in IFNAR -/- BMDMS. n=3, 2-way ANOVA.
(E) PML protein level is not increase upon pI:C in IFNAR -/- BMDMS. Bar plot shows the quantification of PML protein level. n=3, 2-way ANOVA.
Data are represented as mean ± SD. *p < 0.1; **p < 0.01; ***p < 0.001; ****p < 0.0001; ns, not significant.
Burcu Sivri took part in the sample collection of IFNAR -/- mice and BMDMs.
Burcu Sivri made the panels E, F, G.

4.1.3. Arsenic trioxide (ATO), an FDA-approved drug, degrades PML and prevent its upregulation upon pI:C-induced inflammation

ATO was shown to degrade PML by SUMOylation-dependent ubiquitination followed by proteasomal degradation.

First, we studied PML degradation upon 2.5 µM ATO in BMDMs. After 30 minutes of ATO treatment, high molecular-weight bands were observed (figure 30A). Those bands corresponded to SUMOylated forms of PML in line with the findings obtained using immunofluorescence, where an accumulation of SUMO2/3 proteins in PML-NBs was found (figure 30B). Upon 8 hours of ATO treatment, most of PML protein were degraded (figure 30 A&B).

Then, we investigated whether ATO could prevent PML-NBs formation and PML protein level increase. To do so, wt mice were first pretreated with 2.5 µM of ATO, 24 hours later, they were injected by i.p. with 300 µg of pI:C and were sacrificed 5 hours or 12 hours after pI:C injection. As previously shown, PML-NBs were rarely present at steady state in adult microglia and their formation was induced upon pI:C 12 hours. Interestingly, when mice were pretreated with ATO, PML-NBs were not formed (figure 30C), suggesting that ATO degrades PML-NBs and also inhibits their formation upon stimuli. We recapitulated these findings in BV2, an immortalized murine microglia cell line and in BMDMs. Similarly, pI:C induced PML protein level increase, however, when pretreated for 24 hours with ATO, PML was fully degraded, even upon additional pI:C stimulation (figure 30 D&E).

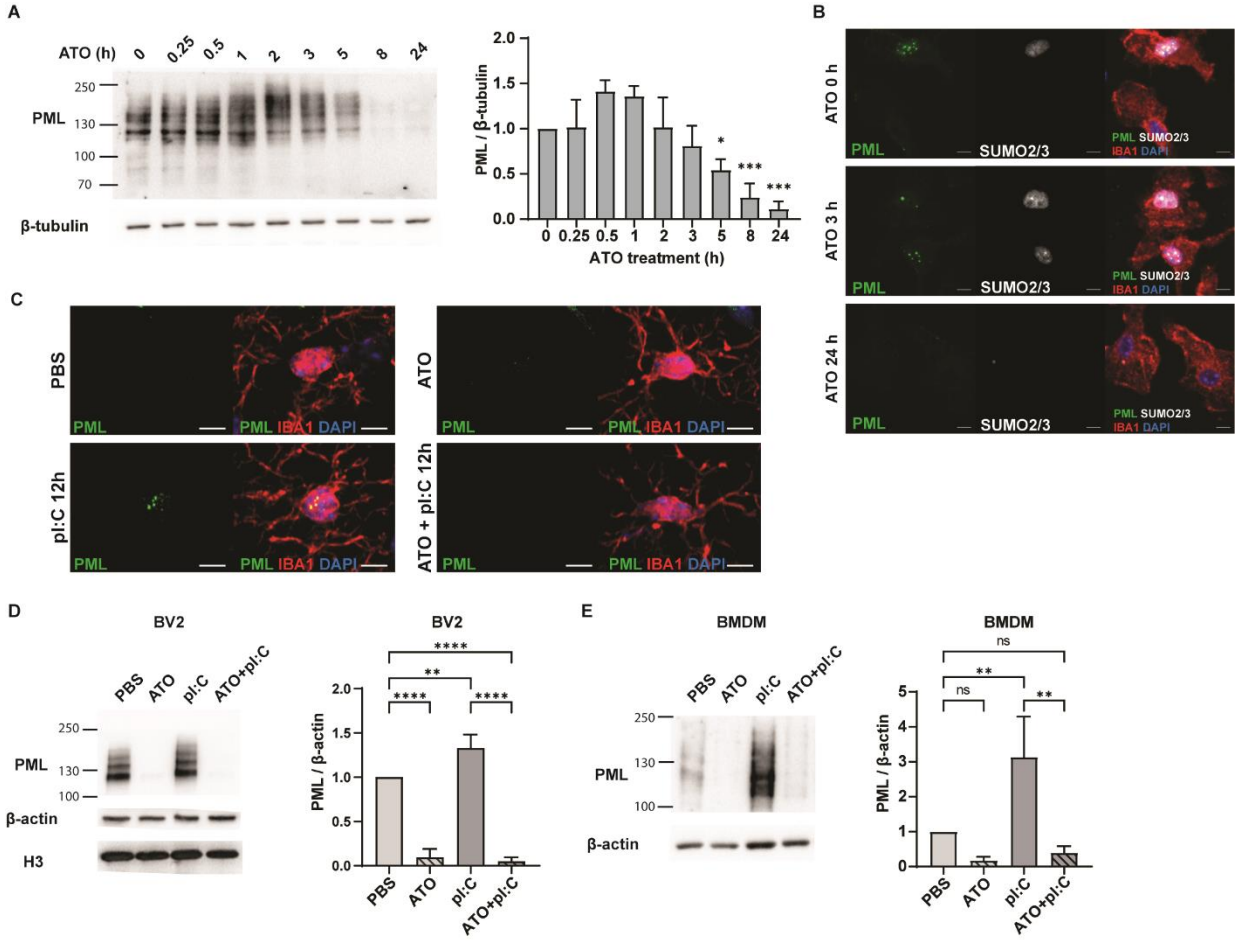

Fig. 30: PML degradation upon ATO.
(A) Western blotting assay showing PML degradation with time upon 2.5 µM of ATO. n=3; 2-way ANOVA.
(B) Representative confocal images of SUMO2/3 and PML in BMDMs show the colocalization of SUMO2/3 with the PML-NBs before their degradation upon ATO.
(C) Representative confocal images of PML in microglia upon *in vivo* ATO and pI:C stimulation. ATO pretreatment inhibits the formation of PML-NBs in microglia upon *in vivo* pI:C stimulation. Scale bars, 10 µm.
(D&E) Western blot assays showing that ATO treatment degrades and inhibits the pI:C-induced PML upregulation in BV2 (D) and in BMDMs (E). Bar plots represent the quantification of PML normalized by actin. n=6, ordinary one-way ANOVA.
Data are represented as mean ± SD. $^{*}p < 0.1$; $^{**}p < 0.01$; $^{***}p < 0.001$; $^{****}p < 0.0001$; ns, not significant.
Burcu Sivri took part in the sample collection of the ATO+pIC12 h treated mice.

4.1.4. Microglia activation markers and cytokines in the serum and BMDM supernatants are reduced with an ATO pre-treatment

Following our findings that ATO prevents PML upregulation and PML-NB formation upon pI:C, we looked at the level of inflammation upon 12 hours of pI:C in ATO pretreated mice. One common inflammation marker in microglia is the Cluster of Differentiation 68

(CD68). CD68 forms little granules in microglia processes and soma and their number and intensity increases in activated microglia. In our pI:C stimulated model, we observed that the pI:C-induced upregulation of CD68 was inhibited in mice pretreated with ATO (figure 31A). A similar trend was shown for IBA1 protein (figure 31B). We therefore hypothesize that the level of microglia activation is inhibited by ATO-pretreatment in the brain.

As ATO and pI:C were intraperitoneally injected, we checked the inflammation levels in the blood. To do so we quantified the cytokines present in the serum upon pI:C in ATO pretreated mice. Since the cytokines are only transiently present in the blood upon pI:C injection, we first determined the time-window to detect them. We were able to detect IFNβ between 3 hours to 6 hours after pI:C injection, therefore, we chose to sacrifice the mice and collect blood 5 hours after pI:C injection to check the cytokine levels in the plasma. As shown in figure 31B, most of the cytokines studied here, IFNβ, IFNα, IFNγ, IL-6, IL-10 and Cxcl10, were significantly downregulated in ATO pre-treated mice upon pI:C. Similarly, we checked the cytokine released by *in vitro* BMDM cultures upon pI:C and ATO pretreatment, discovering that 24 hours of pretreatment with ATO inhibited the pI:C-induced release of IFNβ, IL-6, IL-10 and Cxcl10 (Figure 31C). Also, the phagocytosis activity of BMDMs upon pI:C was significantly downregulated by ATO pretreatment (Figure 31D).

Taken together, our data showed that ATO pretreatment reduced several activation markers upon inflammation: CD68 level, cytokine levels and phagocytosis activity were decreased with ATO pretreatment upon pI:C stimulation.

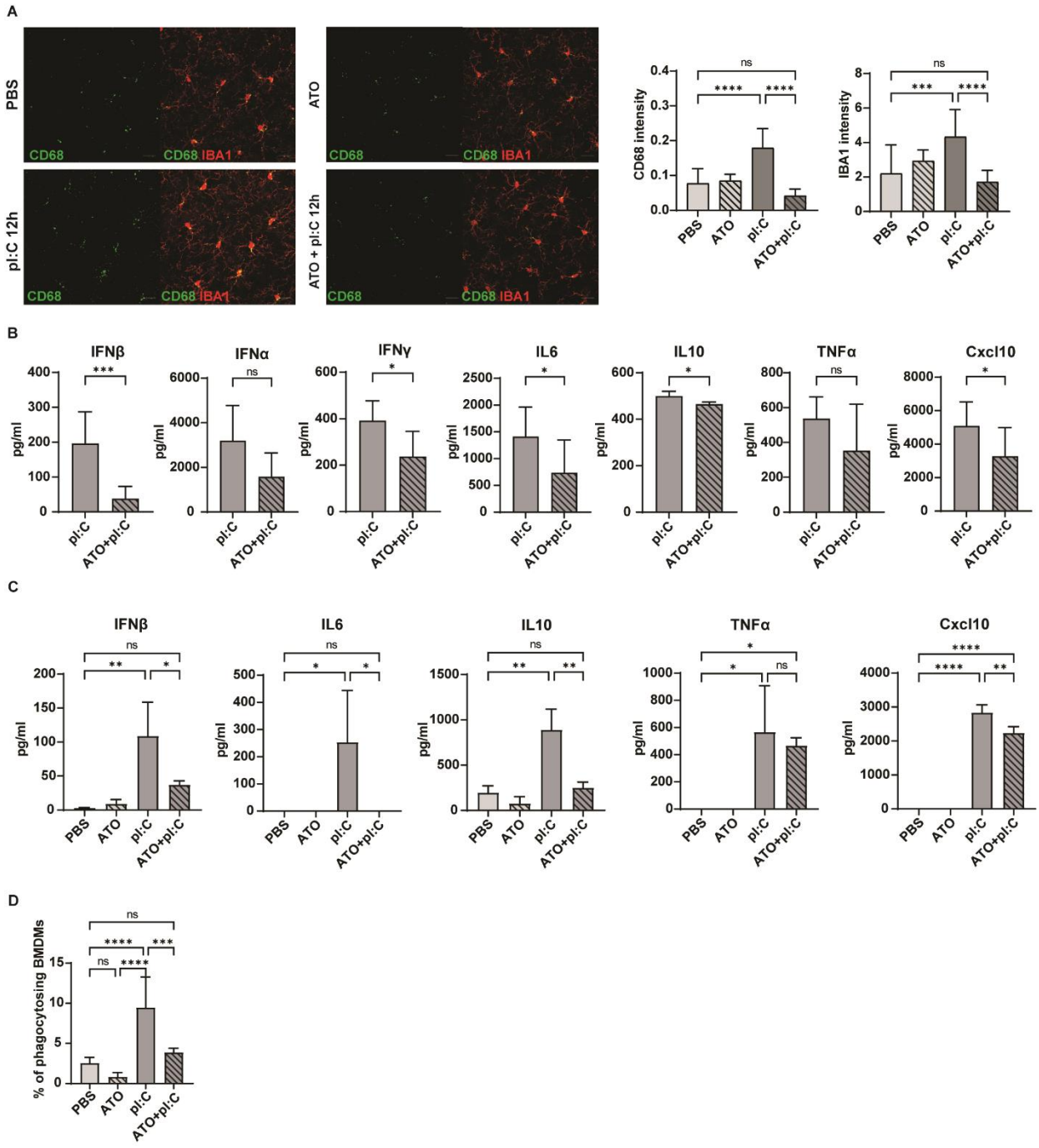

Fig. 31: ATO pretreatment inhibits the increase of inflammation markers.
(A) ATO pretreatment abrogates the CD68 and IBA1 intensity increase upon pI:C12h. n=4, scale bar, 20 µm.
(B) Bar plots showing the cytokine measurement in the serum of ATO+pI:C5h vs. pI:C5h treated mice. Upregulation of cytokines in the serum upon in vivo pI:C treatment is reduced with ATO pretreatment, n=6-9, unpaired t-test.
(C) Bar plots showing that the cytokine release by BMDMs upon hour pI:C is reduced by ATO pretreatment. n=3-6, 2-way ANOVA.
(D) Bar plot showing that the pI:C-induced phagocytosis activity of BMDMs is reduced with ATO pretreatment, biological n=2, technical, n=2; ordinary one-way ANOVA.
Data are represented as mean ± SD. $^{*}p < 0.1$; $^{**}p < 0.01$; $^{***}p < 0.001$; $^{****}p < 0.0001$; ns, not significant.

Burcu Sivri took part in the sample collection of some of the ATO+pI:C5 h treated mice and contributed to C.

4.1.5. ATO does not induce cell death in *in vitro* BMDMs nor *in vivo* microglia

ATO acts against immune-related diseases and autoimmune diseases by triggering the apoptosis of cells spreading the inflammation (K. An et al., 2020; Gao et al., 2015; C. Li et al., 2015; Ye et al., 2020). Thus, we investigated whether the inhibition of pI:C-induced inflammation by ATO pretreatment is due to immune cell death. First, we did not detect any cleaved Caspase 3 positive microglia upon ATO, pI:C, nor ATO+pI:C (figure 32A) unlike in microglia 1 day after middle cerebral artery occlusion (MCAO) (figure 32B). Secondly, the number of microglia was unchanged upon the *in vivo* ATO and pI:C treatments (figure 32C). Both results suggest that the microglia do not go into apoptosis.

In *in vitro* BMDMs culture, brightfield images showed an absence of floating/dead cells as well as a similar confluency upon treatments, suggesting that ATO and pI:C treatments, alone or in combination, do not induce *in vitro* cell death. In addition, the BMDM cell number upon 24 hours of 2.5 µM ATO was similar to the untreated condition, confirming the absence of cell death in BMDMs upon ATO treatment (figure 32E). However, at 2.5 µM, ATO induced the cell death of more than 50 % of HL60, a promyelocytic leukemia cell line derived from a APL patient (figure 32F). Higher doses than 2.5 µM of ATO treatment induced cell death of BMDMs, as shown on the dose response curve (figure 32E).

Finally, it is noteworthy that no other brain cell was positive for cleaved-Caspase 3 upon the ATO nor pI:C treatments.

Taken together, our results suggested that *in* vivo and *in vitro* ATO treatment did not induce cell death of, respectively, microglia and BMDMs.

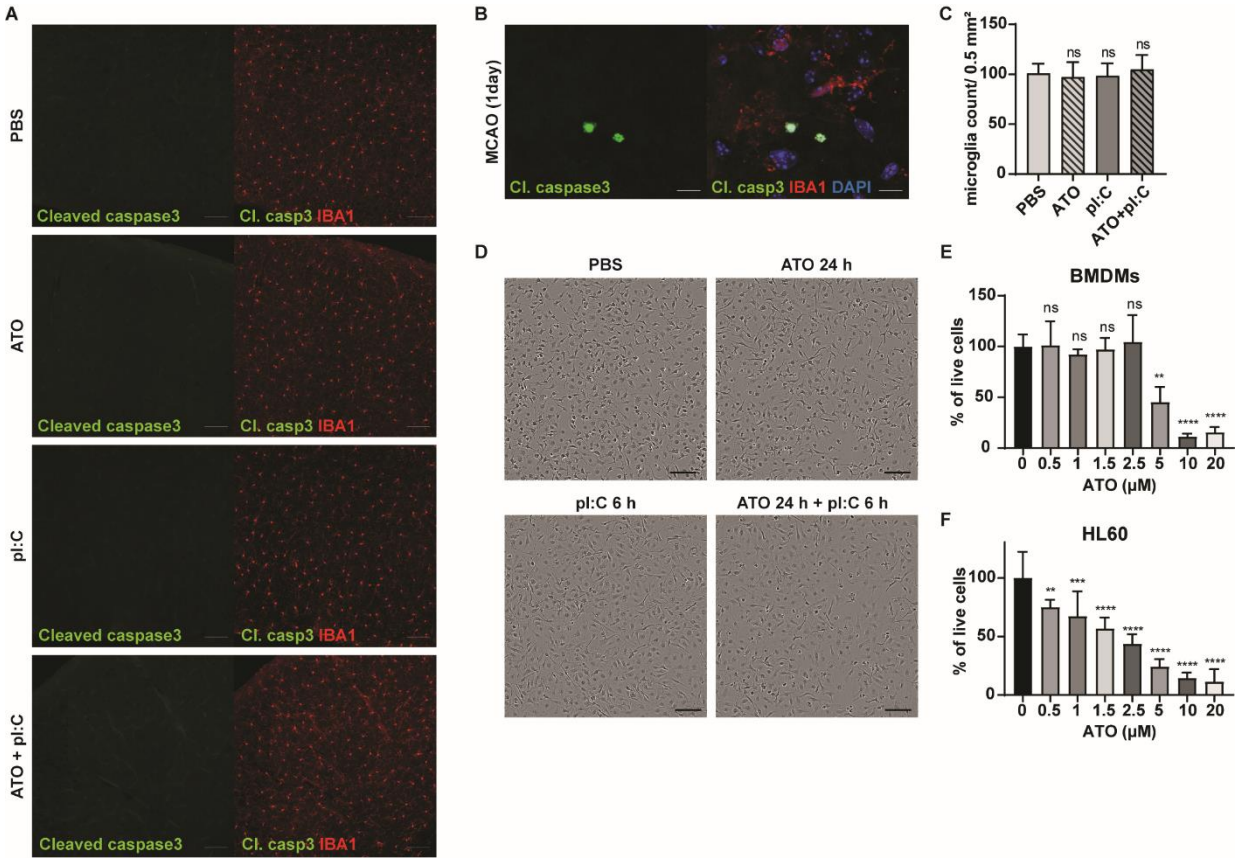

Fig. 32: Cell death is not induced upon ATO treatment in BMDMs and microglia.
(A) Representative confocal images of cleaved Caspase-3 in ATO+pI:C12h treated brains. No cleaved Caspase-3 positive cell are observed. Scale bars, 100 µm.
(B) Positive microglia for cleaved Caspase-3 in the middle cerebral artery occlusion (MCAO) model used as a positive control. Scale bars, 10 µm.
(C) Bar plot representing the microglia number per area in the ATO+pI:C12h treated brains. n=4, ordinary one-way ANOVA.
(D) Representative brightfield images of BMDMs upon pI:C with ATO pretreatment.
(E&F) Bar plots showing the percentage of live cells after 24-hour ATO treatment in BMDMs (E) and HL60 (F). n=3; ordinary one-way ANOVA.
Data are represented as mean ± SD. $^{*}p < 0.1$; $^{**}p < 0.01$; $^{***}p < 0.001$; $^{****}p < 0.0001$; ns, not significant.

4.1.1. ATO inhibits pI:C-induced biological functions

We have shown that the inhibition of inflammation marker induction upon pI:C by ATO is not due to the cell death of inflammation-spreading cells. In order to better understand the effect of ATO pretreatment, bulk RNA sequencing was performed on microglia isolated from the *in vivo* ATO and/or 12-hour pI:C-treated mice. The following three comparisons were studied: 1) ATO vs. PBS, 2) pI:C vs. PBS, 3) ATO+pI:C vs. pI:C.

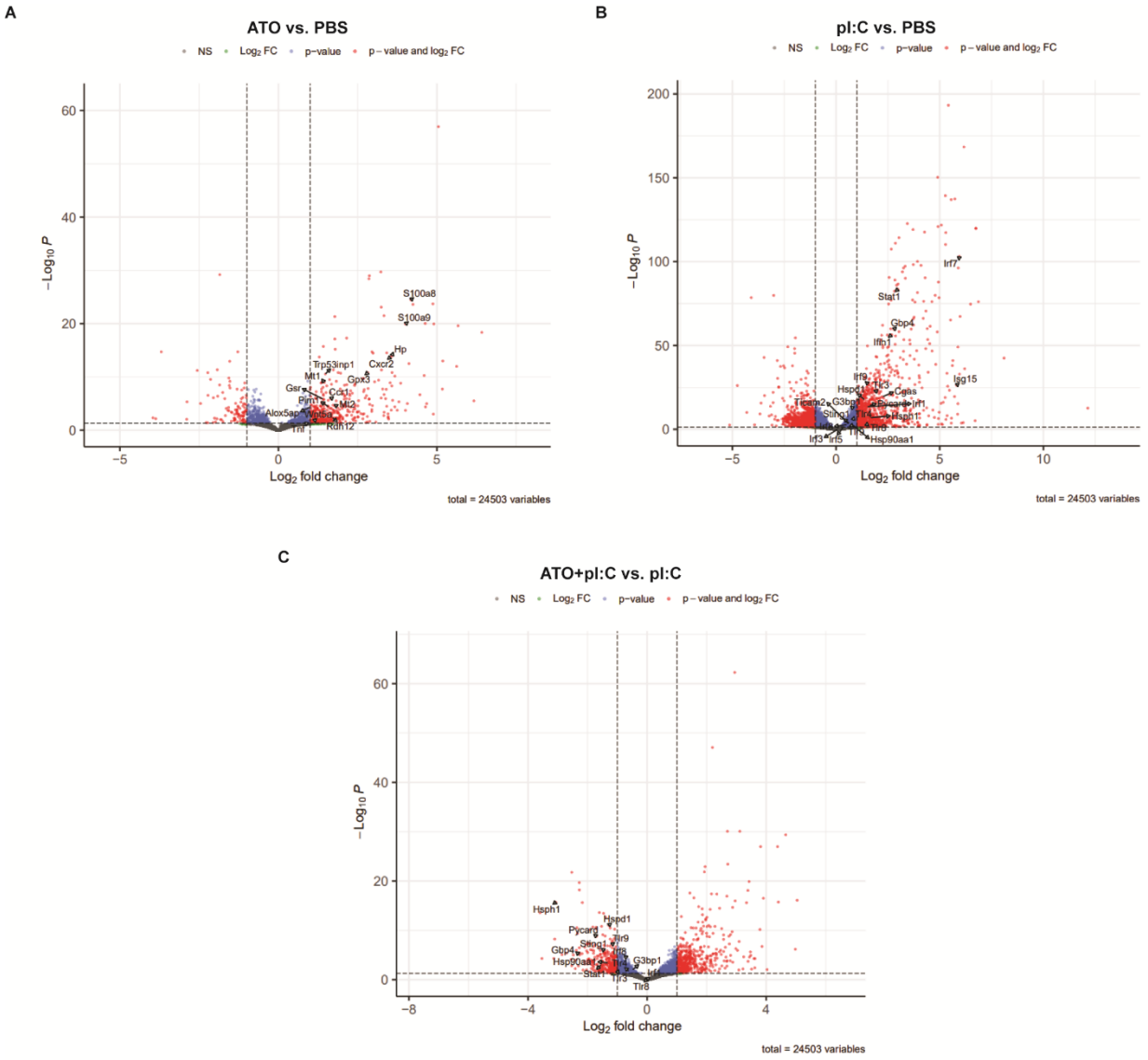

Fig. 33: Volcano plot of each comparison: pI:C vs. PBS, ATO vs. PBS and ATO+pI:C vs pI:C from the RNA sequencing of isolated microglia upon ATO and/or pI:C in vivo treatments
(plots generated by Dr. Hang Mao Lee).

The comparison ATO vs. PBS revealed 180 significantly downregulated genes and 498 upregulated genes. The downregulated genes, due to their few number, did not give any results by gene ontology analysis. The upregulated genes in ATO vs. PBS were associated with several interesting pathways, such as leukocyte chemotaxis, reactive oxygen species metabolism, and response to toxic substance/detoxification (figure 34). The latter was expected since ATO, as an anti-cancer drug, is toxic.

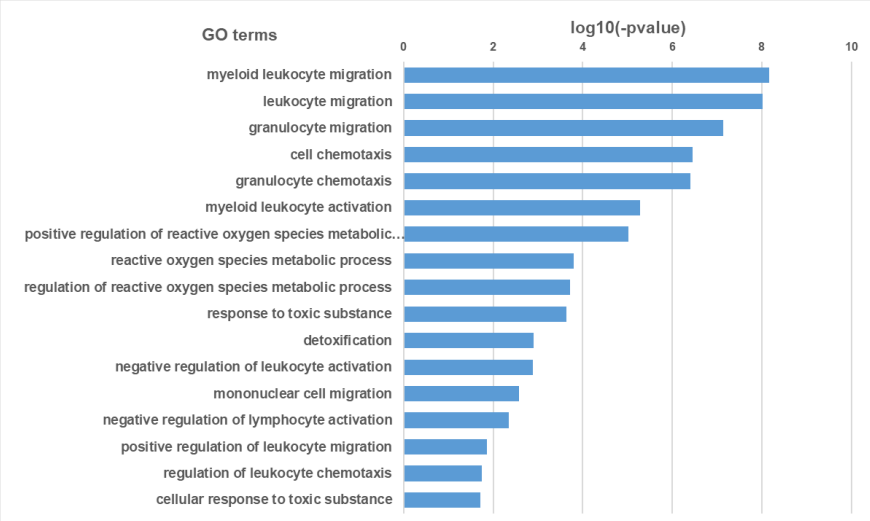

Fig. 34: Significant pathways associated with upregulated genes of ATO vs. PBS in microglia.
GO term analysis was performed on upregulated genes of ATO vs PBS in microglia by Cluego app from Cytoscape with the following settings: only GO terms with a p-value of 0.05, a level 3-4, and minimum 5 % of associated genes are displayed.

The comparison pI:C vs. PBS had the most differentially expressed genes (DEGs), with 2,818 DEGs of which 1,294 genes were upregulated (figure 33A). These upregulated genes were associated to immune-response related gene ontology (GO) terms such as positive regulation of defense response, regulation of innate immune response and response to virus, which was expected as pI:C mimics a virus infection. Interestingly, the top 10 pathways associated with the upregulated genes upon pI:C were also associated with the downregulated DEGs from the ATO+pI:C vs. pI:C comparison (figure 35A). In addition, among the 340 downregulated genes in ATO+pI:C vs. pI:C, 196 were found upregulated in pI:C vs. PBS comparison (figure 35B). This suggests that ATO downregulates genes which are induced upon pI:C and those genes are associated with immune-related pathways.

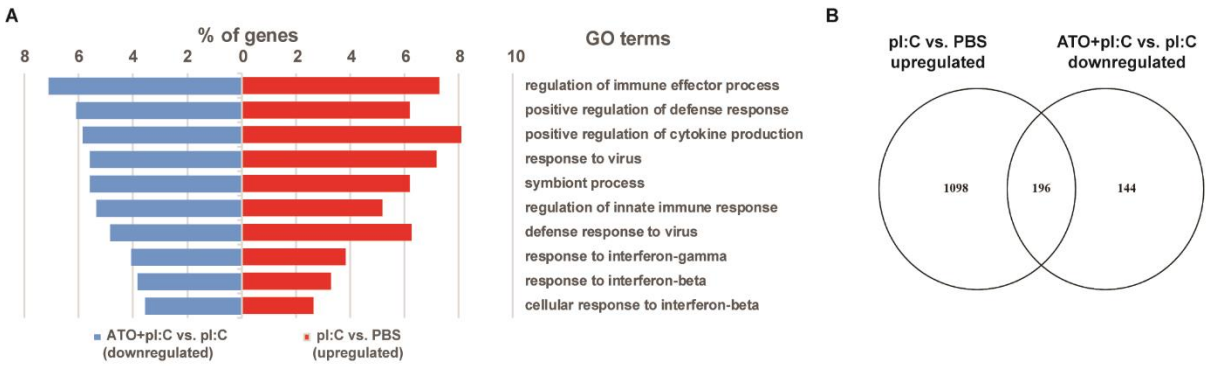

Fig. 35: Biological processes associated with upregulated genes upon pI:C compared to PBS are also associated with the downregulated genes in ATO+pI:C vs. pI:C.
(A) Bar plots showing the percentage of DEGs belonging to the top 10 significant biological functions associated with the upregulated genes of pI:C vs. PBS. n=4.
(B) Venn diagram of the upregulated genes upon pI:C and downregulated genes in ATO+pI:C vs. pI:C showing 196 common genes.

From the functional analysis of the downregulated genes in ATO+pI:C vs pI:C comparison, three main biological functions arise: type I IFN production, the antigen processing/presentation and the protein folding (figure 36). These biological pathways are detailed below.

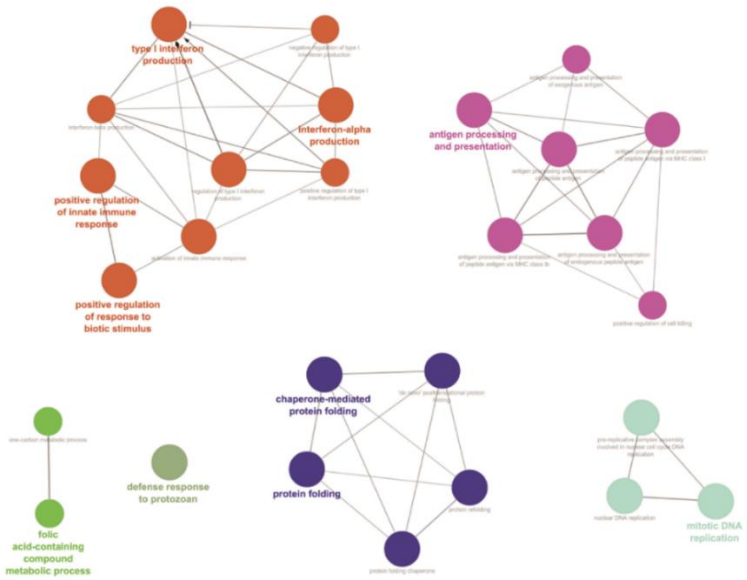

Fig. 36: Biological functions associated with the downregulated genes in microglia upon ATO+pI:C compared to pI:C.
Cluego app from Cytoscape was used with the following settings: only GO terms with a p-value of 0.05, a level 2-4, and minimum 10 % of associated genes are displayed.

4.1.2. ATO inhibits the activation of the interferon response in *in vivo* microglia and in *in vitro* human PBMC-derived monocytes

The functional analysis revealed that the “type I interferon production” biological function was associated with the downregulated genes in ATO+pI:C compared to pI:C in isolated microglia, we therefore sought to validate it. We found that ISGs, such as *pml*, *isg56*, *isg15*, *stat1* and *ifnb* itself, which were upregulated upon pI:C were downregulated with ATO pretreatment (Figure 37A). This was confirmed by the heatmap representing the 50 most significantly downregulated genes in ATO+pI:C vs. pI:C: the genes belonging to the “type I interferon production” were induced upon pI:C, and a pretreatment with ATO inhibited their induction (figure 37B).

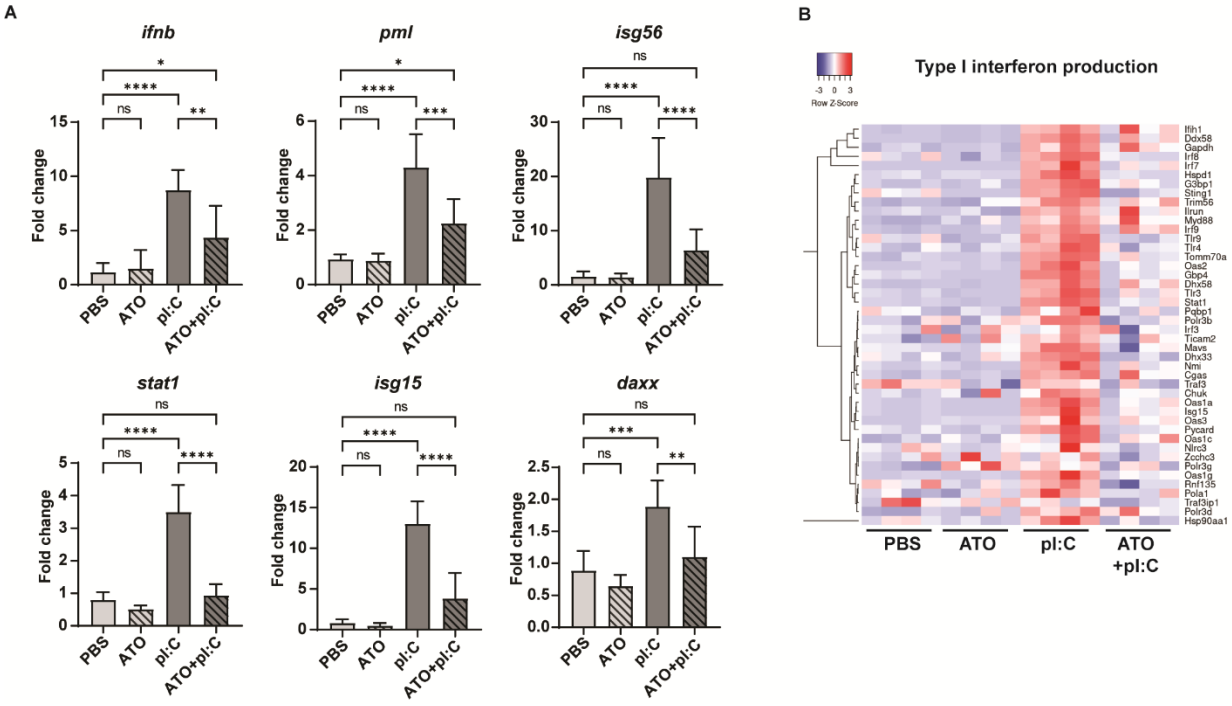

Fig. 37: ATO pretreatment inhibits the interferon response upon pI:C in *in vivo* microglia.
(A) ISGs transcription level in microglia shows that ATO pretreatment inhibits their upregulation upon pI:C stimulation. n=4; ordinary one-way ANOVA.
(B) Heatmap of the top 50 most significant DEGs of ATO+pI:C vs pI:C in *in vivo* microglia related to the “Type I interferon production” biological function.
Data are represented as mean ± SD. *p < 0.1; **p < 0.01; ***p < 0.001; ****p < 0.0001; ns, not significant.

Furthermore, we studied the effect of ATO in pI:C-treated human derived macrophages from 6 different patients, 4 females and 2 males. The buffy coats analyzed were kindly

provided by the University Hospital of Bonn. To do so, we isolated and derived peripheral blood mononuclear cells (PBMCs) into macrophages, which were pretreated with ATO 2.5 µM for 24 hours, followed by 150 µg/ml of pI:C. The cells were collected 6 hours after pI:C treatment and the RNA was isolated and processed for total RNA sequencing. Similarly to the RNA sequencing analysis performed on the *in vivo*-treated microglia shown above, we focused on the upregulated genes upon pI:C compared to PBS-treated cells and on the downregulated genes upon ATO+pI:C vs pI:C stimulation. The functional analysis revealed that the biological functions associated with the upregulated genes upon pI:C were downregulated with ATO pretreatment (figure 38A). Interestingly, these biological processes were all related to immune response. Confirming the RNA sequencing data, the upregulation upon pI:C of the tested ISGs was inhibited by ATO pretreatment (figure 38B). Altogether, our results showed that ATO inhibits the pI:C-induced IFN response in *in vivo* microglia as well as in human PBMC-derived macrophages.

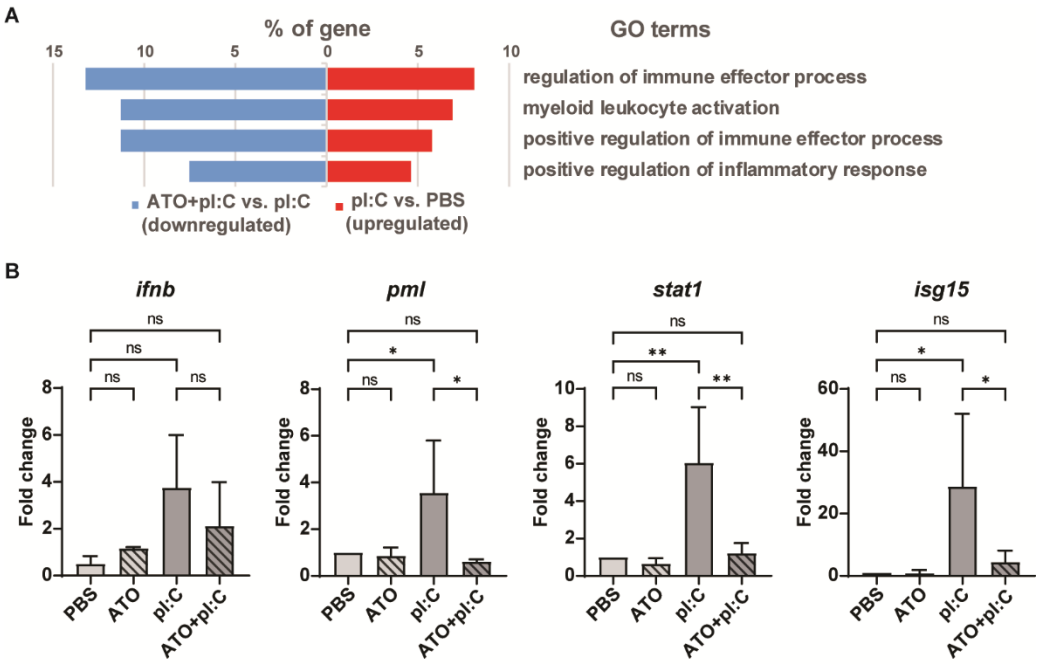

Fig. 38: ATO pretreatment inhibits the pI:C-induced interferon response in *in vitro* PBMC-derived macrophages.
(A) Bar plots showing the percentage of DEGs belonging to the top 4 significant biological functions associated to the upregulated genes in pI:C vs. PBS. n=6.
(B) ISGs transcription level in PBMC-derived macrophages shows that ATO pretreatment inhibits their upregulation upon pI:C stimulation. n=4; ordinary one-way ANOVA.

Data are represented as mean ± SD. *p < 0.1; **p < 0.01; ***p < 0.001; ****p < 0.0001; ns, not significant.
Burcu Sivri performed the differentiation as well as the *in vitro* stimulation and she took part in the *in vitro* PBMC culture and collection.

4.1.3. ATO inhibits the protein folding response *in vivo* microglia

In addition to the “Type I interferon production” function, the “protein folding” biological function was associated to the downregulated genes in ATO+pI:C vs pI:C from brain-isolated microglia (figure 36). On the heatmap representing the 50 most significant DEGs in ATO+pI:C vs. pI:C belonging to the “protein folding” GO term, we observed that those genes were upregulated upon pI:C, and ATO inhibited their upregulation upon pI:C to remain at a steady-state level (figure 39A). From the genes displayed on the heatmap, we noticed that many of them were heat-shock-related proteins of which we confirmed few of them in figure 39D.

We then investigated if there was a common transcription factor affected by ATO. To do so, a transcription factor enrichment analysis (TFEA) was carried out using ChEA3, a web tool created by Maayan lab (Keenan et al., 2019). The TFEA revealed that the transcription factor HSF1 was the most enriched transcription factor from the downregulated genes of ATO+pI:C vs. pI:C belonging to the “protein folding” GO term (figure 39B) and interestingly, *hsf1* upregulation upon pI:C stimulation was also inhibited by ATO pretreatment (figure 39C).

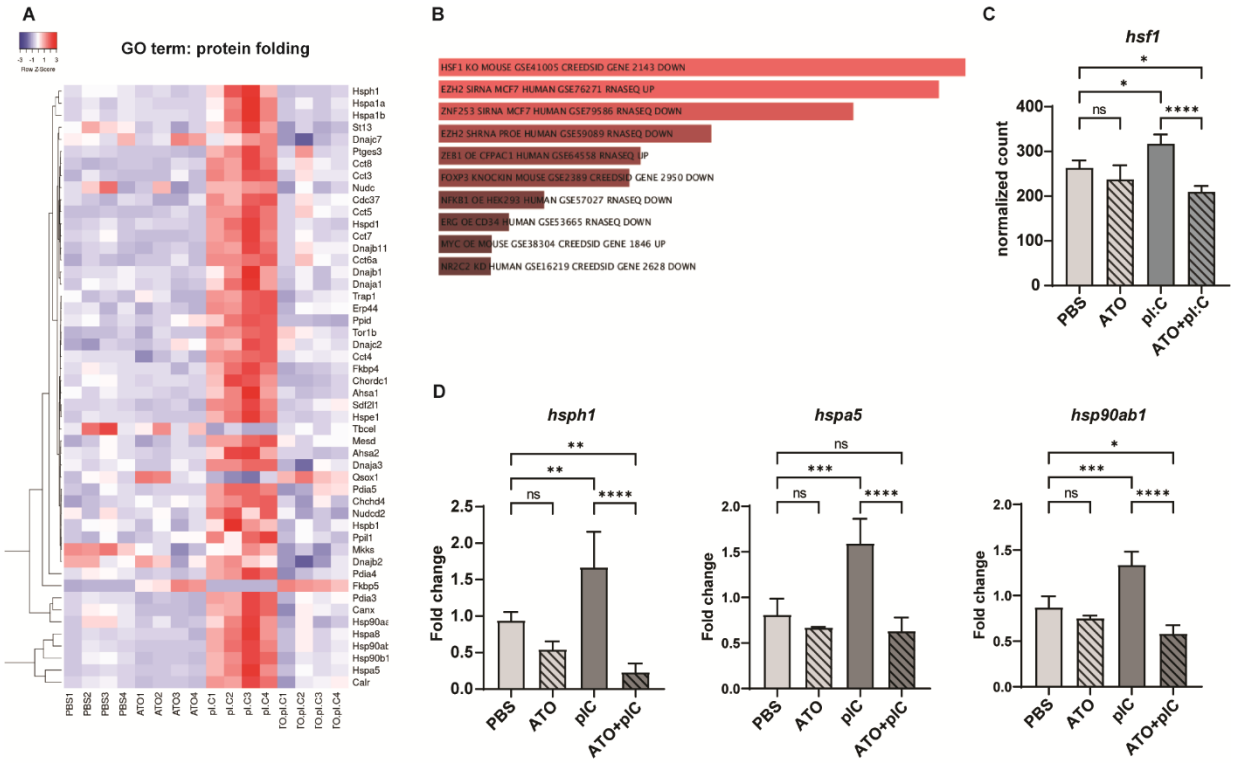

Fig. 39: ATO pretreatment inhibits the protein folding process upon pI:C in *in vivo* microglia.
(A) Heatmap of the top 50 most significant DEGs of ATO+pI:C vs pI:C in *in vivo* microglia related to the “Protein folding” biological function.
(B) Transcription factors enrichment analysis on the downregulated genes of ATO+pI:C vs pI:C in *in vivo* microglia.
(C) Normalized count of *hsf1* gene from the RNA sequencing dataset of brain isolated microglia. n=4, ordinary one-way ANOVA.
(D) Transcription level of hsf1-induced genes in microglia upon in vivo treatment with ATO and pI:C. n=4, ordinary one-way ANOVA.
Data are represented as mean ± SD. *p < 0.1; **p < 0.01; ***p < 0.001; ****p < 0.0001; ns, not significant.

4.1.4. ATO inhibits STAT1 phosphorylation without affecting primary signaling pathways such as TBK1

We have shown that ATO pretreatment inhibits pI:C-induced activation of microglia. We thus investigated pI:C-induced signaling pathways. In a simplified manner, upon pI:C binding TLR3, TRIF induces the phosphorylation of TBK1, which in turn phosphorylates IRF3 and IRF7 transcription factors. Once phosphorylated, IRF3 and IRF7 translocate to the nucleus and induce the transcription of type I IFNs. This primary IFN production is then amplified by IFNs themselves by binding IFNAR and triggering the

phosphorylation and activation of STATs by JAK1/2. STATs transcription factors lead to the amplification of IFN production as well as the transcription of ISGs.

We hypothesized that ATO could indirectly or directly act on the primary signaling, i.e. TLR3/TBK1/IRF, or/and on the IFN pathway, i.e. IFNAR/JAK/STAT (figure 40).

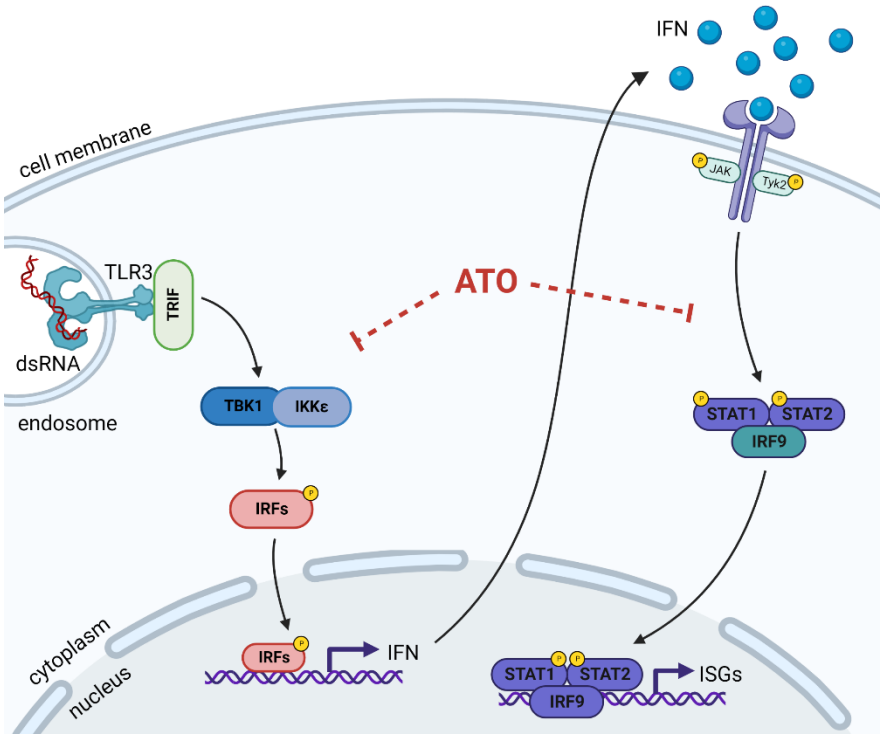

Fig. 40: Potential targets of ATO for repressing pI:C-induced inflammation.

Since ATO pretreatment inhibited the transcription of ISGs as well as production and release of cytokines upon pI:C stimulation, we first studied the phosphorylation of STAT1. We found that 24-hour ATO pretreatment inhibited STAT1 phosphorylation upon 6-hour pI:C stimulation in BMDMs and BV2 cells (figure 41 A&B).

We still need to investigate the TBK1/IRF pathway leading to the primary IFN production in order to assess whether TBK1 phosphorylation is affected by ATO pretreatment.

By checking MAPK P38 which is phosphorylated upon pI:C stimulation, we found that the phosphorylation of MAPK P38 was almost fully abrogated by ATO pretreatment in BMDMs and BV2 (figure 41 A&B). However, as the function of MAPK P38 is not fully understood yet in inflammation, we did not investigate this pathway further and we focused on TBK1/IRF and JAK/STAT pathways.

Since STAT1 phosphorylation was shown to be inhibited by SUMO conjugation (Begitt et al., 2011), we investigated the SUMOylation profile upon ATO and pI:C.

SUMO conjugation by covalent or non-covalent bonds present a weak interaction and proteins are easily deSUMOylated. SUMOylated proteins are thus only detectable by lysing the cells with Laemmli. In BV2 and BMDMs, pI:C induced an increase of SUMOylation, especially of high molecular-weight proteins. Interestingly, this increase of SUMOylated proteins upon pI:C was abrogated by ATO pretreatment (figure 41 C&D).

Taken together, our data suggested that the decrease of cytokine release was due, partially at least, to an inhibition of STAT1 phosphorylation by ATO.

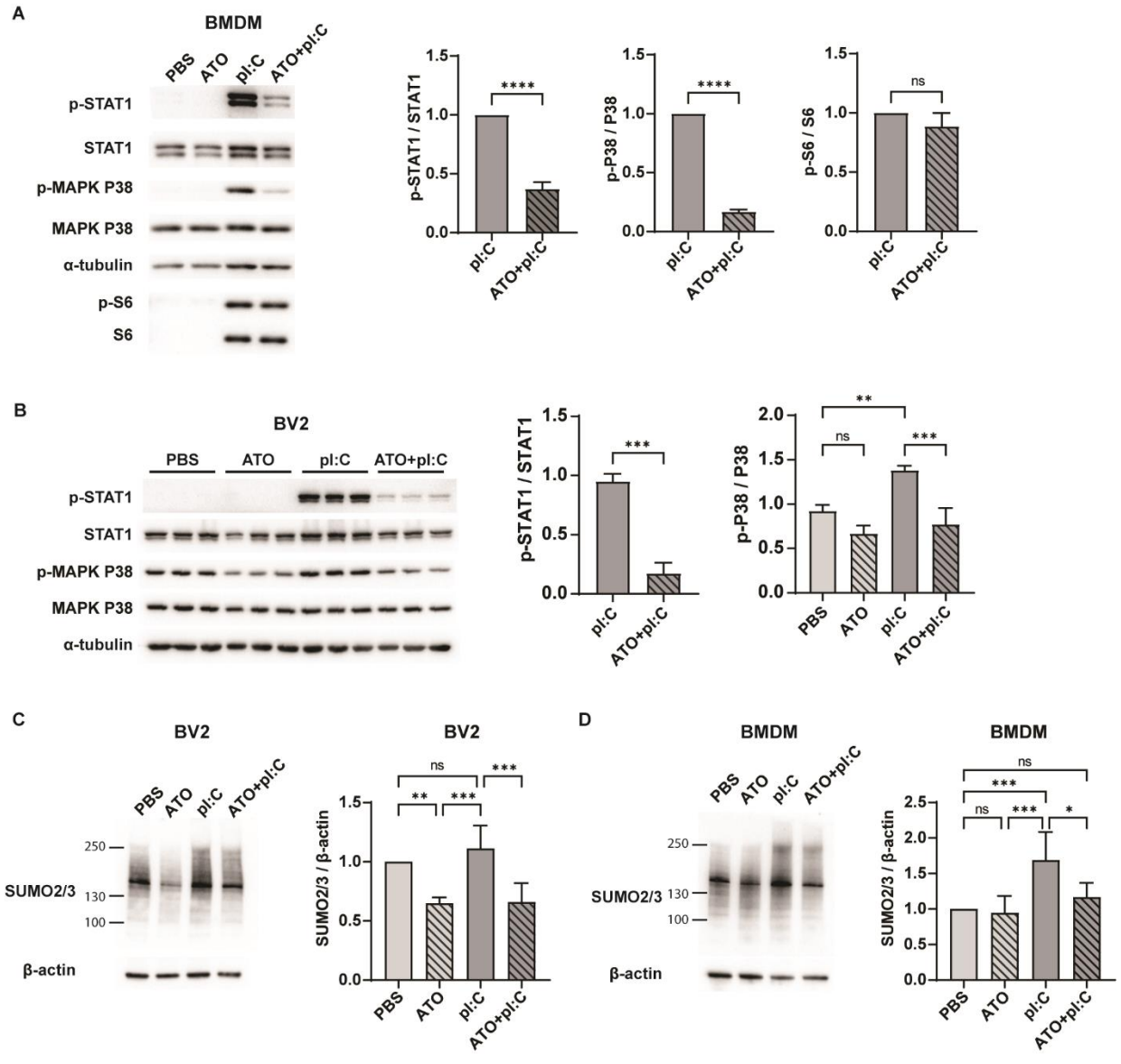

Fig. 41: ATO inhibits the phosphorylation of STAT1 and MAPK P38.

(A) Western blotting showing the phosphorylation and total levels of STAT1, MAPK P38, S6, TBK1 in BMDMs pretreated with ATO and stimulated with pI:C. Bar plots represent the phosphorylated level normalized to the total level of each protein. n=3, t-test
(B) Western blotting showing the phosphorylation and total levels of STAT1 and MAPK P38, in BV2 pretreated with ATO and stimulated with pI:C. Bar plots represent the phosphorylated level normalized to the total level of each protein. n=3, t-test and ordinary one-way ANOVA.
(C&D) Western blot assays of SUMO2/3 in BV2 (F) and BMDMs (G) upon ATO pretreatment and pI:C stimulation. n=5-6; ordinary one-way ANOVA.
All data are represented as mean ± SD. $^{*}p < 0.1$; $^{**}p < 0.01$; $^{***}p < 0.001$; $^{****}p < 0.0001$; ns, not significant.

4.1.5. Inhibition of inflammation by ATO is partially dependent on PML

Our data showed that ATO inhibits pI:C-induced inflammation and that PML is upregulated in microglia upon IFN-mediated inflammation. Also, literature has suggested that PML is required to induce inflammation upon viral infection. We therefore investigated the PML dependency of ATO's inhibition of inflammation. To do so, we compared wt and PML KO mice upon ATO+pI:C treatment described previously.

We found that the pI:C-induction of ISGs was reduced in PML KO microglia, and that ATO pretreatment further inhibited the ISG transcription (figure 42A). Similarly, PML KO brains showed lower level of CD68 activation marker upon pI:C than wt mice, and ATO pretreatment further decreases CD68 level in PML KO brains (figure 42B).

As ATO and pI:C were injected intraperitoneally, we quantified the cytokines present in the serum of wt and PML KO mice upon ATO+pI:C stimulation. Surprisingly, we found that PML KO mice presented a higher level of IFNβ, while no difference were observed for other cytokines. Furthermore, similarly to wt mice, ATO pretreatment lowered the cytokine levels in the serum (figure 42C).

After studying the response to pI:C+ATO in PML KO microglia, we investigated it in BMDMs. Unlike PML KO microglia, PML KO BMDMs did not indicate a reduced transcription level upon pI:C compared to wt BMDMs (figure 43A). Also, in PML KO BMDMs, the phosphorylation of STAT1 was increased upon pI:C and decreased with ATO pretreatment similarly to wt BMDMs (figure 43B). By quantification of cytokines released by BMDMs, no difference were found between wt and PML KO BMDMs release

of IFNβ, IL-6 and Cxcl10 upon pI:C and ATO+pI:C. However, higher levels of IL-10 and lower levels of TNFα in PML KO upon pI:C and ATO+pI:C were observed (figure 43D).

As discussed earlier, the overall SUMOylation was elevated upon pI:C and this was inhibited by ATO pretreatment. Interestingly, the PML KO BMDMs tended to show, overall, lower level of SUMOylation and they did not show any increase of SUMOylation upon pI:C (figure 43C).

Taken together, we showed that PML deletion reduced pI:C-induced inflammation similarly to ATO. We also shown that the pI:C-induced ISGs transcription seemed further inhibited by ATO in PML KO microglia, suggesting that the mechanism of action of ATO might also be independent on PML. Furthermore, we showed that ATO's inhibition of STAT1 phosphorylation was also independent of PML. Further experiments will need to be carried out in order to understand ATO's mechanism better.

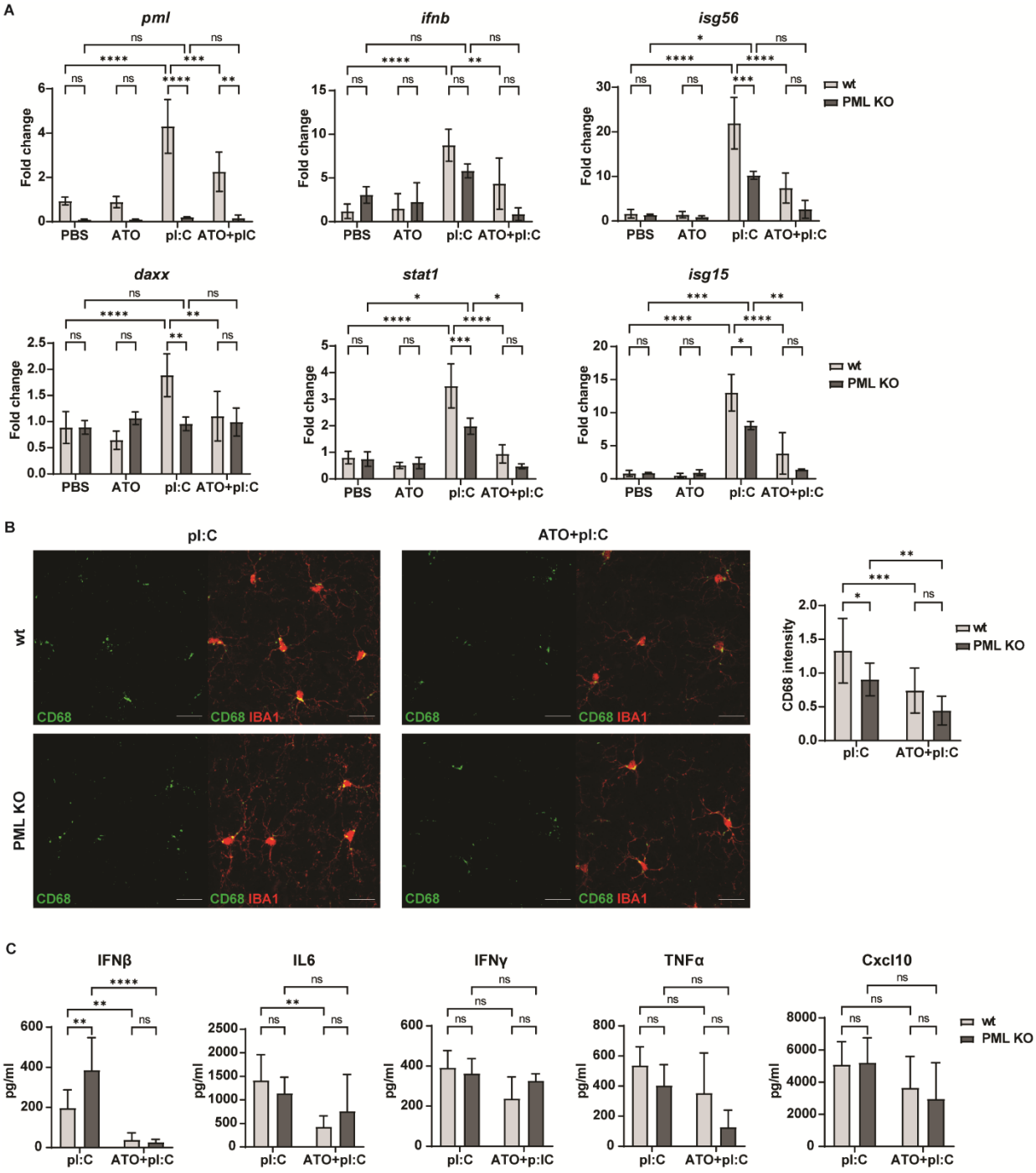

Fig. 42: Effect of ATO in *in vivo* PML KO microglia.
(A) Bar plots showing that the pI:C-induced transcription of ISGs is reduced in PML KO microglia, and ATO has an additional downregulation effect to PML deletion. n=3, 2-way ANOVA.
(B) Representative confocal images of CD68 marker in PML KO microglia upon pI:C and ATO+pI:C. n=3, 2way ANOVA.
(C) Bar plots showing the cytokine measurement in the serum of ATO+pI:C vs. pI:C treated wt and PML KO mice. n=6, 2-way ANOVA.
All data are represented as mean ± SD. $^{*}p < 0.1$; $^{**}p < 0.01$; $^{***}p < 0.001$; $^{****}p < 0.0001$; ns, not significant.

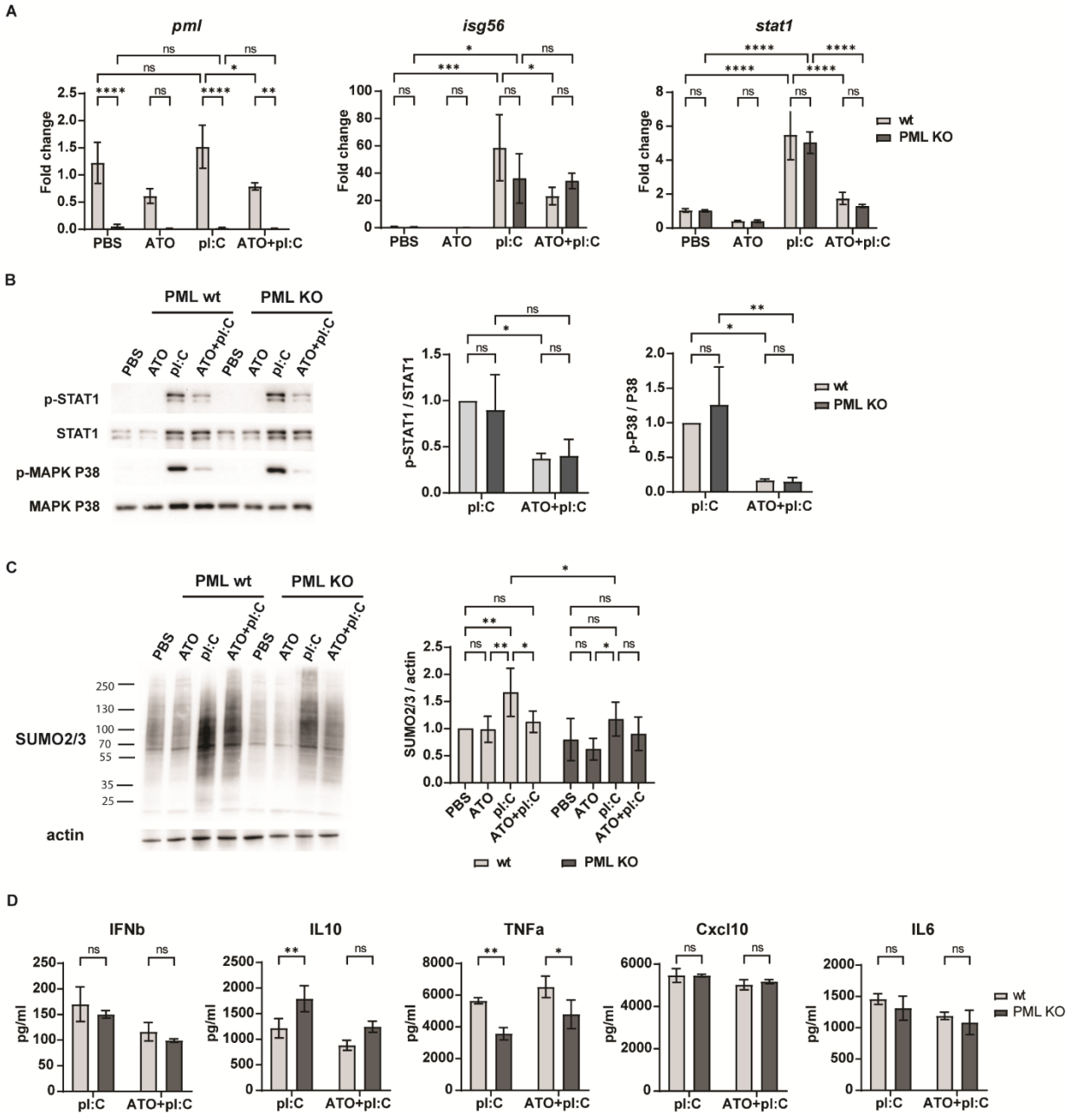

Fig. 43: Effect of ATO in *in vitro* PML KO BMDMs upon pI:C stimulation.
(A) Bar plots showing that the transcription level of ISGs in wt and PML KO microglia upon pI:C with ATO pretreatment. n=3, 2-way ANOVA.
(B) Western blot analysis of phosphorylated and total level of STAT1 and MAPK P38 in wt and PML KO BMDMs upon pI:C with ATO pretreatment. n=3, 2-way ANOVA.
(C) Western blot assay of SUMO2/3 in wt and PML KO BMDMs upon ATO pretreatment and pI:C stimulation. n=5-6; 2-way ANOVA.
(D) Bar plots showing the cytokine release of ATO+pI:C vs. pI:C treated wt and PML KO BMDMs. n=3, 2-way ANOVA.
All data are represented as mean ± SD. $^{*}p < 0.1$; $^{**}p < 0.01$; $^{***}p < 0.001$; $^{****}p < 0.0001$; ns, not significant.

4.1.6. ATO in RQ

After showing that ATO inhibits pI:C-induced inflammation by a mechanism involving the inhibition of STAT1 phosphorylation, we investigated ATO's potential in MDA5 RQ mice. For this purpose, wt and MDA5 RQ mice were i.p. injected once per day, for 6 days, with 2.5 µg/g of ATO and were collected on the 7th day. Preliminary data are shown from the analysis of 2 mice per group.

Interestingly, ATO showed a tendency to decrease PML-NB number in MDA5 RQ microglia, as well as in neurons (figure 44 A, B&C). Furthermore, the activation of MDA5 RQ microglia seemed also reduced by ATO, indeed, treated microglia harbored less and thinner branches, in addition to a lower CD68 activation marker (figure 44 D&E). It is worth mentioning that at steady state, despite harboring an activated morphology, MDA5 RQ microglia did not show higher CD68 level than wt microglia.

Similarly to wt BMDMs, and despite MDA5 RQ BMDMs having higher level of total STAT1 than wt BMDMs upon pI:C (figure 44F), we showed that ATO inhibited STAT1 phosphorylation in MDA5 RQ BMDMs as well (figure 44F). Also, the downregulation of

p-STAT1 in MDA5 RQ BMDMs by ATO is also correlated to a decrease in cytokine release upon pI:C (figure 44G).

Taken together, long term ATO treatment seemed to reduce the inflammation in the MDA5 RQ model, however, further confirmation is required.

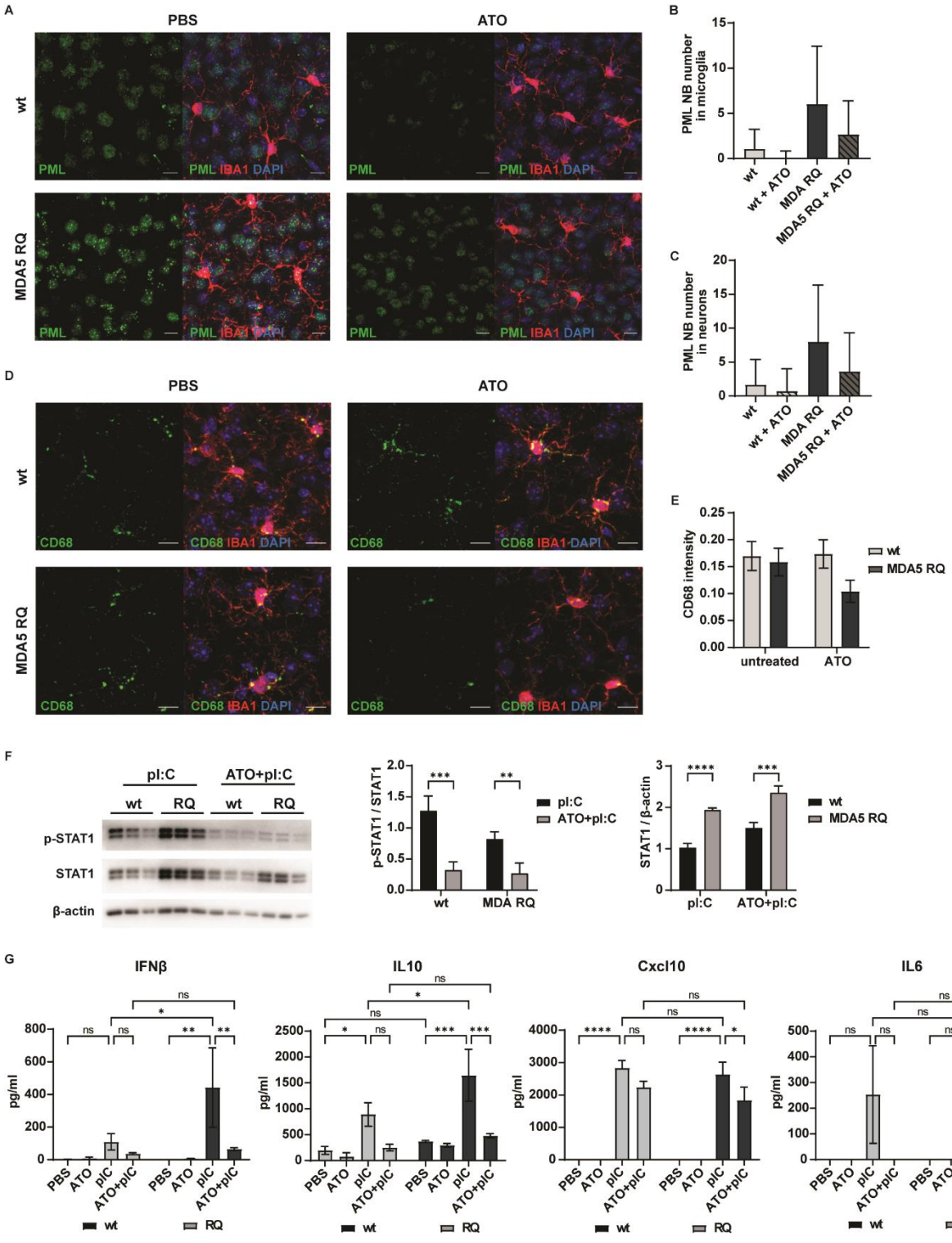

Fig. 44: ATO reduces the inflammation in MDA5 RQ microglia and BMDMs.
(A) Representative confocal images of PML in MDA5 RQ brain. Scale bars, 10 µm.
(B&C) Bar plots show that PML-NBs number tend to decrease in microglia (B) and in neurons (C) upon 6 consecutive days of ATO treatment in MDA5 RQ mice. n=2.
(D) Representative confocal images of CD68 in MDA5 RQ brain. Scale bars, 10 µm.
(E) Bar plot shows that CD68 seems to be reduced by 6-days ATO treatment in MDA5 RQ brain. n=2.
(F) Western blot assay showing a decrease of STAT1 phosphorylation in wt and MDA5 RQ BMDMs upon ATO+pI:C compared to pI:C. Bar plots represent the ratio of phosphorylated vs. total STAT1 level, and the quantification of total STAT1. n=3, t-test.
(G) Level of cytokine release by MDA5 RQ BMDMs. ATO inhibits the cytokine release by MDA5 RQ BMDMs upon pI:C. n=3-6; 2-way ANOVA.
Data are represented as mean ± SD. $^{*}p < 0.1$; $^{**}p < 0.01$; $^{***}p < 0.001$; $^{****}p < 0.0001$; ns, not significant.
Burcu Sivri performed the ATO injections, took part in the mice collection and BMDMs culture, she also contributed to F.

4.1.7. ATO inhibits the cytokine release in DAXX KO BMDMs

DAXX deletion in microglia and BMDMs induces an inflammatory response with type-I IFN signature (data unpublished, Georgopoulou et al.). We thus investigated the presence of PML-NBs in this model. To do so, DAXX fl/fl mice were crossed with an inducible microglia-specific Cx3cr1-Cre-ERT2 line which resulted in DAXX deletion in microglia upon 5 consecutive days of Tamoxifen treatment. 3 weeks after DAXX deletion, the microglia harbored activated morphology, and interestingly, PML-NBs number was increased compared to wt microglia (figure 45A).

Furthermore, we hypothesized that ATO treatment could reduce the IFN-related inflammation caused by DAXX loss. To do so, DAXX fl/fl, Rosa-CreERT2 BMDMs were cultured and the deletion of DAXX was obtained 4 days after a 24-hour pulse of Tamoxifen. Then, DAXX KO and wt BMDMs were pretreated for 24 hours with ATO, followed by a 6-hour pI:C stimulation. We observed that the pI:C-induced release of cytokines, such as IFNβ, IL-10, Cxcl10 and TNFα was highly increased in DAXX KO BMDMs compared to wt BMDMs. Nevertheless, ATO, as in wt and MDA5 RQ BMDMs, inhibited the pI:C-induced release of cytokines in DAXX KO BMDMs (figure 45).

Taken together, these findings suggested that PML is a sensor and potential mediator of IFN-induced inflammation and that ATO inhibits the cytokines release in several IFN-mediated inflammation models.

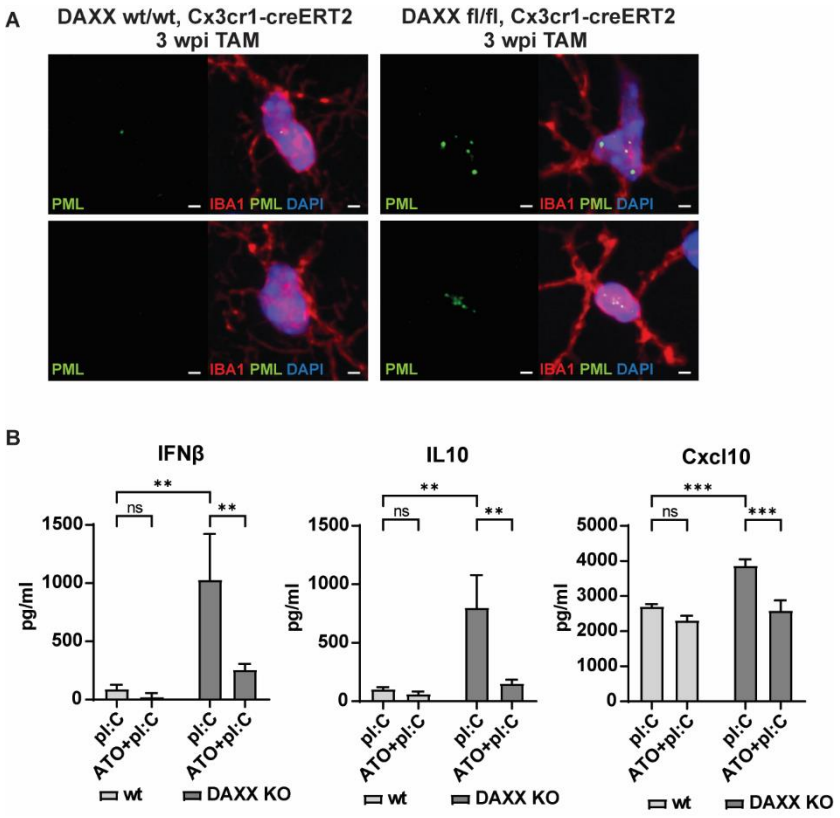

Fig. 45: ATO inhibits the cytokine release in DAXX KO model.
(A) Representative confocal images showing the increase of PML-NBs in DAXX KO microglia. Scale bars, 2 µm.
(B) Bar plots showing the release of cytokines by wt and KO BMDMs with ATO pretreatment upon 6-hour pI:C stimulation. n=3, 2-way ANOVA. Data are represented as mean ± SD. $^{*}p < 0.1$; $^{**}p < 0.01$; $^{***}p < 0.001$; $^{****}p < 0.0001$; ns, not significant.

4.1.8. PML response in other interferon-related diseases

In addition of investigating the PML response in AGS, we were also interested in expanding the research to other disease models presenting elevated type-I IFN signatures.

As a first model, we studied a stroke disease model by transient middle cerebral artery occlusion (tMCAO), where microglia were shown to be activated by IFN (Kuo et al., 2016; McDonough et al., 2017; M. Zhang et al., 2017). In this model, the interruption of blood flow to a part of the brain induces hypoxic and ischemic brain injury (Kleinschnitz et al., 2015). Activated glial cells, such as reactive astrocytes and round-shaped microglia were found around the infarct, and they were assigned to have both

detrimental and beneficial role on stroke outcome (Anttila et al., 2017; L. Li et al., 2022; Qin et al., 2019).

Brain sections from 3-days post tMCAO were kindly provided by AG Petzold (DZNE of Bonn). Interestingly, in the ipsilateral side 3-days post tMCAO, the activated microglia presented one large PML-NB and astrocytes harbored several PML-NBs. Oppositely, in the contralateral side, microglia and astrocytes were not activated and presented no PML-NB (Figure 46A).

The second model studied was a SARS-CoV-2 infected model. From the recent and extended studies on the SARS-CoV-2 infection, it was discovered that a cytokine storm, including IFNs, is induced in late stages after infection (R. P. da Silva et al., 2021; Ragab et al., 2020; Thepmankorn et al., 2021). We thus investigated the presence of PML-NBs in microglia upon SARS-CoV-2 infection in the brain.

Paraffin-embedded brains from SARS-CoV-2 infected K18-hACE2 transgenic mice with or without Nanobody treatment against SARS-CoV-2 were kindly provided by AG Kato (BMZ). Mice were collected 7 to 10 days post-infection, and viral RNA was detected in the brain only when mice were not treated with Nanobodies. The mice treated with Nanobodies will be referred as COVID “-“, while the mice not treated with Nanobodies as COVID “+”.

As indicated in figure 46B, COVID “+” mice presented an activated morphology with thick processes and bulky shape, harboring as well many PML-NBs. On the contrary, COVID ”-“ mice were lacking not only activation signs but also PML-NBs.

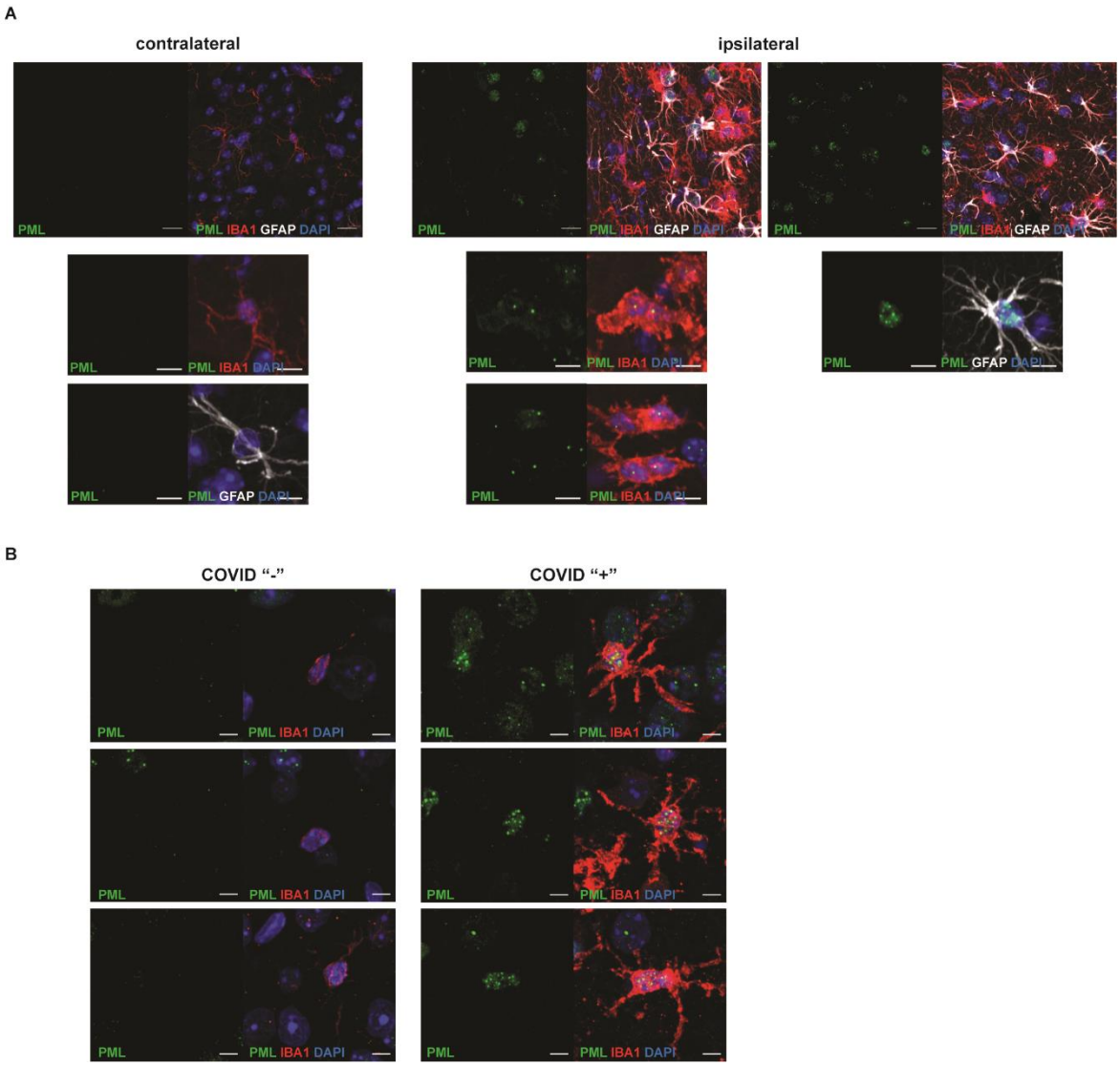

Fig. 46: PML-NBs in other disease models, MCAO and COVID, presenting high type-I IFN signatures.
(A) Representative confocal images of the contralateral and ipsilateral sides of a brain 3-days post hypoxic and ischemic injury due to tMCAO. PML-NB formation is induced in microglia and astrocytes in the ipsilateral but not contralateral side. Scale bars, 10 µm and 5 µm for close up images.
(B) Representative confocal images of PML in microglia of the SARS-CoV-2 infected K18-hACE2 transgenic mice, a COVID model. PML is increased in microglia. Scale bars, 5 µm.

4.2. Discussion

Currently, existing literature presents a lack of research about PML in microglia: not one publication reports the presence of PML in microglia. As shown in the first part of the thesis, PML-NBs are mostly present during postnatal days and disappear during adulthood at steady state.

In this study, we showed that PML transcription and PML-NB formation are induced upon IFN-mediated inflammation in microglia, such as upon pI:C-induced inflammation and in the MDA5 RQ interferonopathy mouse model. This result is in line with previous studies which have revealed an upregulation of PML upon IFN stimuli in peripheral immune cells and mouse embryonic fibroblasts (Chelbi-Alix et al., 1995; Regad et al., 2001; Regad & Chelbi-Alix, 2001; Stadler et al., 1995). Furthermore, we discovered that PML deletion leads to a reduced inflammation state of microglia, accompanied by lower expression of ISGs in microglia and lower protein level of the CD68 lysosomal marker upon pI:C stimulation. Surprisingly, PML deletion in BMDMs did not hinder the pI:C-induced ISGs transcription, neither the cytokines release, nor the phosphorylation of inflammation-mediated transcription factors, such as STAT1. These results did not confirm the previous study showing that PML deletion in mouse embryonic fibroblasts or HEK293 PML -/- cells led to reduced STAT1 phosphorylation and ISG transcription upon IFNγ (el Bougrini et al., 2011).

To explain this difference of results in BMDMs from microglia and previous studies, we suggest that *in vitro* BMDMs might respond differently to stimulation as they are already in a stimulated state due to the culture process of primary cells.

ATO was previously shown to inhibit inflammation in several autoimmune diseases by inducing apoptosis of inflammatory cells: for instance, in multiple sclerosis and in graft-versus host disease, ATO induces T cell apoptosis (K. An, Gao, 2015, li 2015), while in systemic sclerosis, it induces plasmacytoid dendritic cells apoptosis (Ye, 2020). By studying the effect of ATO upon IFN-mediated inflammation, we found that ATO inhibits the pI:C-induced inflammation in the brain and BMDMs independently on cell-death induction. Interestingly, the ATO concentration used on BMDMs induces cell death of a promyelocytic leukemia cell line.

In the CNS, several inflammation markers were inhibited by ATO, such as the CD68 lysosomal marker and the transcription of ISGs in microglia. More generally, we found that the response to interferon and other pI:C-induced pathways were not induced upon pI:C stimulation with ATO pretreatment. Therefore, we hypothesized that ATO could inhibit the interferon response by either affecting the primary signaling,

TLR3/TBK1/IRFs, or the IFN pathway, IFNAR/STATs. We further need to assess the TBK1 phosphorylation level and to optimize the detection of IRF3 phosphorylation in order to confirm that ATO does not affect the primary signaling pathway.

In the IFN pathway, we found that ATO inhibits the phosphorylation of STAT1 which could be explained by several hypotheses : 1) ATO could inhibit JAK activity, 2) ATO could activate PIAS, a STAT inhibitor, 3) ATO could induce STAT1 SUMOylation, which was shown to inhibit its phosphorylation (Begitt et al., 2011; Maarifi et al., 2015; Maroui et al., 2018). In order to support the latter hypothesis, we will assess whether a SUMO inhibitor would restore STAT1 phosphorylation upon pI:C and ATO pretreatment.

More generally, SUMOylation is involved in the regulation of inflammation (El-Asmi et al., 2020a; El-Asmi et al., 2020b; Karhausen et al., 2021; Maarifi et al., 2015; Maroui et al., 2018), however, as the study of SUMOylated proteins is very challenging, a lot is still to be understood in this mechanism. The SUMO-protein bond is weak, which makes its conjugation easily reversible and difficult to detect. In our study, we observed an increase of overall SUMOylation upon pI:C which was inhibited by ATO pretreatment. The decrease in SUMOylation upon ATO could be resulting from an ubiquitin-dependent degradation of SUMOylated proteins or an inhibition of SUMOylation. Finally, we hypothesized that the inhibition of SUMOylation by ATO could also cause the general inhibition of inflammation. Nonetheless, the role of SUMOylation in inflammation would first need to be further understood.

Interestingly, PML deletion and ATO pretreatment similarly inhibit the IFN-mediated inflammation in the CNS: lower level of CD68 lysosomal marker and lower ISG transcription in microglia were found in both models upon pI:C stimulation. These results suggest that ATO has a PML-dependent inhibitory effect on inflammation in microglia. However, ATO seems to further inhibit the transcription levels of ISGs in PML KO microglia, though the decrease is insignificant. Also, ATO inhibits the inflammation in a PML-independent manner in BMDMs: PML deletion does not affect the cytokine release and ISG transcription as mentioned previously, and ATO was found to inhibit pI:C-induced inflammation in PML -/- BMDMs. The difference of response to inflammation between PML KO BMDMs and microglia remains unclear, nonetheless, ATO’s inhibition of inflammation is similar to the one achieved by PML deletion, though it seems to be

mostly independent on PML. It is important to keep in mind that PML deletion in microglia, as well as in other peripheral immune cells, occurs at embryonic stage in our model by the Csf1r promoter, therefore compensatory mechanisms could have been acquired by the microglia to maintain their functions. In order to overcome this limitation, we are creating a new mouse model with an inducible cre system, the cre-ERT2, under the microglia specific Cx3cr1 promoter. This will allow a specific deletion of PML in microglia at any chosen time upon Tamoxifen injections.

Promising preliminary data on the MDA5 RQ interferonopathy model showed that daily injections of ATO reduces the CD68 lysosomal marker and the PML NBs number, which are correlated with high inflammation, in neurons and microglia. Therefore, we suggest that ATO could have a beneficial effect by lowering the inflammation in interferonopathy.

Yet, few limitations of this study have to be kept in mind. First, pI:C is injected intraperitoneally and is therefore transported to the brain by blood flow, however, the ability of pI:C to cross the BBB has never been assessed. We thus need to keep in mind that we might look at a peripheral inflammation inducing CNS inflammation and not a direct pI:C-induced CNS inflammation. In order to confirm the BBB crossing/diffusion and the direct binding of pI:C to TLR3 receptors of microglia, we could, for instance, tag pI:C to be able to follow its propagation in mice after injection. Secondly and similarly, ATO is also intraperitoneally injected and its ability to cross the BBB was evaluated at 18% of the ingested compound (Au et al., 2008). In addition to the lowered CNS inflammation, we also found that ATO inhibits the peripheral inflammation as shown by the reduced production and release of cytokines in the serum. Therefore, assessing the inflammation state of peripheral immune cells and their penetration into the brain have to be studied in order to get new insights on ATO's role in the CNS. Finally, it is important to keep in mind that the MDA5 RQ model shows a systemic inflammation and that since ATO is intraperitoneally injected, lowering the peripheral inflammation could also result in the reduced CNS inflammation suggested by our preliminary data. To overcome those limitation, assessing the ability of ATO to cross the BBB is necessary, as well as determining the contribution of the peripheral inflammation to the CNS inflammation in our models.

As discussed above, the role of PML in IFN-induced inflammation in microglia requires further studies. We have proven that PML-NB formation is induced in several IFN-mediated inflammation models, such as interferonopathies, pI:C-mimicking viral infection, viral infection, as well as in the MCAO stroke model. Interestingly, PML-NB formation is different in interferonopathies and pI:C induced inflammation than in the MCAO model: the microglia harbor respectively several PML-NBs in interferonopathies and pI:C-induced inflammation while only one large PML-NB is observed upon stroke. In order to understand this difference in shape and most likely a difference in function of those PML-NBs, we should first address the cause of the formation of the PML-NBs. By studying PML-NB formation upon MCAO in an IFNAR -/- background, we could assess whether PML is solely induced by IFN signaling or whether PML is induced upon other stress(es), such as the response to cell death stimuli in the stroke model. Interestingly, reducing the inflammatory response by deleting IFNAR1 was shown to lead to a better outcome and reduced CNS injury upon stroke (M. Zhang et al., 2017). It would be interesting to study the role a PML in that mechanism.

Overall, the function of PML in microglia upon hypoxia/ischemia requires further investigation. To date, germline PML -/- showed a reduced CNS injury upon stroke, however, the contribution of PML deletion in neurons and in other brain cells could not be determined.

We could note the similarity of PML-NB pattern in microglia upon stroke and during postnatal days, only one large PML-NB is present per microglia. Similar events are happening during those two phenomena: neuronal death during the first postnatal days is observed (Mosley et al., 2017) while a stroke induces an important cell death in the infarct area (Sekerdag et al., 2018; Yoon et al., 2018). Also, phagocytosis is a common event happening in both contexts: upon stroke, microglia engulf debris, but also apoptotic cells and dead/live neurons (Jia et al., 2022), while during development, “eat me” signals are necessary for pruning (Scott-Hewitt et al., 2020). Thus, we can hypothesize that the pattern of PML-NBs in immune cells could also depict a function.

In conclusion, a new role of ATO against inflammation has been revealed in this thesis. Our study put in light ATO as an inhibitor of IFN-mediated inflammation independently of cell death. We suggest that ATO's inhibition of inflammation is due to a PML-independent reduced STAT1 phosphorylation. We propose that ATO should be further studied to be considered as a potential treatment option for patients suffering from interferonopathies.

5. PML in Alzheimer's disease

5.1. Results

5.1.1. PML-NB formation is induced in microglia in APP/PS1 murine AD model

Inflammation is one of the hallmarks of AD and, interestingly, was recently linked to interferon signaling (Roy et al., 2020). Type I interferon response was shown to be induced in the brain of 6 month-old 5XFAD mice by the presence of nucleic acid in 95 % of amyloid-β plaques. These findings were also extended to several other AD murine models, such as the APP/PS1 transgenic mice. We have previously demonstrated that PML-NBs are formed upon interferon-mediated inflammation in microglia, therefore, we hypothesized that the inflammatory state of microglia, as well as the activated interferon response in the plaque-associated microglia, could trigger PML-NBs formation in AD microglia. In order to confirm this hypothesis, the APP/PS1 model containing the human amyloid precursor protein (APP) bearing the Swedish mutation as well as the human mutated PSEN1, was used in this study. As both mutations lead to the formation of amyloid-β plaques, the presence of PML-NBs was studied in plaque-associated microglia and in microglia distant from amyloid-β plaques. The data shown in this chapter were collected from 10 month-old APP/PS1 mice, when the amyloid-β plaque load is already quite advanced.

Our hypothesis was confirmed as a significant increase of PML-NBs number was observed in APP/PS1 microglia (figure 47 A&C). Furthermore, this increase in PML-NBs had the tendency to negatively correlated with the distance to the closest amyloid-β plaque (figure 47B), indicating that PML-NB formation occurred mostly in the plaque-associated microglia. Surprisingly, the observed increase of PML-NBs was not in line with *pml* transcription level: *pml* was downregulated in brain-isolated APP/PS1 microglia (figure 47D). However, as the RNA was extracted from all microglia in the brain, the transcription level reflects the overall *pml* transcription level in microglia, which might be different in plaque-associated microglia. In order to address this hypothesis, single cell RNA sequencing or RNA-FISH could be performed.

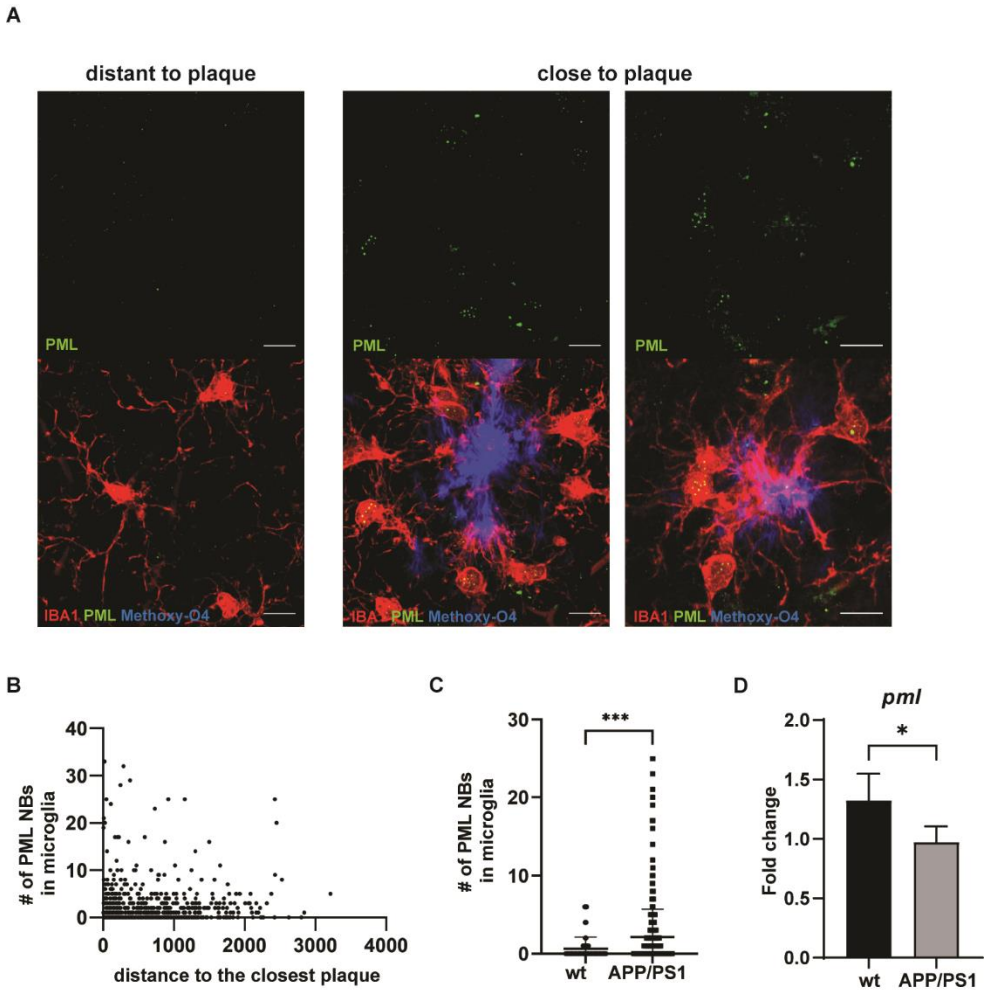

Fig. 47: PML-NB formation is induced in plaque-associated microglia.
(A) Representative confocal image of microglia surrounding an amyloid-β plaque harboring high number of PML-NBs.
(B) Quantification of PML-NB number in microglia in function of the distance to the closest plaque of the PML-NB-containing microglia.
(C) Quantification of PML-NBs in APP/PS1 microglia compared to wt microglia in 10 month-old mice. n=3, number of microglia analyzed per biological replicate > 200, t-test.
(D) *pml* transcript level is downregulated in APP/PS1 brain-isolated microglia compared to wt brain isolated microglia. n=3, t-test.
All data are represented as mean ± SD. $^{*}p < 0.1$; $^{**}p < 0.01$; $^{***}p < 0.001$; ns, not significant.

5.1.2. PML is upregulated in microglia in AD patients

Following our discovery of PML-NB formation in APP/PS1 microglia, we sought to investigate PML presence in microglia in human AD patients. To this aim, paraffin-embedded brain samples of human AD patients and of age-matched control patients were supplied from the Netherland Brain Bank. AD patients were histologically diagnosed when presenting a Braak stage of IV or V, corresponding to the fully developed AD (Braak & Braak, 1995). Control patients were not assessed any neurodegenerative disease. All patients were older than 65 years old (figure 48 D&E) and AD patients presenting an amyloid load of level C were chosen for our survey (figure 48D).

Interestingly, immunohistochemistry analysis revealed a higher intensity of PML staining in AD-patient microglia in the parietal cortex and hippocampus compared to control-patient microglia (figure 48 A,B &C).

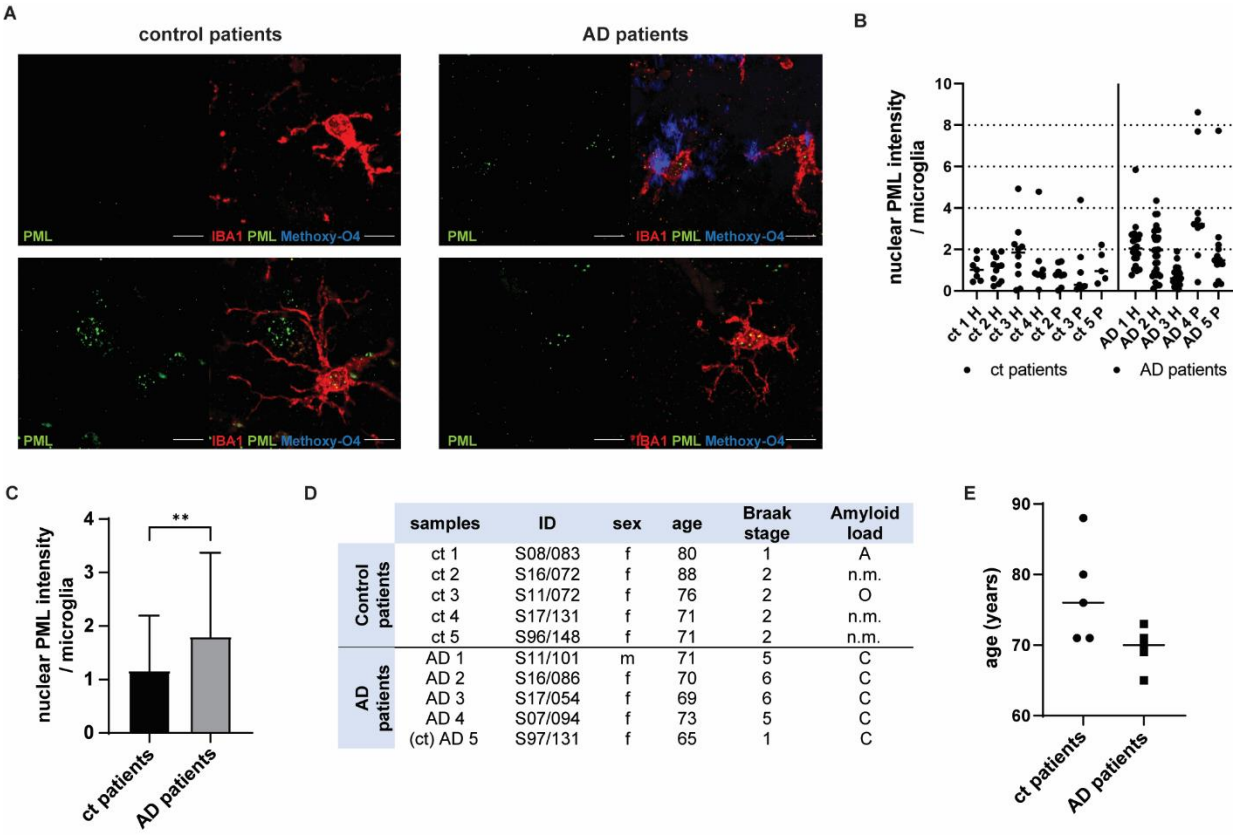

	samples	ID	sex	age	Braak stage	Amyloid load
Control patients	ct 1	S08/083	f	80	1	A
	ct 2	S16/072	f	88	2	n.m.
	ct 3	S11/072	f	76	2	O
	ct 4	S17/131	f	71	2	n.m.
	ct 5	S96/148	f	71	2	n.m.
AD patients	AD 1	S11/101	m	71	5	C
	AD 2	S16/086	f	70	6	C
	AD 3	S17/054	f	69	6	C
	AD 4	S07/094	f	73	5	C
	(ct) AD 5	S97/131	f	65	1	C

Fig. 48: PML intensity is increased in AD patient microglia.
(A) Representative confocal images of PML in microglia in ct patient and AD patients. Scale bars, 10um. ct: control patients.

(B&C) Quantification of nuclear PML intensity in microglia by patient (B) and merged by diagnosis (C) in the hippocampus (H) and parietal cortex (P). n=4 AD patients and n=5 ct patients, t-test. Data are represented as mean ± SD. $^{**}p < 0.01$;
(D) Patients data. n.m.: non measured.
(E) Age of the patients.

5.1.3. PML-NB formation is induced in neurons in APP/PS1 mice

Knowing that PML is mostly present in neurons in the CNS and after observing an upregulation of PML in microglia in APP/PS1 mice and in AD patients, we also looked at the neurons in APP/PS1 mice. Interestingly, APP/PS1 mice harbored higher number of PML-NBs in cortical neurons despite showing a lower intensity of PML nuclear staining (figure 49A). Furthermore, *pml* transcript and protein levels were upregulated in total RNA and protein extracts of APP/PS1 cortex and hippocampus (figure 49 B&C). In line with the increased interferon signaling found in APP/PS1 mice (Roy et al., 2020), transcription levels of ISGs, such as *daxx* and *stat1* were also significantly increased in the total brain (figure 49C).

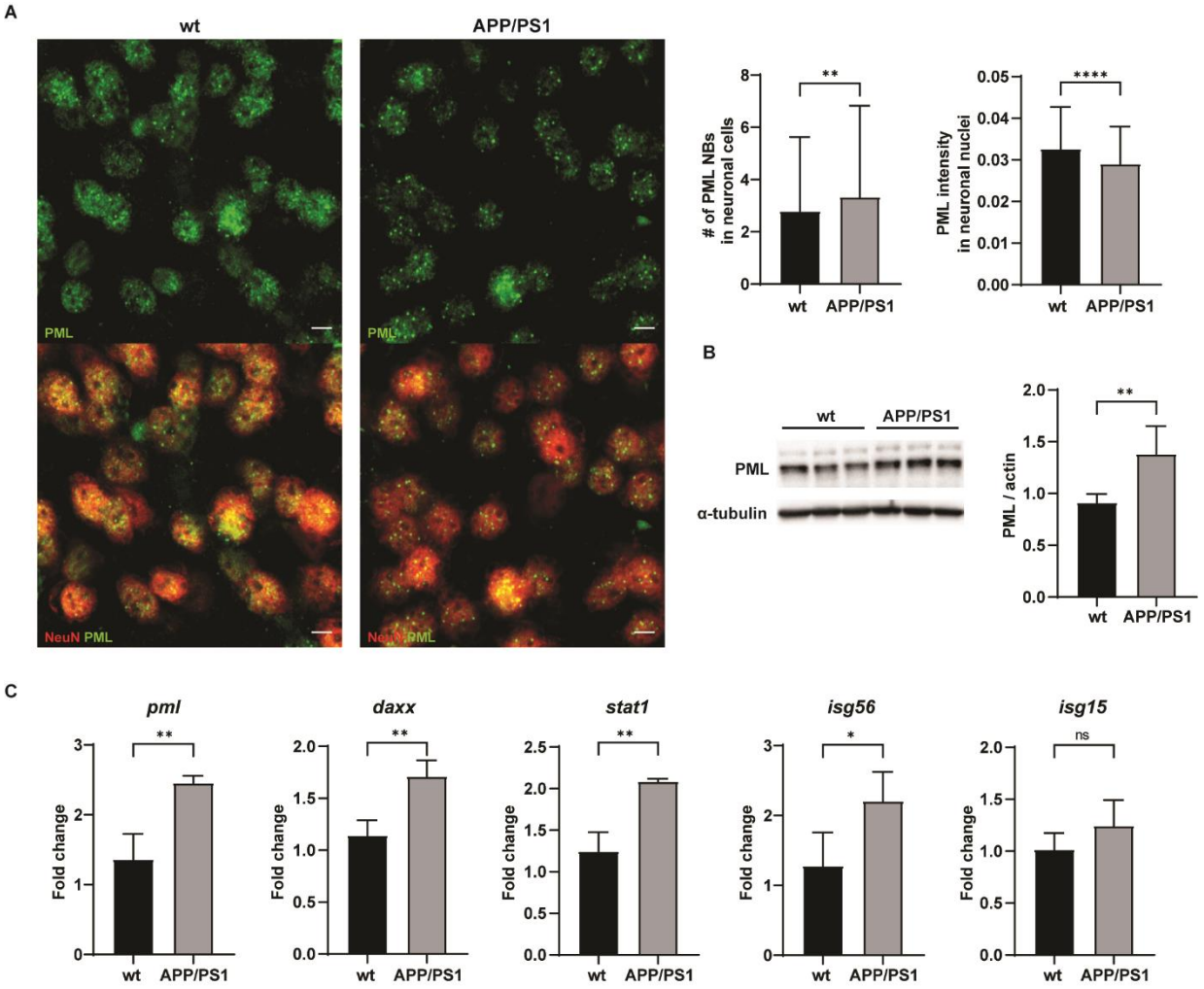

Fig. 49: PML-NBs formation is induced in APP/PS1 neurons.
(A) Representative confocal images of PML in APP/PS1 and wt cortical neurons and the quantification of PML-NB number and PML nuclear intensity in neurons. Scale bars, 10 µm. n=3, t-test, 50-80 neurons analyzed per biological replicate.
(B) Western blot showing the increase of PML in total brain extract of APP/PS1 cortex and hippocampus. n=6, t-test.
(C) Bar plots showing the increased transcription level of ISGs from total RNA isolated from the cortex and hippocampus of wt and APP/PS1 mice. n=3, t-test.
All data are represented as mean ± SD. $^{*}p < 0.1$; $^{**}p < 0.01$; $^{***}p < 0.001$; $^{****}p < 0.0001$; ns, not significant.

5.1.4. Effects of PML deletion in microglia in APP/PS1 mice

After discovering that PML-NB formation is induced in APP/PS1 microglia, we wanted to investigate PML role in disease progression. To do so, we created a new mouse model with PML deleted in microglia in the APP/PS1 background by crossing PML f/f,

Csf1r-cre with APP/PS1 mice. Mice were collected and analyzed at 10 month-old, as the amyloid β-plaque load is already advanced.

Surprisingly, PML deletion in microglia induced an increase of *trem2* transcription levels in APP/PS1 microglia as well as a tendency to higher level of human amyloid β42 in APP/PS1 brain.

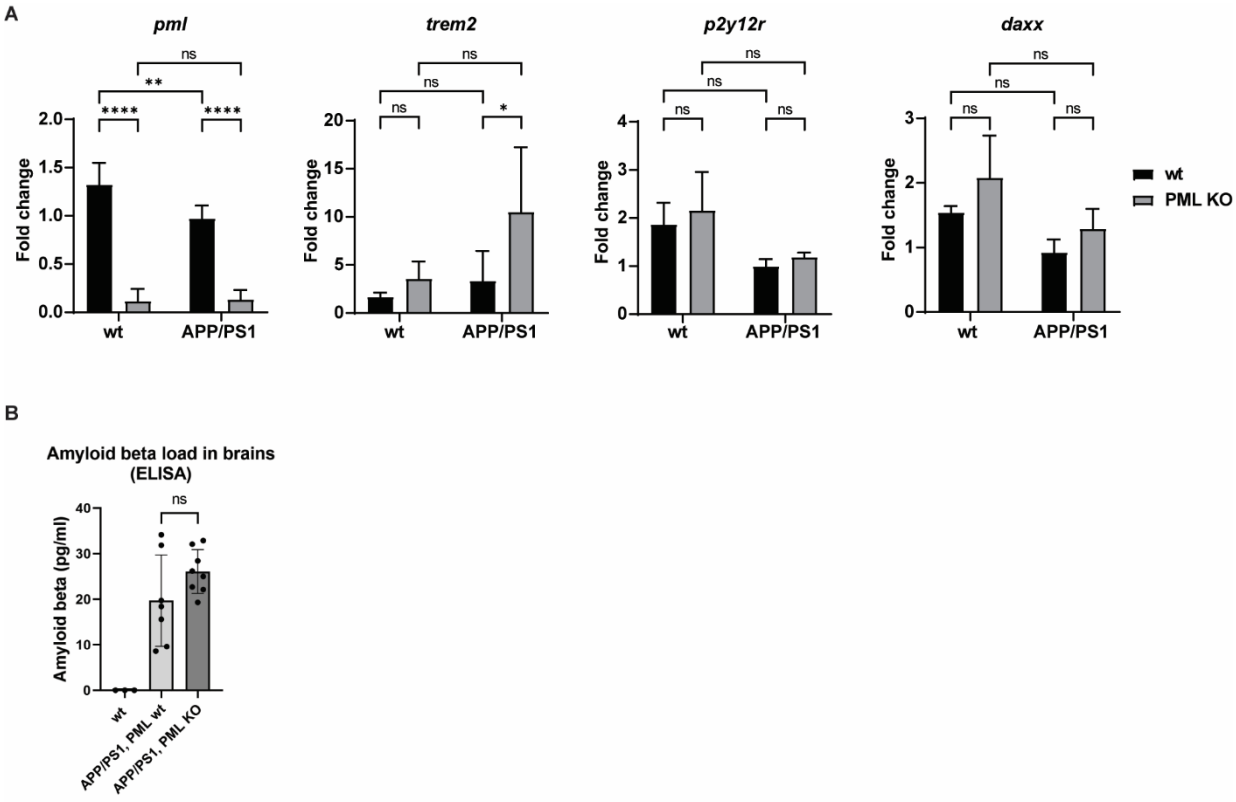

Fig. 50: PML deletion in microglia leads to an increase of *trem2* transcript level and amyloid β42 load.
(A) Bar plots showing the transcription level of ISGs from total RNA isolated from the cortex and hippocampus of wt and APP/PS1 mice. n=3-9, 2-way ANOVA.
(B) Human amyloid β42 quantification by ELISA from wt, APP/PS1 and APP/PS1, PML KO brain extracts. n=7-8, 2-way ANOVA.
All data are represented as mean ± SD. $^{*}p < 0.1$; $^{**}p < 0.01$; $^{***}p < 0.001$; $^{****}p < 0.0001$; ns, not significant.

5.2. Discussion

High CNS inflammation is one of the hallmarks of AD. For the last decades, beneficial or detrimental effects of glial activation on AD progression have been extensively studied, however remaining still controversial (Guzman-Martinez et al., 2019; Hashioka

et al., 2021; Kwon & Koh, 2020; Leng & Edison, 2021). We found higher numbers of PML-NBs in plaque associated microglia as well as in neurons of APP/PS1 model. Furthermore, and more importantly, we confirmed the increase of PML protein in AD patients' microglia. This finding as very exciting as PML is targetable by ATO, as shown previously.

First, in order to understand the role of PML in APP/PS1 microglia, we generated a new APP/PS1 murine model in which PML is deleted from microglia. We discovered that the deletion of PML in APP/PS1 microglia induced an increase of *trem2* transcription in microglia. Interestingly, TREM2 has been associated with an increased phagocytic activity leading to a decrease of amyloid-β accumulation in APP/PS1 mice and therefore an ameliorated phenotype showing less CNS inflammation and cognitive deficits in APP/PS1 mice (Ruganzu et al., 2021). Furthermore, loss of TREM2 was associated with higher risks of developing AD (Gratuze et al., 2018). However, despite the increase of *trem2*, we found that the level of human amyloid β42 is increased in PML KO APP/PS1 brains. This project being only at its start, we will further study the effects of the trem2 increase on plaques formation by quantifying the number and size of amyloid-β plaques in our models. Furthermore, it will be interesting to assess by behavioral tests whether PML deletion would improve or worsen the cognitive deficit in APP/PS1 mice. Finally, as shown previously, PML deletion in microglia inhibits the CNS inflammation, therefore, it will of importance to determine the inflammation level which is also linked to cognitive ability.

Taken altogether, PML seems to play an important role in microglia in response to amyloid-β aggregation and further investigations will be required to understand it. Furthermore, it will also be of interest to investigate whether the anti-inflammatory capacity of ATO could be beneficial to AD disease, and specifically to amyloid-β load progression.

6. Abstract

Activation of interferon type-I (IFN-I) production and downstream signaling pathways mediate the tissue response to pathogens such as viruses, but its aberrant activation has been suggested to contribute to the aging process and aging-associated neurodegenerative diseases. As a result, the identification of therapeutic avenues for inhibition of the IFN response bears promise for countering tissue aging and IFN-associated diseases. Arsenic trioxide (ATO), an FDA-approved drug against Acute Promyelocytic Leukemia, has been suggested having anti-inflammatory effects in peripheral blood cells. However, the effect of ATO in the context of brain inflammation is unknown. ATO targets the Promyelocytic Leukemia nuclear body (PML-NB), a subnuclear structure involved in the response to stress including viral infections. We found PML upregulated in microglia in interferonopathy models and in amyloid-β plaque-associated microglia in Alzheimer's disease. We therefore hypothesized that PML-high microglia may be targetable with ATO for suppression of IFN signaling. To test this, we studied the effect of ATO upon viral mimicry and in an interferonopathy model. *In vitro* and *in vivo*, we observed that poly I:C-induced inflammation markers in brain microglia were markedly reduced upon ATO, including IFNβ, several chemokines, MHC Class I genes as well as interferon stimulated genes. The inhibitory effect of ATO is only in part PML-dependent and is associated with suppression of STAT1 phosphorylation. We are currently investigating further the mechanism(s) of action of ATO in counteracting brain inflammation, with a particular focus on the link between SUMOylation and STAT1 function. Critically, ATO displayed suppressive effects on microglia activation in interferonopathy models. Taken together, these findings suggest that ATO may represent a promising anti-inflammatory agent in the context of the aging CNS and CNS diseases associated with enhanced IFN signaling.

7. List of figures

8. List of tables

9. References

Abe, J., Nakamura, K., Nishikomori, R., Kato, M., Mitsuiki, N., Izawa, K., Awaya, T., Kawai, T., Yasumi, T., Toyoshima, I., Hasegawa, K., Ohshima, Y., Hiragi, T., Sasahara, Y., Suzuki, Y., Kikuchi, M., Osaka, H., Ohya, T., Ninomiya, S., … Heike, T. (2014). A nationwide survey of Aicardi–Goutières syndrome patients identifies a strong association between dominant TREX1 mutations and chilblain lesions: Japanese cohort study. *Rheumatology*, *53*(3), 448–458

Ahmed, A., Wan, X., Mitxitorena, I., Lindsay, A. J., Pandolfi, P. P., McCaffrey, M. W., Keeshan, K., Chen, Y. H., & Carmody, R. J. (2017). Regulation of NF-κB by PML and PML-RARα. *Scientific Reports*, *7*(1), 44539

Alcalay, M., Zangrilli, D., Pandolfi, P. P., Longo, L., Mencarelli, A., Giacomucci, A., Rocchi, M., Biondi, A., Rambaldi, A., & lo Coco, F. (1991). Translocation breakpoint of acute promyelocytic leukemia lies within the retinoic acid receptor alpha locus. *Proceedings of the National Academy of Sciences*, *88*(5), 1977–1981

Alzheimer's disease facts and figures. (2019). *Alzheimer Association*

Amodeo, V., Deli, A., Betts, J., Bartesaghi, S., Zhang, Y., Richard-Londt, A., Ellis, M., Roshani, R., Vouri, M., Galavotti, S., Oberndorfer, S., Leite, A. P., Mackay, A., Lampada, A., Wessel Stratford, E., Li, N., Dinsdale, D., Grimwade, D., Jones, C., … Salomoni, P. (2017). A PML/Slit Axis Controls Physiological Cell Migration and Cancer Invasion in the CNS. *Cell Reports*, *20*(2), 411–426

AM, W., JJ, S., K, N., & PB, T. (2016). Evaluation of Arsenic Trioxide Potential for Lung Cancer Treatment: Assessment of Apoptotic Mechanisms and Oxidative Damage. *Journal of Cancer Science & Therapy*, *8*(1)

An, J., Woodward, J. J., Lai, W., Minie, M., Sun, X., Tanaka, L., Snyder, J. M., Sasaki, T., & Elkon, K. B. (2018). Inhibition of Cyclic GMP-AMP Synthase Using a Novel Antimalarial Drug Derivative in *Trex1* -Deficient Mice. *Arthritis & Rheumatology*, *70*(11), 1807–1819

An, J., Woodward, J. J., Sasaki, T., Minie, M., & Elkon, K. B. (2015). Cutting Edge: Antimalarial Drugs Inhibit IFN-β Production through Blockade of Cyclic GMP-AMP Synthase–DNA Interaction. *The Journal of Immunology*, *194*(9), 4089–4093

An, K., Xue, M. J., Zhong, J. Y., Yu, S. N., Lan, T. S., Qi, Z. Q., & Xia, J. J. (2020). Arsenic trioxide ameliorates experimental autoimmune encephalomyelitis in C57BL/6 mice by inducing CD4+ T cell apoptosis. *Journal of Neuroinflammation*, *17*(1)

Anttila, J. E., Whitaker, K. W., Wires, E. S., Harvey, B. K., & Airavaara, M. (2017). Role of microglia in ischemic focal stroke and recovery: focus on Toll-like receptors. *Progress in Neuro-Psychopharmacology and Biological Psychiatry*, *79*, 3–14

Augusto-Oliveira, M., Arrifano, G. P., Lopes-Araújo, A., Santos-Sacramento, L., Takeda, P. Y., Anthony, D. C., Malva, J. O., & Crespo-Lopez, M. E. (2019). What Do Microglia Really Do in Healthy Adult Brain? *Cells*, *8*(10), 1293

Au, W. Y. (2011). A biography of arsenic and medicine in Hong Kong and China. *Hong Kong Medical Journal = Xianggang Yi Xue Za Zhi*, *17*(6), 507–513

Au, W. Y., Tam, S., Fong, B. M., & Kwong, Y. L. (2008). Determinants of cerebrospinal fluid arsenic concentration in patients with acute promyelocytic leukemia on oral arsenic trioxide therapy. *Blood*, *112*(9), 3587–3590

Banani, S. F., Rice, A. M., Peeples, W. B., Lin, Y., Jain, S., Parker, R., & Rosen, M. K. (2016). Compositional Control of Phase-Separated Cellular Bodies. *Cell*, *166*(3), 651–663

Bateman, R. J., Xiong, C., Benzinger, T. L. S., Fagan, A. M., Goate, A., Fox, N. C., Marcus, D. S., Cairns, N. J., Xie, X., Blazey, T. M., Holtzman, D. M., Santacruz, A., Buckles, V., Oliver, A., Moulder, K., Aisen, P. S., Ghetti, B., Klunk, W. E., McDade, E., … Morris, J. C. (2012). Clinical and Biomarker Changes in Dominantly Inherited Alzheimer's Disease. *New England Journal of Medicine*, *367*(9), 795–804

Begitt, A., Droescher, M., Knobeloch, K.-P., & Vinkemeier, U. (2011). SUMO conjugation of STAT1 protects cells from hyperresponsiveness to IFNγ. *Blood*, *118*(4), 1002–1007

Behrendt, R., & Roers, A. (2013). Mouse models for Aicardi–Goutières syndrome provide clues to the molecular pathogenesis of systemic autoimmunity. *Clinical and Experimental Immunology*, *175*(1), 9–16

Bennett, J. M., Catovsky, D., Daniel, M.-T.,Flandrin, G., Galton, D. A. G., Gralnick, H. R., & Sultan, C. (1976). Proposals for the Classification of the Acute Leukaemias French-American-British (FAB) Co-operative Group. *British Journal of Haematology*, *33*(4), 451–458

Bernardi, R., & Pandolfi, P. P. (2007a). Structure, dynamics and functions of promyelocytic leukaemia nuclear bodies. *Nature Reviews. Molecular Cell Biology*, *8*(12), 1006–1016

Bernardi, R., & Pandolfi, P. P. (2007b). Structure, dynamics and functions of promyelocytic leukaemia nuclear bodies. *Nature Reviews Molecular Cell Biology 2007 8:12*, *8*(12), 1006–1016

Bernardi, R., Scaglioni, P. P., Bergmann, S., Horn, H. F., Vousden, K. H., & Pandolfi, P. P. (2004). PML regulates p53 stability by sequestering Mdm2 to the nucleolus. *Nature Cell Biology*, *6*(7), 665–672

Bloomer, W. A. C., VanDongen, H. M. A., & VanDongen, A. M. J. (2007). Activity-regulated cytoskeleton-associated protein Arc/Arg3.1 binds to spectrin and associates with nuclear promyelocytic leukemia (PML) bodies. *Brain Research*, *1153*(1), 20–33

Boisvert, F. M., Hendzel, M. J., & Bazett-Jones, D. P. (2000). Promyelocytic leukemia (PML) nuclear bodies are protein structures that do not accumulate RNA. *The Journal of Cell Biology*, *148*(2), 283–292

Borrow, J., Goddard, A. D., Sheer, D., & Solomon, E. (1990). Molecular Analysis of Acute Promyelocytic Leukemia Breakpoint Cluster Region on Chromosome 17. *Science*, *249*(4976), 1577–1580

Braak, H., & Braak, E. (1995). Staging of alzheimer's disease-related neurofibrillary changes. *Neurobiology of Aging*, *16*(3), 271–278

Butler, K., Martinez, L. A., & Tejada-Simon, M. v. (2013). Impaired cognitive function and reduced anxiety-related behavior in a promyelocytic leukemia (PML) tumor suppressor protein-deficient mouse. *Genes, Brain and Behavior*, *12*(2), 189–202

Campanaro, F., Batticciotto, A., Zaffaroni, A., Cappelli, A., Donadini, M. P., & Squizzato, A. (2021). JAK inhibitors and psoriatic arthritis: A systematic review and meta-analysis. *Autoimmunity Reviews*, *20*(10), 102902

Caselli, R. J., & Reiman, E. M. (2013). Characterizing the preclinical stages of Alzheimer's disease and the prospect of presymptomatic intervention. *Journal of Alzheimer's Disease: JAD*, *33 Suppl 1*(0 1)

Castoldi, G. L., Liso, V., Specchia, G., & Tomasi, P. (1994). Acute promyelocytic leukemia: morphological aspects. *Leukemia*, *8*(9), 1441–1446

Chang, H. R., Munkhjargal, A., Kim, M. J., Park, S. Y., Jung, E., Ryu, J. H., Yang, Y., Lim, J. S., & Kim, Y. (2018). The functional roles of PML nuclear bodies in genome maintenance. *Mutation Research/Fundamental and Molecular Mechanisms of Mutagenesis*, *809*, 99–107

Chelbi-Alix, M. K., Pelicano, L., Quignon, F., Koken, M. H., Venturini, L., Stadler, M., Pavlovic, J., Degos, L., & de Thé, H. (1995). Induction of the PML protein by interferons in normal and APL cells. *Leukemia*, *9*(12), 2027–2033

Chen, G. F., Xu, T. H., Yan, Y., Zhou, Y. R., Jiang, Y., Melcher, K., & Xu, H. E. (2017). Amyloid beta: structure, biology and structure-based therapeutic development. *Acta Pharmacologica Sinica*, *38*(9), 1205–1235

Cheng, X., Guo, S., Liu, Y., Chu, H., Hakimi, P., Berger, N. A., Hanson, R. W., & Kao, H. Y. (2013). Ablation of Promyelocytic Leukemia Protein (PML) Re-patterns Energy Balance and Protects Mice from Obesity Induced by a Western Diet. *The Journal of Biological Chemistry*, *288*(41), 29746

Ching, R. W., Ahmed, K., Boutros, P. C., Penn, L. Z., & Bazett-Jones, D. P. (2013). Identifying gene locus associations with promyelocytic leukemia nuclear bodies using immuno-TRAP. *The Journal of Cell Biology*, *201*(2), 325–335

Choi, Y. H., Bernardi, R., Pandolfi, P. P., & Benveniste, E. N. (2006). The promyelocytic leukemia protein functions as a negative regulator of IFN-γ signaling. *Proceedings of the National Academy of Sciences of the United States of America*, *103*(49), 18715–18720

Chort, A., Alves, S., Marinello, M., Dufresnois, B., Dornbierer, J. G., Tesson, C., Latouche, M., Baker, D. P., Barkats, M., el Hachimi, K. H., Ruberg, M., Janer, A.,

Stevanin, G., Brice, A., & Sittler, A. (2013). Interferon beta induces clearance of mutant ataxin 7 and improves locomotion in SCA7 knock-in mice. *Brain*, *136*(6), 1732–1745

Chow, S. K. Y., Chan, J. Y. W., & Fung, K. P. (2004). Inhibition of cell proliferation and the action mechanisms of arsenic trioxide (As2O3) on human breast cancer cells. *Journal of Cellular Biochemistry*, *93*(1), 173–187

Chung, H., Calis, J. J. A., Wu, X., Sun, T., Yu, Y., Sarbanes, S. L., Dao Thi, V. L., Shilvock, A. R., Hoffmann, H. H., Rosenberg, B. R., & Rice, C. M. (2018). Human ADAR1 Prevents Endogenous RNA from Triggering Translational Shutdown. *Cell*, *172*(4), 811-824

Chung, I., Osterwald, S., Deeg, K. I., & Rippe, K. (2012). PML body meets telomere: The beginning of an ALTernate ending? *Nucleus*, *3*(3), 263

Chu, Y., & Yang, X. (2011). SUMO E3 ligase activity of TRIM proteins. *Oncogene*, *30*(9), 1108–1116

Condemine, W., Takahashi, Y., Zhu, J., Puvion-Dutilleul, F., Guegan, S., Janin, A., & de Thé, H. (2006). Characterization of endogenous human promyelocytic leukemia isoforms. *Cancer Research*, *66*(12), 6192–6198

Corpet, A., Kleijwegt, C., Roubille, S., Juillard, F., Jacquet, K., Texier, P., & Lomonte, P. (2020). PML nuclear bodies and chromatin dynamics: catch me if you can! *Nucleic Acids Research*, *48*(21), 11890–11912

Crow, Y. J. (2016). Aicardi-Goutières Syndrome. *Handbook of Clinical Neurology*, *113*, 1629–1635

Crow, Y. J., & Manel, N. (2015). Aicardi-Goutières syndrome and the type I interferonopathies. *Nature Reviews. Immunology*, *15*(7), 429–440

Crow, Y. J., & Rehwinkel, J. (2009). Aicardi-Goutières syndrome and related phenotypes: linking nucleic acid metabolism with autoimmunity. *Human Molecular Genetics*, *18*(R2), R130

Cummings, J., Aisen, P., Apostolova, L. G., Atri, A., Salloway, S., & Weiner, M. (2021). Aducanumab: Appropriate Use Recommendations. *The Journal of Prevention of Alzheimer's Disease*, *8*(4), 398

d'Angelo, D. M., di Filippo, P., Breda, L., & Chiarelli, F. (2021). Type I Interferonopathies in Children: An Overview. *Frontiers in Pediatrics*, *9*, 11

da Silva, R. P., Gonçalves, J. I. B., Zanin, R. F., Schuch, F. B., & de Souza, A. P. D. (2021). Circulating Type I Interferon Levels and COVID-19 Severity: A Systematic Review and Meta-Analysis. *Frontiers in Immunology*, *12*

DeForte, S., & Uversky, V. N. (2016). Intrinsically disordered proteins in PubMed: what can the tip of the iceberg tell us about what lies below? *RSC Advances*, *6*(14), 11513–11521

Delbarre, E., Ivanauskiene, K., Küntziger, T., & Collas, P. (2013). DAXX-dependent supply of soluble (H3.3-H4) dimers to PML bodies pending deposition into chromatin. *Genome Research*, *23*(3), 440–451

Delbarre, E., Ivanauskiene, K., Spirkoski, J., Shah, A., Vekterud, K., Moskaug, J., Bøe, S. O., Wong, L. H., Küntziger, T., & Collas, P. (2017). PML protein organizes heterochromatin domains where it regulates histone H3.3 deposition by ATRX/DAXX. *Genome Research*, *27*(6), 913–921

Dellaire, G., Farrall, R., & Bickmore, W. A. (2003). The Nuclear Protein Database (NPD): sub-nuclear localisation and functional annotation of the nuclear proteome. *Nucleic Acids Research*, *31*(1), 328–330

de Stanchina, E., Querido, E., Narita, M., Davuluri, R. v, Pandolfi, P. P., Ferbeyre, G., & Lowe, S. W. (2004). PML is a direct p53 target that modulates p53 effector functions. *Molecular Cell*, *13*(4), 523–535

de Thé, H., & Chen, Z. (2010). Acute promyelocytic leukaemia: novel insights into the mechanisms of cure. *Nature Reviews. Cancer*, *10*(11), 775–783

de Thé, H., Chomienne, C., Lanotte, M., Degos, L., & Dejean, A. (1990). The t(15;17) translocation of acute promyelocytic leukaemia fuses the retinoic acid receptor α gene to a novel transcribed locus. *Nature*, *347*(6293), 558–561

de Thé, H., le Bras, M., & Lallemand-Breitenbach, V. (2012). The cell biology of disease: Acute promyelocytic leukemia, arsenic, and PML bodies. *The Journal of Cell Biology*, *198*(1), 11

Ditlev, J. A., Case, L. B., & Rosen, M. K. (2018). Who's In and Who's Out-Compositional Control of Biomolecular Condensates. *Journal of Molecular Biology*, *430*(23), 4666–4684

Dunker, A. K., Cortese, M. S., Romero, P., Iakoucheva, L. M., & Uversky, V. N. (2005). Flexible nets. The roles of intrinsic disorder in protein interaction networks. *The FEBS Journal*, *272*(20), 5129–5148

Dunker, A. K., Garner, E., Guilliot, S., Romero, P., Albrecht, K., Hart, J., Obradovic, Z., Kissinger, C., & Villafranca, J. E. (1998). Protein disorder and the evolution of molecular recognition: theory, predictions and observations. *Pacific Symposium on Biocomputing. Pacific Symposium on Biocomputing*, 473–484

Dunker, A. K., Lawson, J. D., Brown, C. J., Williams, R. M., Romero, P., Oh, J. S., Oldfield, C. J., Campen, A. M., Ratliff, C. M., Hipps, K. W., Ausio, J., Nissen, M. S., Reeves, R., Kang, C. H., Kissinger, C. R., Bailey, R. W., Griswold, M. D., Chiu, W., Garner, E. C., & Obradovic, Z. (2001). Intrinsically disordered protein. *Journal of Molecular Graphics & Modelling*, *19*(1), 26–59

Dutrieux, J., Maarifi, G., Portilho, D. M., Arhel, N. J., Chelbi-Alix, M. K., & Nisole, S. (2015). PML/TRIM19-Dependent Inhibition of Retroviral Reverse-Transcription by Daxx. *PLoS Pathogens*, *11*(11)

Edwards, G. A., Gamez, N., Escobedo, G., Calderon, O., & Moreno-Gonzalez, I. (2019). Modifiable Risk Factors for Alzheimer's Disease. *Frontiers in Aging Neuroscience*, *11*(JUN)

El-Asmi, F., El-Mchichi, B., Maroui, M. A., Dianoux, L., & Chelbi-Alix, M. K. (2019). TGF-β induces PML SUMOylation, degradation and PML nuclear body disruption. *Cytokine*, *120*, 264–272

El-Asmi, F., McManus, F. P., Brantis-de-Carvalho, C. E., Valle-Casuso, J. C., Thibault, P., & Chelbi-Alix, M. K. (2020). Cross-talk between SUMOylation and ISGylation in response to interferon. *Cytokine*, *129*, 155025

El-Asmi, F., McManus, F. P., Thibault, P., & Chelbi-Alix, M. K. (2020). Interferon, restriction factors and SUMO pathways. *Cytokine & Growth Factor Reviews*, *55*, 37–47

el Bougrini, J., Dianoux, L., & Chelbi-Alix, M. K. (2011). PML positively regulates interferon gamma signaling. *Biochimie*, *93*(3), 389–398.

Fang, Y., & Zhang, Z. (2020). Arsenic trioxide as a novel anti-glioma drug: a review. *Cellular & Molecular Biology Letters*, *25*, 44. https://doi.org/10.1186/S11658-020-00236-7

Fan, H. C., Ho, L. I., Chi, C. S., Chen, S. J., Peng, G. S., Chan, T. M., Lin, S. Z., & Harn, H. J. (2014). Polyglutamine (PolyQ) diseases: Genetics to treatments. *Cell Transplantation*, *23*(4–5), 441–458

fda, & cder. (2021). *PRESCRIBING INFORMATION Aducanumab*. www.fda.gov/medwatch

Ferbeyre, G., de Stanchina, E., Querido, E., Baptiste, N., Prives, C., & Lowe, S. W. (2000). PML is induced by oncogenic ras and promotes premature senescence. *Genes & Development*, *14*(16), 2015–2027

Ferri, C. P., & Jacob, K. S. (2017). Dementia in low-income and middle-income countries: Different realities mandate tailored solutions. *PLOS Medicine*, *14*(3), e1002271

Fleischmann, R., Kremer, J., Cush, J., Schulze-Koops, H., Connell, C. A., Bradley, J. D., Gruben, D., Wallenstein, G. v., Zwillich, S. H., & Kanik, K. S. (2012). Placebo-Controlled Trial of Tofacitinib Monotherapy in Rheumatoid Arthritis. *New England Journal of Medicine*, *367*(6), 495–507

Frege, T., & Uversky, V. N. (2015). Intrinsically disordered proteins in the nucleus of human cells. *Biochemistry and Biophysics Reports*, *1*(1), 33–51

Funabiki, M., Kato, H., Miyachi, Y., Toki, H., Motegi, H., Inoue, M., Minowa, O., Yoshida, A., Deguchi, K., Sato, H., Ito, S., Shiroishi, T., Takeyasu, K., Noda, T., & Fujita, T. (2014). Autoimmune Disorders Associated with Gain of Function of the Intracellular Sensor MDA5. *Immunity*, *40*(2), 199–212

Fu, S., Wei, J., Wang, G., Wang, B., Wang, Y., Lai, X., & Huang, H. (2015). The key role of PML in IFN-α induced cellular senescence of human mesenchymal stromal cells. *International Journal of Oncology*, *46*(1), 351–359

Gall, A., Treuting, P., Elkon, K. B., Loo, Y. M., Gale, M., Barber, G. N., & Stetson, D. B. (2012). Autoimmunity initiates in nonhematopoietic cells and progresses via lymphocytes in an interferon-dependent autoimmune disease. *Immunity*, *36*(1), 120–131

Gao, C., Jiang, J., Ma, P., Cheng, P., Lian, Y., Zhao, B., Li, C., Peng, Y., Wang, F., Lin, Y., Jin, N., Li, J., Wang, L., Li, Q., Leng, Y., Xia, J., & Qi, Z. (2015). Arsenic Trioxide Induces T Cell Apoptosis and Prolongs Islet Allograft Survival in Mice. *Transplantation*, *99*(9), 1796–1806

Gärtner, A., & Muller, S. (2014). PML, SUMO, and RNF4: guardians of nuclear protein quality. *Molecular Cell*, *55*(1), 1–3

Gilbert, N., Gilchrist, S., & Bickmore, W. A. (2004). Chromatin organization in the mammalian nucleus. *International Review of Cytology*, *242*, 283–336

Golomb, H., Rowley, J., Vardiman, J., Testa, J., & Butler, A. (1980). “Microgranular” acute promyelocytic leukemia: a distinct clinical, ultrastructural, and cytogenetic entity. *Blood*, *55*(2), 253–259

Gratuze, M., Leyns, C. E. G., & Holtzman, D. M. (2018). New insights into the role of TREM2 in Alzheimer’s disease. *Molecular Neurodegeneration*, *13*(1), 66

Gray, E. E., Treuting, P. M., Woodward, J. J., & Stetson, D. B. (2015). Cutting Edge: cGAS Is Required for Lethal Autoimmune Disease in the Trex1-Deficient Mouse Model of Aicardi–Goutières Syndrome. *The Journal of Immunology*, *195*(5), 1939–1943

Greth, W., Robbie, G. J., Brohawn, P., Hultquist, M., & Yao, B. (2017). Targeting the interferon pathway with sifalimumab for the treatment of systemic lupus erythematosus. *Immunotherapy*, *9*(1), 57–70

Grupe, A., Abraham, R., Li, Y., Rowland, C., Hollingworth, P., Morgan, A., Jehu, L., Segurado, R., Stone, D., Schadt, E., Karnoub, M., Nowotny, P., Tacey, K., Catanese, J., Sninsky, J., Brayne, C., Rubinsztein, D., Gill, M., Lawlor, B., … Williams, J. (2007). Evidence for novel susceptibility genes for late-onset Alzheimer’s disease from a genome-wide association study of putative functional variants. *Human Molecular Genetics*, *16*(8), 865–873

Guan, D., & Kao, H. Y. (2015). The function, regulation and therapeutic implications of the tumor suppressor protein, PML. *Cell & Bioscience 2015 5:1*, *5*(1), 1–14

Guerreiro, R. J., Gustafson, D. R., & Hardy, J. (2012). The genetic architecture of Alzheimer’s disease: beyond APP, PSENs and APOE. *Neurobiology of Aging*, *33*(3), 437–456

Guion, L. G., & Sapp, M. (2020). The Role of Promyelocytic Leukemia Nuclear Bodies During HPV Infection. *Frontiers in Cellular and Infection Microbiology*, *10*, 35

Guo, L., Giasson, B. I., Glavis-Bloom, A., Brewer, M. D., Shorter, J., Gitler, A. D., & Yang, X. (2014). A cellular system that degrades misfolded proteins and protects against neurodegeneration. *Molecular Cell*, *55*(1), 15

Guo, X., Wiley, C. A., Steinman, R. A., Sheng, Y., Ji, B., Wang, J., Zhang, L., Wang, T., Zenatai, M., Billiar, T. R., & Wang, Q. (2021). Aicardi-Goutières syndrome-associated mutation at ADAR1 gene locus activates innate immune response in mouse brain. *Journal of Neuroinflammation*, *18*(1), 1–16

Guzman-Martinez, L., Maccioni, R. B., Andrade, V., Navarrete, L. P., Pastor, M. G., & Ramos-Escobar, N. (2019). Neuroinflammation as a Common Feature of Neurodegenerative Disorders. *Frontiers in Pharmacology*, *10*

Haettig, J., Stefanko, D. P., Multani, M. L., Figueroa, D. X., McQuown, S. C., & Wood, M. A. (2011). HDAC inhibition modulates hippocampus-dependent long-term memory for object location in a CBP-dependent manner. *Learning & Memory*, *18*(2), 71–79

Hashioka, S., Wu, Z., & Klegeris, A. (2021). Glia-Driven Neuroinflammation and Systemic Inflammation in Alzheimer's Disease. *Current Neuropharmacology*, *19*(7), 908–924

Hemphill, W. O., Simpson, S. R., Liu, M., Salsbury, F. R., Hollis, T., Grayson, J. M., & Perrino, F. W. (2021). TREX1 as a Novel Immunotherapeutic Target. *Frontiers in Immunology*, *12*

Hodges, H. (1996). Maze procedures: the radial-arm and water maze compared. *Cognitive Brain Research*, *3*(3–4), 167–181

Hoonjan, M., Jadhav, V., & Bhatt, P. (2018). Arsenic trioxide: insights into its evolution to an anticancer agent. *JBIC Journal of Biological Inorganic Chemistry 2018 23:3*, *23*(3), 313–329

Hsu, K. S., & Kao, H. Y. (2018). PML: Regulation and multifaceted function beyond tumor suppression. *Cell & Bioscience*, *8*(1)

Huang, K.-L., Marcora, E., Pimenova, A. A., di Narzo, A. F., Kapoor, M., Jin, S. C., Harari, O., Bertelsen, S., Fairfax, B. P., Czajkowski, J., Chouraki, V., Grenier-Boley, B., Bellenguez, C., Deming, Y., McKenzie, A., Raj, T., Renton, A. E., Budde, J., Smith, A., … Goate, A. M. (2017). A common haplotype lowers PU.1 expression in myeloid cells and delays onset of Alzheimer's disease. *Nature Neuroscience*, *20*(8), 1052–1061

Huang, L. K., Chao, S. P., & Hu, C. J. (2020). Clinical trials of new drugs for Alzheimer disease. *Journal of Biomedical Science*, *27*(1)

Huang, X. (2020). Alzheimer's Disease: Drug Discovery. *Alzheimer's Disease: Drug Discovery*

Hubbard, N. W., Ames, J. M., Maurano, M., Chu, L. H., Somfleth, K. Y., Gokhale, N. S., Werner, M., Snyder, J. M., Lichauco, K., Savan, R., Stetson, D. B., & Oberst, A. (2022). ADAR1 mutation causes ZBP1-dependent immunopathology. *Nature*, *607*(7920), 769–775

Hu, J., Liu, Y.-F., Wu, C.-F., Xu, F., Shen, Z.-X., Zhu, Y.-M., Li, J.-M., Tang, W., Zhao, W.-L., Wu, W., Sun, H.-P., Chen, Q.-S., Chen, B., Zhou, G.-B., Zelent, A., Waxman, S., Wang, Z.-Y., Chen, S.-J., & Chen, Z. (2009). Long-term efficacy and safety of all-trans retinoic acid/arsenic trioxide-based therapy in newly diagnosed acute promyelocytic leukemia. *Proceedings of the National Academy of Sciences of the United States of America*, *106*(9), 3342–3347

Iakoucheva, L. M., Brown, C. J., Lawson, J. D., Obradović, Z., & Dunker, A. K. (2002). Intrinsic disorder in cell-signaling and cancer-associated proteins. *Journal of Molecular Biology*, *323*(3), 573–584

Insinga, A., Monestiroli, S., Ronzoni, S., Carbone, R., Pearson, M., Pruneri, G., Viale, G., Appella, E., Pelicci, P., & Minucci, S. (2004). Impairment of p53 acetylation, stability and function by an oncogenic transcription factor. *The EMBO Journal*, *23*(5), 1144–1154

Jackson, D. A., Hassan, A. B., Errington, R. J., & Cook, P. R. (1993). Visualization of focal sites of transcription within human nuclei. *The EMBO Journal*, *12*(3), 1059–1065

Janer, A., Martin, E., Muriel, M. P., Latouche, M., Fujigasaki, H., Ruberg, M., Brice, A., Trottier, Y., & Sittler, A. (2006). PML clastosomes prevent nuclear accumulation of mutant ataxin-7 and other polyglutamine proteins. *The Journal of Cell Biology*, *174*(1), 65

Jeanne, M., Lallemand-Breitenbach, V., Ferhi, O., Koken, M., le Bras, M., Duffort, S., Peres, L., Berthier, C., Soilihi, H., Raught, B., & de Thé, H. (2010). PML/RARA Oxidation and Arsenic Binding Initiate the Antileukemia Response of As2O3. *Cancer Cell*, *18*(1), 88–98.

Jensen, K., Shiels, C., & Freemont, P. S. (2001). PML protein isoforms and the RBCC/TRIM motif. *Oncogene*, *20*(49), 7223–7233

Jia, J., Yang, L., Chen, Y., Zheng, L., Chen, Y., Xu, Y., & Zhang, M. (2022). The Role of Microglial Phagocytosis in Ischemic Stroke. *Frontiers in Immunology*, *12*

Jiao, H., Wachsmuth, L., Wolf, S., Lohmann, J., Nagata, M., Kaya, G. G., Oikonomou, N., Kondylis, V., Rogg, M., Diebold, M., Tröder, S. E., Zevnik, B., Prinz, M., Schell, C., Young, G. R., Kassiotis, G., & Pasparakis, M. (2022). ADAR1 averts fatal type I interferon induction by ZBP1. *Nature*, *607*(7920), 776–783

Jones, B. J., & Roberts, D. J. (1968). A rotarod suitable for quantitative measurements of motor incoordination in naive mice. *Naunyn-Schmiedebergs Archiv Fur Pharmakologie Und Experimentelle Pathologie*, *259*(2), 211–211

Jo, Y., & Jung, Y. (2019). Interplay between intrinsically disordered proteins inside membraneless protein liquid droplets. *Chemical Science*, *11*(5), 1269–1275

Kahle, T., Volkmann, B., Eissmann, K., Herrmann, A., Schmitt, S., Wittmann, S., Merkel, L., Reuter, N., Stamminger, T., & Gramberg, T. (2015). TRIM19/PML Restricts HIV Infection in a Cell Type-Dependent Manner. *Viruses*, *8*(1), 2

Karch, C. M., & Goate, A. M. (2015). Alzheimer's disease risk genes and mechanisms of disease pathogenesis. *Biological Psychiatry*, *77*(1), 43–51

Karhausen, J., Ulloa, L., & Yang, W. (2021). SUMOylation Connects Cell Stress Responses and Inflammatory Control: Lessons From the Gut as a Model Organ. *Frontiers in Immunology*, *12*

Keenan, A. B., Torre, D., Lachmann, A., Leong, A. K., Wojciechowicz, M. L., Utti, V., Jagodnik, K. M., Kropiwnicki, E., Wang, Z., & Ma'ayan, A. (2019). ChEA3: transcription factor enrichment analysis by orthogonal omics integration. *Nucleic Acids Research*, *47*(W1), W212–W224

Kerbauy, D. M. B., Lesnikov, V., Abbasi, N., Seal, S., Scott, B., & Joachim Deeg, H. (2005). NF-κB and FLIP in arsenic trioxide (ATO)-induced apoptosis in myelodysplastic syndromes (MDSs). *Blood*, *106*(12), 3917

Khoury, R., & Ghossoub, E. (2019). Diagnostic biomarkers of Alzheimer's disease: A state-of-the-art review. *Biomarkers in Neuropsychiatry*, *1*

Kim, M. K., Yang, S., Lee, K. H., Um, J. H., Liu, M., Kang, H., Park, S. J., & Chung, J. H. (2011). Promyelocytic leukemia inhibits adipogenesis, and loss of promyelocytic leukemia results in fat accumulation in mice. *American Journal of Physiology - Endocrinology and Metabolism*, *301*(6), E1130

Kim, Y. E., & Ahn, J. H. (2015). Positive Role of Promyelocytic Leukemia Protein in Type I Interferon Response and Its Regulation by Human Cytomegalovirus. *PLOS Pathogens*, *11*(3), e1004785

Kindler, H. L., Aklilu, M., Nattam, S., & Vokes, E. E. (2008). Arsenic trioxide in patients with adenocarcinoma of the pancreas refractory to gemcitabine: a phase II trial of the University of Chicago Phase II Consortium. *American Journal of Clinical Oncology*, *31*(6), 553–556

Kleinschnitz, C., Fluri, F., & Schuhmann, M. (2015). Animal models of ischemic stroke and their application in clinical research. *Drug Design, Development and Therapy*, 3445

Korb, E., & Finkbeiner, S. (2013). PML in the Brain: From Development to Degeneration. *Frontiers in Oncology*, *3*

Korf, K., Wodrich, H., Haschke, A., Ocampo, C., Harder, L., Gieseke, F., Pollmann, A., Dierck, K., Prall, S., Staege, H., Ma, H., Horstmann, M. A., Evans, R. M., & Sternsdorf, T. (2014). The PML domain of PML-RARα blocks senescence to promote leukemia. *Proceedings of the National Academy of Sciences of the United States of America*, *111*(33), 12133–12138

Kunkle, B. W., Grenier-Boley, B., Sims, R., Bis, J. C., Damotte, V., Naj, A. C., Boland, A., Vronskaya, M., van der Lee, S. J., Amlie-Wolf, A., Bellenguez, C., Frizatti, A., Chouraki, V., Martin, E. R., Sleegers, K., Badarinarayan, N., Jakobsdottir, J., Hamilton-Nelson, K. L., Moreno-Grau, S., … Pericak-Vance, M. A. (2019). Genetic meta-analysis

of diagnosed Alzheimer's disease identifies new risk loci and implicates Aβ, tau, immunity and lipid processing. *Nature Genetics*, *51*(3), 414–430

Kuo, P., Scofield, B. A., Yu, I., Chang, F., Ganea, D., & Yen, J. (2016). Interferon-β Modulates Inflammatory Response in Cerebral Ischemia. *Journal of the American Heart Association*, *5*(1)

Kurihara, M., Kato, K., Sanbo, C., Shigenobu, S., Ohkawa, Y., Fuchigami, T., & Miyanari, Y. (2020). Genomic Profiling by ALaP-Seq Reveals Transcriptional Regulation by PML Bodies through DNMT3A Exclusion. *Molecular Cell*, *78*(3), 493-505

Kwon, H. S., & Koh, S.-H. (2020). Neuroinflammation in neurodegenerative disorders: the roles of microglia and astrocytes. *Translational Neurodegeneration*, *9*(1), 42

Lallemand-Breitenbach, V., & de Thé, H. (2010). PML nuclear bodies. *Cold Spring Harbor Perspectives in Biology*, *2*(5)

Lallemand-Breitenbach, V., Jeanne, M., Benhenda, S., Nasr, R., Lei, M., Peres, L., Zhou, J., Zhu, J., Raught, B., & de Thé, H. (2008). Arsenic degrades PML or PML–RARα through a SUMO-triggered RNF4/ubiquitin-mediated pathway. *Nature Cell Biology*, *10*(5), 547–555

Lallemand-Breitenbach, V., Zhu, J., Puvion, F., Koken, M., Honoré, N., Doubeikovsky, A., Duprez, E., Pandolfi, P. P., Puvion, E., Freemont, P., & de Thé, H. (2001). Role of promyelocytic leukemia (PML) sumolation in nuclear body formation, 11S proteasome recruitment, and As2O3-induced PML or PML/retinoic acid receptor alpha degradation. *The Journal of Experimental Medicine*, *193*(12), 1361–1371

Lång, A., Lång, E., & Bøe, S. O. (2019). PML Bodies in Mitosis. *Cells*, *8*(8)

Lemons, R. S., Eilender, D., Waldmann, R. A., Rebentisch, M., Frej, A.-K., Ledbetter, D. H., Willman, C., McConnell, T., & O'Connell, P. (1990). Cloning and characterization of the T(15;17) translocation breakpoint region in acute promyelocytic leukemia. *Genes, Chromosomes and Cancer*, *2*(2), 79–87

Leng, F., & Edison, P. (2021). Neuroinflammation and microglial activation in Alzheimer disease: where do we go from here? *Nature Reviews Neurology*, *17*(3), 157–172

Li, C., Guan, T., Gao, C., Lin, Y., Yan, G., Zhu, M., Lv, C., Xia, J., & Qi, Z. (2015). Arsenic trioxide inhibits accelerated allograft rejection mediated by alloreactive CD8(+) memory T cells and prolongs allograft survival time. *Transplant Immunology*, *33*(1), 30–36

Liddicoat, B. J., Piskol, R., Chalk, A. M., Ramaswami, G., Higuchi, M., Hartner, J. C., Li, J. B., Seeburg, P. H., & Walkley, C. R. (2015). RNA editing by ADAR1 prevents MDA5 sensing of endogenous dsRNA as nonself. *Science (New York, N.Y.)*, *349*(6252), 1115–1120

Li, L., Zhou, J., Han, L., Wu, X., Shi, Y., Cui, W., Zhang, S., Hu, Q., Wang, J., Bai, H., Liu, H., Guo, W., Feng, D., & Qu, Y. (2022). The Specific Role of Reactive Astrocytes in Stroke. *Frontiers in Cellular Neuroscience*, *16*

Lim, J. H., Liu, Y., Reineke, E., & Kao, H. Y. (2011). Mitogen-activated Protein Kinase Extracellular Signal-regulated Kinase 2 Phosphorylates and Promotes Pin1 Protein-dependent Promyelocytic Leukemia Protein Turnover. *Journal of Biological Chemistry*, *286*(52), 44403–44411

Lin, H. K., Bergmann, S., & Pandolfi, P. P. (2004). Cytoplasmic PML function in TGF-beta signalling. *Nature*, *431*(7005), 205–211

Lister, RichardG. (1987). The use of a plus-maze to measure anxiety in the mouse. *Psychopharmacology*, *92*(2)

Livak, K. J., & Schmittgen, T. D. (2001). Analysis of relative gene expression data using real-time quantitative PCR and the 2(-Delta Delta C(T)) Method. *Methods (San Diego, Calif.)*, *25*(4), 402–408

Long, J. M., & Holtzman, D. M. (2019). Alzheimer Disease: An Update on Pathobiology and Treatment Strategies. *Cell*, *179*(2), 312–339

Louria-Hayon, I., Alsheich-Bartok, O., Levav-Cohen, Y., Silberman, I., Berger, M., Grossman, T., Matentzoglu, K., Jiang, Y. H., Muller, S., Scheffner, M., Haupt, S., & Haupt, Y. (2009). E6AP promotes the degradation of the PML tumor suppressor. *Cell Death & Differentiation 2009 16:8*, *16*(8), 1156–1166

Lunardi, A., Gaboli, M., Giorgio, M., Rivi, R., Bygrave, A., Antoniou, M., Drabek, D., Dzierzak, E., Fagioli, M., Salmena, L., Botto, M., Cordon-Cardo, C., Luzzatto, L., Pelicci, P. G., Grosveld, F., & Pandolfi, P. P. (2011). A Role for PML in Innate Immunity. *Genes & Cancer*, *2*(1), 10–19

Maarifi, G., Maroui, M. A., Dutrieux, J., Dianoux, L., Nisole, S., & Chelbi-Alix, M. K. (2015). Small Ubiquitin-like Modifier Alters IFN Response. *The Journal of Immunology*, *195*(5), 2312–2324

Mao, Y. S., Zhang, B., & Spector, D. L. (2011). Biogenesis and Function of Nuclear Bodies. *Trends in Genetics : TIG*, *27*(8), 295

Maroui, M. A., Kheddache-Atmane, S., el Asmi, F., Dianoux, L., Aubry, M., & Chelbi-Alix, M. K. (2012a). Requirement of PML SUMO Interacting Motif for RNF4- or Arsenic Trioxide-Induced Degradation of Nuclear PML Isoforms. *PLOS ONE*, *7*(9), e44949

Maroui, M. A., Maarifi, G., McManus, F. P., Lamoliatte, F., Thibault, P., & Chelbi-Alix, M. K. (2018). Promyelocytic Leukemia Protein (PML) Requirement for Interferon-induced Global Cellular SUMOylation. *Molecular & Cellular Proteomics : MCP*, *17*(6), 1196–1208

Mathieu, J., & Besançon, F. (2006). Arsenic trioxide represses NF-kappaB activation and increases apoptosis in ATRA-treated APL cells. *Annals of the New York Academy of Sciences*, *1090*, 203–208

McDonough, A., Lee, R. v., Noor, S., Lee, C., Le, T., Iorga, M., Phillips, J. L. H., Murphy, S., Möller, T., & Weinstein, J. R. (2017). Ischemia/Reperfusion Induces Interferon-Stimulated Gene Expression in Microglia. *The Journal of Neuroscience*, *37*(34), 8292–8308

Medda, N., De, S. K., & Maiti, S. (2021). Different mechanisms of arsenic related signaling in cellular proliferation, apoptosis and neo-plastic transformation. *Ecotoxicology and Environmental Safety*, *208*, 111752

Mendez, M. F. (2019). Early-onset Alzheimer Disease and Its Variants. *Continuum (Minneapolis, Minn.)*, *25*(1), 34–51

Mendoza, R., Banerjee, I., Manna, D., Reghupaty, S. C., Yetirajam, R., & Sarkar, D. (2022). *Mouse Bone Marrow Cell Isolation and Macrophage Differentiation*, 85–91

Miki, T., Xu, Z., Chen-Goodspeed, M., Liu, M., van Oort-Jansen, A., Rea, M. A., Zhao, Z., Lee, C. C., & Chang, K. S. (2012). PML regulates PER2 nuclear localization and circadian function. *The EMBO Journal*, *31*(6), 1427–1439

Molliex, A., Temirov, J., Lee, J., Coughlin, M., Kanagaraj, A. P., Kim, H. J., Mittag, T., & Taylor, J. P. (2015). Phase separation by low complexity domains promotes stress granule assembly and drives pathological fibrillization. *Cell*, *163*(1), 123–133

Morand, E. F., Furie, R. A., Bruce, I. N., Vital, E. M., Dall'Era, M., Maho, E., Pineda, L., & Tummala, R. (2022). Efficacy of anifrolumab across organ domains in patients with moderate-to-severe systemic lupus erythematosus: a post-hoc analysis of pooled data from the TULIP-1 and TULIP-2 trials. *The Lancet Rheumatology*, *4*(4), e282–e292

Morris, G. P., Clark, I. A., Zinn, R., & Vissel, B. (2013). Microglia: A new frontier for synaptic plasticity, learning and memory, and neurodegenerative disease research. *Neurobiology of Learning and Memory*, *105*, 40–53

Mosley, M., Shah, C., Morse, K. A., Miloro, S. A., Holmes, M. M., Ahern, T. H., & Forger, N. G. (2017). Patterns of cell death in the perinatal mouse forebrain. *Journal of Comparative Neurology*, *525*(1), 47–64

Mumby, D. G., Gaskin, S., Glenn, M. J., Schramek, T. E., & Lehmann, H. (2002). Hippocampal Damage and Exploratory Preferences in Rats: Memory for Objects, Places, and Contexts. *Learning & Memory*, *9*(2), 49–57

Mura, E., Masnada, S., Antonello, C., Parazzini, C., Izzo, G., Garau, J., Sproviero, D., Cereda, C., Orcesi, S., Veggiotti, P., Zuccotti, G., Dilillo, D., Penagini, F., & Tonduti, D. (2021). Ruxolitinib in Aicardi-Goutières syndrome. *Metabolic Brain Disease*, *36*(5), 859–863

Murthy, A. C., & Fawzi, N. L. (2020). The (un)structural biology of biomolecular liquid-liquid phase separation using NMR spectroscopy. *Journal of Biological Chemistry*, *295*(8), 2375–2384

Nakahama, T., Kato, Y., Shibuya, T., Inoue, M., Kim, J. I., Vongpipatana, T., Todo, H., Xing, Y., & Kawahara, Y. (2021). Mutations in the adenosine deaminase ADAR1 that prevent endogenous Z-RNA binding induce Aicardi-Goutières-syndrome-like encephalopathy. *Immunity*, *54*(9), 1976-1988

Nisole, S., Maroui, M. A., Mascle, X. H., Aubry, M., & Chelbi-Alix, M. K. (2013). Differential Roles of PML Isoforms. *Frontiers in Oncology*, *3*

Niwa-Kawakita, M., Ferhi, O., Soilihi, H., le Bras, M., Lallemand-Breitenbach, V., & de Thé, H. (2017). PML is a ROS sensor activating p53 upon oxidative stress. *The Journal of Experimental Medicine*, *214*(11), 3197–3206

Onizawa, H., Kato, H., Kimura, H., Kudo, T., Soda, N., Shimizu, S., Funabiki, M., Yagi, Y., Nakamoto, Y., Priller, J., Nishikomori, R., Heike, T., Yan, N., Tsujimura, T., Mimori, T., & Fujita, T. (2021). Aicardi–Goutières syndrome-like encephalitis in mutant mice with constitutively active MDA5. *International Immunology*, *33*(4), 225–240

Orecchini, E., Frassinelli, L., & Michienzi, A. (2017). Restricting retrotransposons: ADAR1 is another guardian of the human genome. *RNA Biology*, *14*(11), 1485–1491

Palibrk, V., Suganthan, R., Scheffler, K., Wang, W., Bjørås, M., & Bøe, S. O. (2016). PML regulates neuroprotective innate immunity and neuroblast commitment in a hypoxic–ischemic encephalopathy model. *Cell Death & Disease*, *7*(7), e2320

Pandolfi, P. P., Grignani, F., Alcalay, M., Mencarelli, A., Biondi, A., LoCoco, F., Grignani, F., & Pelicci, P. G. (1991). Structure and origin of the acute promyelocytic leukemia myl/RAR alpha cDNA and characterization of its retinoid-binding and transactivation properties. *Oncogene*, *6*(7), 1285–1292

Park, K., Ryoo, J., Jeong, H., Kim, M., Lee, S., Hwang, S. Y., Ahn, J., Kim, D., Moon, H. C., Baek, D., Kim, K., Park, H. Y., & Ahn, K. (2021). Aicardi-Goutières syndrome-associated gene SAMHD1 preserves genome integrity by preventing R-loop formation at transcription–replication conflict regions. *PLOS Genetics*, *17*(4), e1009523

Pearson, M., Carbone, R., Sebastiani, C., Cloce, M., Fagloll, M., Saito, S., Higashimoto, Y., Appella, E., Minucci, S., Pandolfi, P. P., & Pellcci, P. G. (2000). PML regulates p53 acetylation and premature senescence induced by oncogenic Ras. *Nature*, *406*(6792), 207–210

Penagos-Puig, A., & Furlan-Magaril, M. (2020). Heterochromatin as an Important Driver of Genome Organization. *Frontiers in Cell and Developmental Biology*, *8*, 982

Pirrotta, V., & Li, H. B. (2012). A view of nuclear Polycomb bodies. *Current Opinion in Genetics & Development*, *22*(2), 101

Podcasy, J. L., & Epperson, C. N. (2016). Considering sex and gender in Alzheimer disease and other dementias. *Dialogues in Clinical Neuroscience*, *18*(4), 437

Qin, C., Zhou, L.-Q., Ma, X.-T., Hu, Z.-W., Yang, S., Chen, M., Bosco, D. B., Wu, L.-J., & Tian, D.-S. (2019). Dual Functions of Microglia in Ischemic Stroke. *Neuroscience Bulletin*, *35*(5), 921–933

Quignon, F., de Bels, F., Koken, M., Feunteun, J., Ameisen, J.-C., & de Thé, H. (1998). PML induces a novel caspase-independent death process. *Nature Genetics*, *20*(3), 259–265

Rabellino, A., Carter, B., Konstantinidou, G., Wu, S. Y., Rimessi, A., Byers, L. A., Heymach, J. v., Girard, L., Chiang, C. M., Teruya-Feldstein, J., & Scaglioni, P. P. (2012).

The SUMO E3-ligase PIAS1 regulates the tumor suppressor PML and its oncogenic counterpart PML-RARA. *Cancer Research*, *72*(9), 2275–2284

Rabinovici, G. D., Gatsonis, C., Apgar, C., Chaudhary, K., Gareen, I., Hanna, L., Hendrix, J., Hillner, B. E., Olson, C., Lesman-Segev, O. H., Romanoff, J., Siegel, B. A., Whitmer, R. A., & Carrillo, M. C. (2019). Association of Amyloid Positron Emission Tomography With Subsequent Change in Clinical Management Among Medicare Beneficiaries With Mild Cognitive Impairment or Dementia. *JAMA*, *321*(13), 1286–1294

Ragab, D., Salah Eldin, H., Taeimah, M., Khattab, R., & Salem, R. (2020). The COVID-19 Cytokine Storm; What We Know So Far. *Frontiers in Immunology*, *11*

Rapoport, S. I. (2000). Osmotic Opening of the Blood–Brain Barrier: Principles, Mechanism, and Therapeutic Applications. *Cellular and Molecular Neurobiology 2000 20:2*, *20*(2), 217–230

Regad, T., Bellodi, C., Nicotera, P., & Salomoni, P. (2009). The tumor suppressor Pml regulates cell fate in the developing neocortex. *Nature Neuroscience*, *12*(2), 132–140

Regad, T., & Chelbi-Alix, M. K. (2001). Role and fate of PML nuclear bodies in response to interferon and viral infections. *Oncogene*, *20*(49), 7274–7286

Regad, T., Saib, A., Lallemand-Breitenbach, V., Pandolfi, P. P., de Thé, H., & Chelbi-Alix, M. K. (2001). PML mediates the interferon-induced antiviral state against a complex retrovirus via its association with the viral transactivator. *The EMBO Journal*, *20*(13), 3495

Reuter, N., Schilling, E.-M., Scherer, M., Müller, R., & Stamminger, T. (2017). The ND10 Component Promyelocytic Leukemia Protein Acts as an E3 Ligase for SUMOylation of the Major Immediate Early Protein IE1 of Human Cytomegalovirus. *Journal of Virology*, *91*(10)

Reymond, A., Meroni, G., Fantozzi, A., Merla, G., Cairo, S., Luzi, L., Riganelli, D., Zanaria, E., Messali, S., Cainarca, S., Guffanti, A., Minucci, S., Pelicci, P. G., & Ballabio, A. (2001). The tripartite motif family identifies cell compartments. *The EMBO Journal*, *20*(9), 2140

Rice, G. I., del Toro Duany, Y., Jenkinson, E. M., Forte, G. M. A., Anderson, B. H., Ariaudo, G., Bader-Meunier, B., Baildam, E. M., Battini, R., Beresford, M. W., Casarano, M., Chouchane, M., Cimaz, R., Collins, A. E., Cordeiro, N. J. v, Dale, R. C., Davidson, J. E., de Waele, L., Desguerre, I., … Crow, Y. J. (2014). Gain-of-function mutations in IFIH1 cause a spectrum of human disease phenotypes associated with upregulated type I interferon signaling. *Nature Genetics*, *46*(5), 503–509

Rice, G. I., Kasher, P. R., Forte, G. M. A., Mannion, N. M., Greenwood, S. M., Szynkiewicz, M., Dickerson, J. E., Bhaskar, S. S., Zampini, M., Briggs, T. A., Jenkinson, E. M., Bacino, C. A., Battini, R., Bertini, E., Brogan, P. A., Brueton, L. A., Carpanelli, M., de Laet, C., de Lonlay, P., … Crow, Y. J. (2012). Mutations in ADAR1 cause Aicardi-Goutières syndrome associated with a type I interferon signature. *Nature Genetics*, *44*(11), 1243–1248

Rice, G. I., Meyzer, C., Bouazza, N., Hully, M., Boddaert, N., Semeraro, M., Zeef, L. A. H., Rozenberg, F., Bondet, V., Duffy, D., Llibre, A., Baek, J., Sambe, M. N., Henry, E., Jolaine, V., Barnerias, C., Barth, M., Belot, A., Cances, C., … Crow, Y. J. (2018). Reverse-Transcriptase Inhibitors in the Aicardi–Goutières Syndrome. *The New England Journal of Medicine*, *379*(23), 2275–2277

Rice, G., Patrick, T., Parmar, R., Taylor, C. F., Aeby, A., Aicardi, J., Artuch, R., Montalto, S. A., Bacino, C. A., Barroso, B., Baxter, P., Benko, W. S., Bergmann, C., Bertini, E., Biancheri, R., Blair, E. M., Blau, N., Bonthron, D. T., Briggs, T., … Crow, Y. J. (2007). Clinical and molecular phenotype of Aicardi-Goutieres syndrome. *American Journal of Human Genetics*, *81*(4), 713–725

Rogaeva, E. (2002). The solved and unsolved mysteries of the genetics of early-onset Alzheimer's disease. *Neuromolecular Medicine*, *2*(1), 1–10

Rowley, J. D., Golomb, H. M., & Dougherty, C. (1977). 15/17 translocation, a consistent chromosomal change in acute promyelocytic leukemia. *The Lancet*, *309*(8010), 549–550

Roy, E. R., Wang, B., Wan, Y., Chiu, G., Cole, A., Yin, Z., Propson, N. E., Xu, Y., Jankowsky, J. L., Liu, Z., Lee, V. M.-Y., Trojanowski, J. Q., Ginsberg, S. D., Butovsky, O., Zheng, H., & Cao, W. (2020). Type I interferon response drives neuroinflammation and synapse loss in Alzheimer disease. *Journal of Clinical Investigation*, *130*(4), 1912–1930

Ruganzu, J. B., Zheng, Q., Wu, X., He, Y., Peng, X., Jin, H., Zhou, J., Ma, R., Ji, S., Ma, Y., Qian, Y., Wang, Y., & Yang, W. (2021). TREM2 overexpression rescues cognitive deficits in APP/PS1 transgenic mice by reducing neuroinflammation via the JAK/STAT/SOCS signaling pathway. *Experimental Neurology*, *336*, 113506

Sahin Umut, U., Ferhi, O., Jeanne, M., Benhenda, S., Berthier, C., Jollivet, F., Niwa-Kawakita, M., Faklaris, O., Setterblad, N., de Thé, H., & Lallemand-Breitenbach, V. (2014). Oxidative stress–induced assembly of PML nuclear bodies controls sumoylation of partner proteins. *Journal of Cell Biology*, *204*(6), 931–945

Salomoni, P., & Betts-Henderson, J. (2011). The role of PML in the nervous system. *Molecular Neurobiology*, *43*(2), 114–123

Salomoni, P., Ferguson, B., Wyllie, A., & Rich, T. (2008). New insights into the role of PML in tumour suppression. *Cell Research*, *18*(6), 622–640

Sanyal, T., Bhattacharjee, P., Paul, S., & Bhattacharjee, P. (2020). Recent Advances in Arsenic Research: Significance of Differential Susceptibility and Sustainable Strategies for Mitigation. *Frontiers in Public Health*, *8*

Scaglioni, P. P., Yung, T. M., Cai, L. F., Erdjument-Bromage, H., Kaufman, A. J., Singh, B., Teruya-Feldstein, J., Tempst, P., & Pandolfi, P. P. (2006). A CK2-Dependent Mechanism for Degradation of the PML Tumor Suppressor. *Cell*, *126*(2), 269–283

Schafer, S. L., Lin, R., Moore, P. A., Hiscott, J., & Pitha, P. M. (1998). Regulation of Type I Interferon Gene Expression by Interferon Regulatory Factor-3. *Journal of Biological Chemistry*, *273*(5), 2714–2720

Scherer, M., Klingl, S., Sevvana, M., Otto, V., Schilling, E.-M., Stump, J. D., Müller, R., Reuter, N., Sticht, H., Muller, Y. A., & Stamminger, T. (2014). Crystal Structure of Cytomegalovirus IE1 Protein Reveals Targeting of TRIM Family Member PML via Coiled-Coil Interactions. *PLoS Pathogens*, 10(11)

Scherer, M., & Stamminger, T. (2016). Emerging Role of PML Nuclear Bodies in Innate Immune Signaling. *Journal of Virology*, *90*(13), 5850

Scott-Hewitt, N., Perrucci, F., Morini, R., Erreni, M., Mahoney, M., Witkowska, A., Carey, A., Faggiani, E., Schuetz, L. T., Mason, S., Tamborini, M., Bizzotto, M., Passoni, L., Filipello, F., Jahn, R., Stevens, B., & Matteoli, M. (2020). Local externalization of phosphatidylserine mediates developmental synaptic pruning by microglia. *The EMBO Journal*, *39*(16)

Sekerdag, E., Solaroglu, I., & Gursoy-Ozdemir, Y. (2018). Cell Death Mechanisms in Stroke and Novel Molecular and Cellular Treatment Options. *Current Neuropharmacology*, *16*(9), 1396–1415

Se Thoe, E., Fauzi, A., Tang, Y. Q., Chamyuang, S., & Chia, A. Y. Y. (2021). A review on advances of treatment modalities for Alzheimer's disease. *Life Sciences*, *276*, 119129

Sevigny, J., Chiao, P., Bussière, T., Weinreb, P. H., Williams, L., Maier, M., Dunstan, R., Salloway, S., Chen, T., Ling, Y., O'Gorman, J., Qian, F., Arastu, M., Li, M., Chollate, S., Brennan, M. S., Quintero-Monzon, O., Scannevin, R. H., Arnold, H. M., … Sandrock, A. (2016). The antibody aducanumab reduces Aβ plaques in Alzheimer's disease. *Nature 2016 537:7618*, *537*(7618), 50–56

Shin, Y., & Brangwynne, C. P. (2017). Liquid phase condensation in cell physiology and disease. *Science (New York, N.Y.)*, *357*(6357)

Sierksma, A., Lu, A., Mancuso, R., Fattorelli, N., Thrupp, N., Salta, E., Zoco, J., Blum, D., Buée, L., de Strooper, B., & Fiers, M. (2020). Novel Alzheimer risk genes determine the microglia response to amyloid-β but not to TAU pathology. *EMBO Molecular Medicine*, *12*(3)

Silva, M. V. F., Loures, C. D. M. G., Alves, L. C. V., de Souza, L. C., Borges, K. B. G., & Carvalho, M. D. G. (2019). Alzheimer's disease: risk factors and potentially protective measures. *Journal of Biomedical Science*, *26*(1)

Song, Y.-K., Song, J., Kim, K., & Kwon, J.-W. (2022). Potential Adverse Events Reported With the Janus Kinase Inhibitors Approved for the Treatment of Rheumatoid Arthritis Using Spontaneous Reports and Online Patient Reviews. *Frontiers in Pharmacology*, *12*

Spector, D. L., & Gasser, S. M. (2003). A molecular dissection of nuclear function. *EMBO Reports*, *4*(1), 18–23

Stadler, M., Chelbi-Alix, M. K., Koken, M. H., Venturini, L., Lee, C., Saïb, A., Quignon, F., Pelicano, L., Guillemin, M. C., & Schindler, C. (1995). Transcriptional induction of the PML growth suppressor gene by interferons is mediated through an ISRE and a GAS element. *Oncogene*, *11*(12), 2565–2573

Stahl, M., & Tallman, M. S. (2019). Acute promyelocytic leukemia (APL): remaining challenges towards a cure for all. *Leukemia & Lymphoma*, *60*(13), 3107–3115

Stetson, D. B., Ko, J. S., Heidmann, T., & Medzhitov, R. (2008a). Trex1 prevents cell-intrinsic initiation of autoimmunity. *Cell*, *134*(4), 587

Stetson, D. B., Ko, J. S., Heidmann, T., & Medzhitov, R. (2008b). Trex1 prevents cell-intrinsic initiation of autoimmunity. *Cell*, *134*(4), 587–598

Stuurman, N., Floore, A., Colen, A., de Jong, L., & van Driel, R. (1992). Stabilization of the nuclear matrix by disulfide bridges: Identification of matrix polypeptides that form disulfides. *Experimental Cell Research*, *200*(2), 285–294

Szentirmay, M. N., & Sawadogo, M. (2000). Spatial organization of RNA polymerase II transcription in the nucleus. *Nucleic Acids Research*, *28*(10), 2019

Takahashi, J., Fujigasaki, H., Iwabuchi, K., Bruni, A. C., Uchihara, T., el Hachimi, K. H., Stevanin, G., Dürr, A., Lebre, A. S., Trottier, Y., de Thé, H., Tanaka, J., Hauw, J. J., Duyckaerts, C., & Brice, A. (2003). PML nuclear bodies and neuronal intranuclear inclusion in polyglutamine diseases. *Neurobiology of Disease*, *13*(3), 230–237

Takeuchi, T., Tanaka, Y., Matsumura, R., Saito, K., Yoshimura, M., Amano, K., Atsumi, T., Suematsu, E., Hayashi, N., Wang, L., & Tummala, R. (2020). Safety and tolerability of sifalimumab, an anti-interferon-α monoclonal antibody, in Japanese patients with systemic lupus erythematosus: A multicenter, phase 2, open-label study. *Modern Rheumatology*, *30*(1), 93–100

Thepmankorn, P., Bach, J., Lasfar, A., Zhao, X., Souayah, S., Chong, Z. Z., & Souayah, N. (2021). Cytokine storm induced by SARS-CoV-2 infection: The spectrum of its neurological manifestations. *Cytokine*, *138*, 155404

Thomas, X. (2019). Acute Promyelocytic Leukemia: A History over 60 Years-From the Most Malignant to the most Curable Form of Acute Leukemia. *Oncology and Therapy*, *7*(1), 33–65

Tiwari, S., Atluri, V., Kaushik, A., Yndart, A., & Nair, M. (2019). Alzheimer's disease: pathogenesis, diagnostics, and therapeutics. *International Journal of Nanomedicine*, *14*, 5541

Tonduti, D., Fazzi, E., Badolato, R., & Orcesi, S. (2020). Novel and emerging treatments for Aicardi-Goutières syndrome. *Expert Review of Clinical Immunology*, *16*(2), 189–198

Trotman, L. C., Alimonti, A., Scaglioni, P. P., Koutcher, J. A., Cordon-Cardo, C., & Pandolfi, P. P. (2006). Identification of a tumour suppressor network opposing nuclear Akt function. *Nature*, *441*(7092), 523–527

Uversky, V. N., Oldfield, C. J., & Dunker, A. K. (2005). Showing your ID: intrinsic disorder as an ID for recognition, regulation and cell signaling. *Journal of Molecular Recognition : JMR*, *18*(5), 343–384

Vancurova, M., Hanzlikova, H., Knoblochova, L., Kosla, J., Majera, D., Mistrik, M., Burdova, K., Hodny, Z., & Bartek, J. (2019). PML nuclear bodies are recruited to persistent DNA damage lesions in an RNF168-53BP1 dependent manner and contribute to DNA repair. *DNA Repair*, *78*, 114–127

van Damme, E., Laukens, K., Dang, T. H., & van Ostade, X. (2010). A manually curated network of the PML nuclear body interactome reveals an important role for PML-NBs in SUMOylation dynamics. *International Journal of Biological Sciences*, *6*(1), 51–67

van der Lee, R., Buljan, M., Lang, B., Weatheritt, R. J., Daughdrill, G. W., Dunker, A. K., Fuxreiter, M., Gough, J., Gsponer, J., Jones, D. T., Kim, P. M., Kriwacki, R. W., Oldfield, C. J., Pappu, R. v., Tompa, P., Uversky, V. N., Wright, P. E., & Babu, M. M. (2014). Classification of intrinsically disordered regions and proteins. *Chemical Reviews*, *114*(13), 6589–6631

Vanderver, A., Adang, L., Gavazzi, F., McDonald, K., Helman, G., Frank, D. B., Jaffe, N., Yum, S. W., Collins, A., Keller, S. R., Lebon, P., Meritet, J.-F., Rhee, J., Takanohashi, A., Armangue, T., Ulrick, N., Sherbini, O., Koh, J., Peer, K., … Shults, J. (2020). Janus Kinase Inhibition in the Aicardi-Goutières Syndrome. *The New England Journal of Medicine*, *383*(10), 986–989

Vogel-Ciernia, A., Matheos, D. P., Barrett, R. M., Kramár, E. A., Azzawi, S., Chen, Y., Magnan, C. N., Zeller, M., Sylvain, A., Haettig, J., Jia, Y., Tran, A., Dang, R., Post, R. J., Chabrier, M., Babayan, A. H., Wu, J. I., Crabtree, G. R., Baldi, P., … Wood, M. A. (2013). The neuron-specific chromatin regulatory subunit BAF53b is necessary for synaptic plasticity and memory. *Nature Neuroscience*, *16*(5), 552–561

Walsh, R. N., & Cummins, R. A. (1976). The open-field test: A critical review. *Psychological Bulletin*, *83*(3), 482–504

Wang, H., Cao, F., Li, J., Li, L., Li, Y., Shi, C., Lan, W., Li, D., Zhao, H., Zhang, Y., Zhang, Z., Liu, X., Meng, R., Yang, B., & Zhou, J. (2014). Arsenic trioxide and mannitol for the treatment of acute promyelocytic leukemia relapse in the central nervous system. *Blood*, *124*(12), 1998

Wang, J., Shiels, C., Sasieni, P., Wu, P. J., Islam, S. A., Freemont, P. S., & Sheer, D. (2004). Promyelocytic leukemia nuclear bodies associate with transcriptionally active genomic regions. *Journal of Cell Biology*, *164*(4), 515–526

Wang, K., Wang, P., Shi, J., Zhu, X., He, M., Jia, X., Yang, X., Qiu, F., Jin, W., Qian, M., Fang, H., Mi, J., Yang, X., Xiao, H., Minden, M., Du, Y., Chen, Z., & Zhang, J. (2010).

PML/RARalpha targets promoter regions containing PU.1 consensus and RARE half sites in acute promyelocytic leukemia. *Cancer Cell*, *17*(2), 186–197

Wang, Z.-Y., & Chen, Z. (2008). Acute promyelocytic leukemia: from highly fatal to highly curable. *Blood*, *111*(5), 2505–2515

Weller, J., & Budson, A. (2018). Current understanding of Alzheimer's disease diagnosis and treatment. *F1000Research*, *7*

Xiao, Y.-F., Liu, S.-X., Wu, D.-D., Chen, X., & Ren, L.-F. (2006). Inhibitory effect of arsenic trioxide on angiogenesis and expression of vascular endothelial growth factor in gastric cancer. *World Journal of Gastroenterology*, *12*(36), 5780–5786

Xue, B., Dunbrack, R. L., Williams, R. W., Dunker, A. K., & Uversky, V. N. (2010). PONDR-FIT: a meta-predictor of intrinsically disordered amino acids. *Biochimica et Biophysica Acta*, *1804*(4), 996–1010

Xu, Z.-X., Timanova-Atanasova, A., Zhao, R.-X., & Chang, K.-S. (2003). PML Colocalizes with and Stabilizes the DNA Damage Response Protein TopBP1. *Molecular and Cellular Biology*, *23*(12), 4247–4256

Yamada, M., Sato, T., Shimohata, T., Hayashi, S., Igarashi, S., Tsuji, S., & Takahashi, H. (2001). Interaction between neuronal intranuclear inclusions and promyelocytic leukemia protein nuclear and coiled bodies in CAG repeat diseases. *The American Journal of Pathology*, *159*(5), 1785–1795

Yang, S., Jeong, J. H., Brown, A. L., Lee, C. H., Pandolfi, P. P., Chung, J. H., & Kim, M. K. (2006). Promyelocytic leukemia activates Chk2 by mediating Chk2 autophosphorylation. *The Journal of Biological Chemistry*, *281*(36), 26645–26654

Yang, Y., Zhang, X., Jia, S., Yang, S., Yang, Y., & Yang, T. (2012). Arsenic trioxide induces G2/M arrest in hepatocellular carcinoma cells by increasing the tumor suppressor PTEN expression. *Journal of Cellular Biochemistry*, *113*(11), 3528–3535

Ye, Y., Ricard, L., Siblany, L., Stocker, N., de Vassoigne, F., Brissot, E., Lamarthée, B., Mekinian, A., Mohty, M., Gaugler, B., & Malard, F. (2020). Arsenic trioxide induces regulatory functions of plasmacytoid dendritic cells through interferon-α inhibition. *Acta Pharmaceutica Sinica B*, *10*(6), 1061–1072

Yoon, J. S., Jo, D., Lee, H.-S., Yoo, S.-W., Lee, T.-Y., Hwang, W. S., Choi, J.-M., Kim, E., Kim, S.-S., & Suh-Kim, H. (2018). Spatiotemporal Protein Atlas of Cell Death-Related Molecules in the Rat MCAO Stroke Model. *Experimental Neurobiology*, *27*(4), 287–298

Ytterberg, S. R., Bhatt, D. L., Mikuls, T. R., Koch, G. G., Fleischmann, R., Rivas, J. L., Germino, R., Menon, S., Sun, Y., Wang, C., Shapiro, A. B., Kanik, K. S., & Connell, C. A. (2022). Cardiovascular and Cancer Risk with Tofacitinib in Rheumatoid Arthritis. *New England Journal of Medicine*, *386*(4), 316–326

Yu, Q., Herrero del Valle, A., Singh, R., & Modis, Y. (2021). MDA5 disease variant M854K prevents ATP-dependent structural discrimination of viral and cellular RNA. *Nature Communications 2021 12:1*, *12*(1), 1–12

Zhang, J. M., Genois, M. M., Ouyang, J., Lan, L., & Zou, L. (2021). Alternative lengthening of telomeres is a self-perpetuating process in ALT-associated PML bodies. *Molecular Cell*, *81*(5), 1027-1042

Zhang, M., Downes, C. E., Wong, C. H. Y., Brody, K. M., Guio-Agulair, P. L., Gould, J., Ates, R., Hertzog, P. J., Taylor, J. M., & Crack, P. J. (2017). Type-I interferon signalling through IFNAR1 plays a deleterious role in the outcome after stroke. *Neurochemistry International*, *108*, 472–480

Zhang, N., Wu, Z. M., McGowan, E., Shi, J., Hong, Z. B., Ding, C. W., Xia, P., & Di, W. (2009). Arsenic trioxide and cisplatin synergism increase cytotoxicity in human ovarian cancer cells: therapeutic potential for ovarian cancer. *Cancer Science*, *100*(12), 2459–2464

Zhang, S., Song, J., Yang, Y., Miao, H., Yang, L., Liu, Y., Zhang, X., Liu, Y., & Wang, T. (2021). Type I interferonopathies with novel compound heterozygous TREX1 mutations in two siblings with different symptoms responded to tofacitinib. *Pediatric Rheumatology*, *19*(1), 1–8

Zhang, X.-W., Yan, X.-J., Zhou, Z.-R., Yang, F.-F., Wu, Z.-Y., Sun, H.-B., Liang, W.-X., Song, A.-X., Lallemand-Breitenbach, V., Jeanne, M., Zhang, Q.-Y., Yang, H.-Y., Huang, Q.-H., Zhou, G.-B., Tong, J.-H., Zhang, Y., Wu, J.-H., Hu, H.-Y., de Thé, H., … Chen, Z. (2010). Arsenic trioxide controls the fate of the PML-RARalpha oncoprotein by directly binding PML. *Science (New York, N.Y.)*, *328*(5975), 240–243

Zhong, S., Salomoni, P., Ronchetti, S., Guo, A., Ruggero, D., & Pandolfi, P. P. (2000). Promyelocytic leukemia protein (PML) and Daxx participate in a novel nuclear pathway for apoptosis. *The Journal of Experimental Medicine*, *191*(4), 631–639

Zhu, L., Richardson, T. M., Wacheul, L., Wei, M. T., Feric, M., Whitney, G., Lafontaine, D. L. J., & Brangwynne, C. P. (2019). Controlling the material properties and rRNA processing function of the nucleolus using light. *Proceedings of the National Academy of Sciences of the United States of America*, *116*(35), 17330–17335

Zhu, Y., Zhang, Q., Zhang, W., Li, N., Dai, Y., Tu, J., Yang, F., Brann, D. W., & Wang, R. (2017). Protective Effect of 17β-Estradiol Upon Hippocampal Spine Density and Cognitive Function in an Animal Model of Vascular Dementia. *Scientific Reports*, *7*(1), 42660

10. Acknowledgments

I would like, first, to thank Paolo for giving me the opportunity to complete the PhD in his lab. For the last five years, you supervised and supported me in achieving my projects, but you also allow me to personally grow and take responsibilities in the lab. It was a real pleasure as well as an inspiration to work for somebody as driven, curious and open about science. I have learnt a lot from you, the hard work of course, but mostly the dedication for research. Thanks a lot for everything.

I would also like to thank all my former and current colleagues of AG Salomoni, and in particular the ones involved in my projects: Miriam for helping me with all the never-ending animal applications and genotyping, and Erik for analyzing my RNAseq datasets (I hope you won't have many "another day"!).

Many thanks to Pr. Kato, I really appreciated the collaboration we built during the last two years and it was a pleasure to work on this exciting project! On this, I would also like to thank Burcu from AG Kato, with who we performed many long experiments together.

I am really grateful of achieving my PhD at the DZNE and I owe a big thank to the core facilities (PRECISE, LMF, ARF), you made my work possible and easier! To all the groups, for the help and feedbacks on my projects, and especially to AG Capasso and AG Bano for sharing reagents and protocols with me.

In AG Capasso, I would like to particularly thank Ezio for your passionate discussions about our projects, our mutual motivation during this PhD, and your help for the university paperwork! It was great to get to know you!

Finally, to Lena, I am beyond grateful that you were next door! Not only for helping me in my projects, answering all my questions and saving me (many times) by letting me borrow anything that I ran out of, but you were, most of all, an example to me! Your passion, your authenticity and your modesty are qualities that I look up to!

More personnaly, je voudrais remercier toute ma famille et mes parents pour toujours me suivre et me soutenir dans mes aventures les moins conventionelles sans meme les comprendre. A ma soeur qui est mon exemple dans beaucoup de domaines et dont je suis les pas annees apres annees.

Je remercie tous mes amis, “les copains”, Colin, Alexi, Tampax, Francesca… qui, malgres le fait que je n’ai pas ete assez presente pour eux pendant ces 5 dernieres annees, ont toujours ete derriere moi.

Special thanks to my lovely and best flatmate, Super Dani. We started the PhD together and it was great to grow in it side by side… Looking back, I loved our philosophical discussions (even when I was too tired to think) and your efforts to understand my work and project! However, the doubt will forever stay about your field of research: psychology, sociology... all the same to me! Thanks for opening my mind! Eventually, I cannot think of a better flatmate to spend 4 years of PhD with!

I am also grateful for meeting Christina, one of the best persons I met recently. You joined the lab 2 years ago, and I couldn’t have asked for a better colleague and friend during this period. We went through a lot together and I deeply thank you for always understanding me, motivating me and teaching me at so many levels. Also, I owe you one for proofreading my thesis even though you are still not able to pronounce “cabin/camping” and “think”! Eventually, I am not sure how much I should trust your proofreading… That said, I feel very lucky I got to meet you and your sense of humour! About that… as you suggested me to end my acknowledgments: “Finally, I would like to thank me!”.

Actually, the real final thank goes to Tim, I couldn’t have done it without you! I am grateful that my PhD led our paths to cross, this is one of the best things I got from those 5 years! I will never stop thanking you for everything, you never stop supporting, motivating and helping me. You even understood my project and listened to all my ideas but also complains! I can’t thank you enough for your and your family’s support!